NATURALNESS, MONOPOLES, AND DARK MATTER

A Dissertation

Presented to the Faculty of the Graduate School

of Cornell University

in Partial Fulfillment of the Requirements for the Degree of

Doctor of Philosophy

by

Nicolas Rey-Le Lorier

August 2016

NATURALNESS, MONOPOLES, AND DARK MATTER

Nicolas Rey-Le Lorier, Ph.D.

Cornell University 2016

This thesis consists of four papers on which I worked during the course of studies as a graduate student at Cornell University. The first paper, presented in Chapter 2, presents a nearly model-independent method of establishing the degree of fine-tuning in the Standard Model by measuring the coupling of the Higgs to gauge bosons. The second paper, presented in Chapter 3, is an analysis of the phenomenology of the minimal supersymmetric models with spin-one top partners, dubbed the "Swan" model. The third paper, presented In Chapter 4, demonstrates how to use dimensional reduction to go from s-confining four-dimensional theories to three dimensional theories of chiral fields which contain dressed monopoles, bound states of monopoles and matter fields. The fourth and final paper, presented in Chapter 5, presents a novel scenario for the production of thermal relic dark matter. In this scenario, the dark matter candidate is an Elastically Decoupling Relic, or ELDER, whose relic abundance is controlled almost uniquely by its elastic, non-preserving scattering with the Standard Model.

BIOGRAPHICAL SKETCH

Nicolas Rey-Le Lorier was born in Montréal in 1987, which has been a source of endless amusement to his American friends. On a fateful night in the early 2000's he was tempted into doing Physics by an online discussion of special relativity and he has been unable to stay clean since then.

To Alisa, who made me believe it could happen.

I urge you to please notice when you are happy, and exclaim or murmur or think at some point, 'If this isn't nice, I don't know what is.'

Kurt Vonnegut

ACKNOWLEDGEMENTS

Despite the fact that only a single name resides in the place reserved for the "author", this thesis was very much a collaborative work which would never have come to be were it not the efforts of a great many people over the years. In approximate chronological order: my parents, Évelyne and Jacques, who supported me in all the possible ways during the many difficult times; my cousin and godfather Frédéric, who always encouraged my interest in science and insisted, against all the evidence to the contrary, that I was a person worth knowing; my cousin Émmanuel, my aunt Marie-Christine and my uncle Phillippe, for all the happy childhood memories; my sister Magali, who drove me crazy for most of her existence, but then adopted two cats; my friend Vincent, who I've known for close to 25 years now, to the point that we only need to use half of all available syllables to communicate; my CEGEP friends Marie-Claire, Véronique, Phillippe, Adrien, Lynn, Bich, Inge and Consuelo, who made me appreciate the company of people once again; my friends at Université de Montréal Julien, Alex, Kim and Dan, for all those times you made me laugh so hard it made me cry; Françoise, who sent me otters during my Master's thesis and cooking lessons during my PhD.; my Master's advisor, David London, who taught me what a force is; my PhD. advisor, Maxim Perelstein, who kept me on the right track for five years; all of my collaborators throughout the years: Maxime, Marco, Bithaka, Jack, Mario, Antonio, Eric, Gowari and Yu-Dai; Csaba Csáki, who took an interest in my future at a time where I perhaps wasn't doing so myself; Julia Thom-Levy, who allowed me to discover what it was that I really wanted to do, and convinced me that I could do it; my friends at Cornell University, Flip, Bibhushan, Mario, Jack, John, Wee-Hao, Math: thank you for the laughs, the physics, and the poker; Cody and Julia, who made me feel

welcome and useful and appreciated, and let me hang out with their cats; Alisa, who made sure I'll never forget Ithaca and its gorges; and finally all of my students, from my undergraduate days to this very week: thank you for wanting to learn, and thank you for giving me a chance to help you.

CONTENTS

Biographical Sketch . . . iii
Dedication . . . iv
Acknowledgements . . . v
Contents . . . vii
List of Tables . . . ix
List of Figures . . . x

1 Introduction **1**
1.1 The Hierarchy Problem . . . 1
1.1.1 Bottom-Up Explanation . . . 2
1.1.2 Top-Down Explanation . . . 4
1.1.3 Proposed Solutions to the Hierarchy Problem . . . 6
1.1.4 The Topic of Chapter 2: Higgs Couplings and Naturalness 7
1.1.5 Supersymmetric Models . . . 8
1.1.6 The Topic of Chapter 3: Swan Models . . . 9
1.2 Dualities in 3D Field Theories . . . 10
1.2.1 A Duality for QCD . . . 11
1.2.2 Seiberg Dualities and S-Confinement . . . 12
1.2.3 Test of the Duality: Anomaly Matching . . . 15
1.2.4 Gauge Theories in Three Dimensions . . . 16
1.2.5 An Example: SQED . . . 18
1.2.6 From Four Dimensions to Three Dimensions: Dimensional Reduction . . . 26
1.2.7 The Topic of Chapter 4: Dressed Monopoles Operators . . 31
1.3 Thermal Dark Matter Relics . . . 32
1.3.1 The Case for Dark Matter . . . 32
1.3.2 Dark Matter as Thermal Relic . . . 35
1.3.3 The Topic of Chapter 5: ELDERs . . . 39

2 Higgs Couplings and Naturalness **41**
2.1 Introduction . . . 41
2.2 General Argument: Top Partners, Naturalness, and the Higgs Couplings . . . 43
2.3 Benchmark Model: a Single Top Partner . . . 49
2.4 Two Top Partners . . . 54
2.5 Conclusions . . . 57

3 Spin-One Top Partner: Phenomenology **60**
3.1 Introduction . . . 60
3.2 Review of the Model . . . 63
3.2.1 Structure and Particle Content . . . 63
3.2.2 Gauge Boson Spectrum . . . 68

3.2.3 Beta Functions and the Strong-Coupling Scale 70
3.3 Precision Electroweak Constraints 71
3.4 Direct Searches at the LHC 74
3.5 Higgs Mass and EWSB Fine-Tuning 77
3.6 Higgs Couplings to Photons and Gluons 80
3.7 Future Prospects for Direct Searches 83
3.8 Conclusions and Outlook 85
3.9 Appendix A: Masses and Couplings of Z' States 86
3.10 Appendix B: Non-Decoupling D-Terms 88
3.11 Appendix C: Parton-Level Cross Sections for Swan Production . . 90

4 From S-confinement to 3D Chiral Theories: Dressing the Monopoles 92
4.1 Introduction 92
4.2 3D IR Duality in a Chiral $SU(6)$ Gauge Theory 95
4.2.1 The Coulomb Branch Operators 96
4.2.2 Consistency Check from the Partition Function 106
4.3 Appendix 109
4.3.1 Real Mass Deformation 109

5 Elastically Decoupling Dark Matter 111
5.1 Introduction 111
5.2 The elastically decoupling thermal relic 114
5.3 The Boltzmann Equations 118
5.4 Constraints 121

Bibliography 125

LIST OF TABLES

1.1 Matter and symmetry content of SQCD with $N_F = N_c + 1$flavours. 13
1.2 Matter and symmetry content of the dual of SQCD with $N_F = N_c + 1$ flavours. 14

3.1 Chiral superfields of the model, and their gauge quantum numbers. Here, $i = 1 \ldots 3$ is the flavor index. 63
3.2 Field content after the UV symmetry breaking; all entries with spin 0 correspond to complex scalar fields. The MSSM fields are not included in this table. 66
3.3 Mass matrix for fermions in the $(\mathbf{3}, \mathbf{2}, 1/6)$ (and conjugate) sector. 67

4.1 Matter content of the 3D duality obtained from the 4D theory by applying the dimensional reduction procedure. 96
4.2 Matter content of the 4D s-confining theory along with the global symmetries and the charges of the confined mesons. 109

LIST OF FIGURES

1.1 Feynman diagram representing the quantum corrections from ψ loops to the mass of the h particle in the toy-model given by Eq. 1.1. 2

1.2 Pictorial representation of the moduli space of $\mathcal{N} = 2$, three-dimensional SQED with one flavour. The shaded region cannot be studied using weakly-coupled methods. 20

1.3 Pictorial representation of the *classical* moduli space of $\mathcal{N} = 2$, three-dimensional SQCD with N_F flavours. All of the shaded regions involve strongly-coupled dynamics and cannot be analyzed using perturbative methods. 25

1.4 Representation of the RG flow of various theories during the process of dimensional reduction. 29

1.5 The life of a thermal relic, part 1. The dashed blue line represent the yield, or energy density of a thermal relic normalized by the entropy density of the photon bath, if it stayed in thermal and chemical equilibrium throughout its life. The solid orange line corresponds to the observed yield of dark matter in our universe. When $T \lesssim m$, the number density becomes exponentially suppressed and plummets downward to zero. 38

1.6 The life of a thermal relic, part 2. For a real thermal relic (solid black line), the interactions that keep the particle in thermal and chemical equilibrium stop being effective when $T \lesssim m$, and the yield stops following the equilibrium distribution. After decoupling, the yield is constant. 39

2.1 Fractional deviation of the Higgs coupling to gluons (left panel) and photons (right panel) from the SM value, as a function of the top partner mass. Top row: Spin-0 top partner. Bottom row: Spin-1/2 top partner. Regions currently allowed by the LHC and Tevatron data are shown in green (68 % c.l.) and yellow (95 % c.l.). 48

2.2 Regions allowed by the LHC and Tevatron measurements of the Higgs rates in the $R_\gamma - R_g$ plane, at the 68 % c.l. (green) and 95 % c.l. (yellow). The spin-0 top partner model predicts deviations along the blue line, while the spin-1/2 top partner induces deviations along the red line. The points on both lines correspond to the partner masses of 350, 500, 650, and 800 GeV. For comparison, projected constraints from the LHC-14 [1] are shown by red lines. 50

2.3 Regions allowed by the LHC and Tevatron data in the $\Delta - \log\Lambda$ plane, at the 68 % c.l. (green) and 95 % c.l. (yellow). Here, Λ is the scale (in GeV) where the logarithmic divergence in the Higgs mass renormalization is cut off. Left panel: Spin-0 top partner. Right panel: Spin-1/2 top partner. 51
2.4 Fine-tuning as a function of the fractional deviation of the Higgs coupling to gluons (left panel) and photons (right panel) from the SM value, and the energy scale Λ (in GeV) where the logarithmic divergence in the Higgs mass renormalization is cut off. Top row: Spin-0 top partner. Bottom row: Spin-1/2 top partner. Regions currently allowed by the LHC and Tevatron data are shown in green (68 % c.l.) and yellow (95 % c.l.). 52
2.5 Contours of fine tuning (in blue) and R_g (in red) for fixed values of θ, with $\Lambda = 20$ TeV. The regions shaded in green correspond to points where $|R_g - 1| < 0.01$ but for which the amount of fine tuning is less than what is predicted for a one scalar partner model with $R_g = 0.01$. The regions shaded in gray corresponds to points where $|c_i v^2/m_{0,i}^2| > 1$. The top partner mass m_1 is in units of GeV. . 55
2.6 Fine tuning (in blue) as a function of θ for fixed values of μ and R_g, with $\Lambda = 20$ TeV. The regions shaded in in gray indicate values of θ where $|c_i v^2/m_{0,i}^2| > 1$; the regions shaded in red are unphysical due to $m_1^2 < 0$. Green regions indicate values of θ for which the fine tuning is less than what is predicted for a one scalar partner model with $R_g = 0.01$. 56

3.1 Ratio of the masses of the spin-1 top partner ("swan") and the lightest Z'. Left panel: full parameter space (gray regions indicate regions where one of the gauge couplings becomes non-perturbative). Right panel: the region where the ratio is minimized. In both plots, $\tan\beta = 0.95$; the ratio scales as $\sqrt{1 + \tan^2\beta}$. . 69
3.2 Lower bound on the swan mass (in TeV) from precision electroweak constraints. Left panel: full parameter space (gray regions indicate regions where one of the gauge couplings becomes non-perturbative). Right panel: the region where the constraint is minimized. In both plots, $\tan\beta = 0.95$; the bounds scale as $\sqrt{1 + \tan^2\beta}$. 72
3.3 Lower bounds on the swan mass (in TeV) from direct searches for the Z' at the LHC (left panel) and the combination of direct search and precision electroweak constraint (right panel). In both plots, $\tan\beta = 0.95$; the bounds scale as $\sqrt{1 + \tan^2\beta}$. 75

3.4 Solid lines: The difference δ between the value of the Higgs quartic $\lambda_{\rm SM}(\Lambda_{\rm susy})$ needed to accommodate the 125 GeV Higgs, and the value predicted by a SUSY theory with the SM gauge group. Top to bottom: $\Lambda_{\rm susy} = 5, 10, 100$ TeV. Dashed lines: The additional contribution to λ from non-decoupling D-terms possibly present in the CCT model. Top to bottom: $\rho = 2.0, 1.0, 0.5$. (For definition of ρ and other details, see Appendix 3.10.) 78
3.5 Swan contribution to Higgs couplings to gluons and photons, at the one-loop level. 80
3.6 Fractional deviation in the hgg (left panel) and $h\gamma\gamma$ (right panel) couplings from the SM in the CCT model, as a function of the swan mass and $\tan\beta$. (See text for details on the values of other model parameters.) The shaded region is disfavored by precision electroweak constraints and direct LHC searches for a Z'. . . 82
3.7 Swan production cross sections at a 100 TeV pp collider: $pp \to \vec{Q}\vec{Q}$ (blue), $\vec{Q}\widetilde{g}$ (green dashed), $\vec{Q}\widetilde{\chi}_1^0$ (red dashed). 83

5.1 Dark matter yield, as a function of the SM plasma temperature T, for elastically decoupling dark matter with $m_\chi = 10$ MeV, $\epsilon = 8.5 \times 10^{-9}$, and $\alpha = 1$ (**purple**/solid line). For comparison, the dashed curves show the equilibrium yield assuming the DM and SM plasmas are in equilibrium (**blue**/dashed), and assuming the DM plasma is in chemical equilibrium with itself after decoupling (**red**/dashed). Decoupling of the $\chi\chi \to \gamma\gamma$ annihilations occurs roughly at $x \sim 3$. 116
5.2 Regions of parameters corresponding to the observed relic density. For each mass, the vertical section of the line of the left/top corresponds to the elastically decoupling relic (ELDER) scenario proposed in this paper; the horizontal line to the SIMP scenario; and the vertical section on the right/bottom to the WIMP scenario. 119
5.3 Constraints on ϵ vs. m_χ, from dark matter couplings to photons. The blue line corresponds to the ELDER scenario while the region above it corresponds to the SIMP scenario. Also shown are the exclusion limits from: supernova cooling (purple region); CMB constraints on DM annihilations into photons before recombination (blue region); and modification to $N_{\rm eff}^\nu$ from DM decoupling (red region). 121

CHAPTER 1

INTRODUCTION

The body of this thesis is a set of four papers on which I worked during my five years at Cornell University as a Ph.D. student. While these papers all deal with current subjects of interests and unsolved problems in the domain of particle and field theory, they tend to deal with very separate areas in this field of research, with little direct relationship with each other. Chapters 2 and 3 contain two papers which can broadly be said to consider what is called the "naturalness problem" of particle physics; Chapter 4 is a study of non-perturbative effects in three-dimensional field theory, with little immediate phenomenological applications; and Chapter 5 presents a novel scenario for the thermal production of dark matter particles.

This introduction aims to provide an overview of these three topics for non-experts, with a special emphasis on the subjects treated in the following chapters.

1.1 The Hierarchy Problem

The "hierarchy problem" of particle physics refers to the fact that the value of the electroweak scale (or, equivalently, the Higgs mass) seems to be dramatically different from what we should "reasonably" expect it to be. This is also often stated by saying that the weak scale is "fine-tuned" or "unnatural". To establish what is meant exactly by "reasonable", it can be helpful to think about the situation from two different directions: a "bottom-up" and a "top-down" approach.

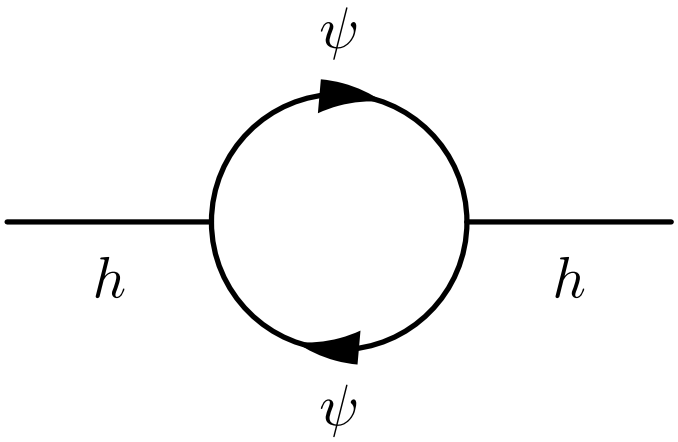

Figure 1.1: Feynman diagram representing the quantum corrections from ψ loops to the mass of the h particle in the toy-model given by Eq. 1.1.

1.1.1 Bottom-Up Explanation

A common way to present the hierarchy problem is to consider this simplified toy model for the Higgs sector of the Standard Model:

$$\mathcal{L} = \frac{1}{2}\partial_\mu h \partial^\mu h - \frac{1}{2}m^2 h^2 + \overline{\psi}\partial\!\!\!/\psi + y h \overline{\psi}\psi \tag{1.1}$$

This theory describes a scalar particle interacting with a fermion. We can use the standard methods of Feynman diagrams to compute observable from this Lagrangian. As is usually the case, however, "loop" diagrams will exhibit divergences when the momentum integration is taken to arbitrarily high energies. This, however, does not affect the predictive power of the theory: renormalization theory allows us to "absorb" these divergences, properly regulated, into the values of the "bare" parameters of the theory. Let's be more explicit about this. The mass of the scalar h receives a correction from the loop shown in Figure 1.1. This correction is divergent; however, if we regularize it by cutting off

the momentum integral at the scale Λ, we get a finite value:

$$\delta m^2 = -\frac{y^2}{8\pi^2}\Lambda^2 + \dots , \tag{1.2}$$

where the omitted terms are sub-leading in Λ. The *observed* mass of the scalar, then, will be the sum of this loop correction and of the tree-level value:

$$m^2_{\text{obs}} = m^2 + \delta m^2 = m^2 - \frac{y^2}{8\pi^2}\Lambda^2 \tag{1.3}$$

In a renormalizable theory, such as this one, we can set the value of the tree-level mass m by demanding that m_{obs} reproduce the observed mass of the scalar: this will introduce a Λ dependance in m, but it can be shown that all *physical* predictions will only depend on m_{obs}, not on m and δm separately, so that the physics in in fact independent of the cut-off Λ. The hierarchy problem will rear its head if we insist on assigning physical meaning to the scale Λ; for example, we might think of Λ as the mass scale of some new, very heavy particles, so that our computations are only valid up that scale, at which our toy-model should be UV-completed. This does not affect our (low-energy) physical predictions at all, since, as stated above, they are Λ independent. However, if we want m_{obs} to be much smaller than Λ, Eq. (1.3) indicates that we should have some very fine cancellation between the two large (but finite) terms m^2 and δm^2. This is not *incoherent*, but it is *uncomfortable*: it would be much more "natural", in a sense, if the three terms m_{obs}, m, and δm were not too far from each other, so that no very precise cancellation were needed. A theory where $\Lambda >> m_{\text{obs}}$ might be said to be "fine-tuned" in that sense, and would suffer from the hierarchy problem. The above discussion can be applied directly to the Standard Model, where the role of the field h is played by the Higgs boson; the fermion ψ is usually taken to be top quark, since it is the fermion whose coupling to the Higgs is largest.

1.1.2 Top-Down Explanation

I would guess that the "bottom-up" approach presented above is the one most commonly used to introduce the hierarchy problem. Unfortunately, it can easily lead to confusion if we start thinking about massless regularization schemes such as dimensional regularization. If we use these regularization schemes then we do not have any explicit cut-off scale playing the role of Λ in the above example, which might lead us to think that the hierarchy problem is just some sort of notational red-herring.

To convince ourselves that this is not the case, it might help to approach the issue from the opposite direction; that is, start with a high energy theory and consider what it might look like at low energy[1]. Consider once again the toy model given in Eq. (1.1), but this time let's give a large mass M to the fermion:

$$\mathcal{L} = \frac{1}{2}\partial_\mu h \partial^\mu h - \frac{1}{2}m^2 h^2 + \overline{\psi}\left(\not{\partial} - M\right)\psi + y h \overline{\psi}\psi \tag{1.4}$$

If we use dimensional regularization, then there is no cut-off scale Λ in this theory, and the issue brought up in the previous section does not appear. There will be a price to pay, however: dimensional regularization becomes problematic when we use it at scales below the masses of some of the particles of theory. Physically, heavy particles should decouple from the dynamics of the theory at low energies: that's why we can afford to ignore contributions from hypothetical as yet undiscovered heavy particles when doing QED loop computations, for example. But this will not happen in dimensional regularization! A naive application of this regularization scheme would show that the heavy fermion ψ, for example, would keep on contributing to the running of the h mass even at scales far below M.

[1] This is a simplified version of the much thorough presentation given in [2]

There is a way to correct for this flaw of dimensional regularization: we have to manually *integrate out* the heavy fermion when we go to scales below M. Formally, this consist of deriving an effective low-energy Lagrangian $\mathcal{L}_{\text{eff}}(h)$ which contain only the field h and which should be valid at energies below the scale M. $\mathcal{L}_{\text{eff}}(h)$ is defined by:

$$\int \mathcal{D}h e^{i\int \mathcal{L}_{\text{eff}}(h)} = \int \mathcal{D}h\mathcal{D}\psi\mathcal{D}\overline{\psi} e^{i\int \mathcal{L}(h,\psi,\overline{\psi})} \,, \tag{1.5}$$

where $\mathcal{L}(h,\psi,\overline{\psi})$ is the full Lagrangian given in Eq. (1.4). In practice, $\mathcal{L}_{\text{eff}}(h)$ is derived by computing low-energy observables with both $\mathcal{L}_{\text{eff}}(h)$ and $\mathcal{L}(h,\psi,\overline{\psi})$ and *matching* the two. This can be done systematically to the n-loop level. If we apply this procedure to the theory specified in Eq. (1.4) we will obtain a mass term $m_{\text{eff}}^2 h^2$ in $\mathcal{L}_{\text{eff}}$ which can be obtained, at the one-loop level, by demanding that it matches the one-loop computations for the two-point function in $\mathcal{L}(h,\psi,\overline{\psi})$. The point is that, even in dimensional regularization, the diagram in Figure 1.1 has a *finite* part which is proportional to the mass of the fermion running in the loop. The matching procedure tells us that this contribution should be added to the m_{eff}^2 term in the low-energy Lagrangian, giving us:

$$m_{\text{eff}}^2 \sim m^2 + \frac{c}{(4\pi)^2} M^2 \,, \tag{1.6}$$

where c is an $O(1)$ number. The hierarchy problem strikes again! Eq. (1.6) leads us to expect that, if this theory contains a heavy fermion, it should try to "drag" the mass of the scalar h to a scale $\sim M$; that is, it tries to raise the scalar mass to its own level by radiative corrections. The only way to have a light scalar in this theory is to choose the tree-level UV mass term, m^2, to precisely cancel out the radiative correction in Eq. (1.6): then m_{eff}^2 can be light. But once again, this involve an uncomfortable of fine-tuning which we would not reasonably expect to see.

There is a way to avoid the hierarchy problem as discussed in this section: don't have heavy degrees of freedom in your theory! Then there be no large scale M^2 trying to make the scalar h heavy. Unfortunately, this "solution" cannot help the Standard Model, as we have very good reasons to believe that there really should be heavier scales present in nature. For one thing, quantum gravitational effects should become important around the Planck scale, $M_P \approx 10^{19}$ GeV, so that some sort of new dynamics at that scale seems unavoidable.

1.1.3 Proposed Solutions to the Hierarchy Problem

There are, roughly speaking, two distinct ways of solving the hierarchy problem. The first solution consists of "simply" choosing the scale Λ of Section 1.1.1 (or equivalently, the scale M of Section 1.1.2) to be close enough to the electroweak scale that the tuning required between m^2 and δm^2 to obtain the physical Higgs mass is not too large. Above the scale Λ, we should have new dynamics which come in to prevent further corrections to the Higgs mass from higher scales. This could be because these dynamics enhance the symmetries of the model, forbidding corrections to the Higgs mass; or it could be because, at that scale, the Higgs is revealed to be a bound state of some more fundamental constituents. Either way, this solution requires new, observable phenomena to take place at a scale not too far above the mass of the Higgs.

The second solution calls upon the *anthropic principle*: we begin with the idea that our universe is only one out of vast "landscape" of universes, each of which contains different dynamics. For example, if there is a more fundamental UV theory with many different meta-stable vacua, each of these could constitute a possible universe. The hierarchy problem implies that in a generic theory it

is very unlikely for the Higgs mass to be at its observed value, but if we have enough universes in the landscape, some of them will, probabilistically, have a light mass for the Higgs. The anthropic principle comes in with the realization that life as we know it would be impossible if the Higgs was much more massive than it is [3]. Therefore, life will only form in one of those comparatively few universes where the Higgs is light: in most universes, the Higgs has a much more "reasonable" mass, but no physicists can exist in those universes. The anthropic principle is sometimes pithily stated as "things are the way they are because if they weren't, we wouldn't be around to wonder why they are the way they are".

1.1.4 The Topic of Chapter 2: Higgs Couplings and Naturalness

As has been pointed out above, a common feature of solutions to the hierarchy problem (with the exception of the anthropic principle) is the appearance of new physics not too far away from the electroweak scale. Given a specific example of such physics, we can then try to directly detect the new particles at a collider experiment. This approach, while entirely valid, is also very model-dependent. In Chapter 2, we present an approach which tries to detect the effects of naturalness-restoring physics in a much more model-independent way. The main idea is as follows: since the main contributors of radiative corrections to the Higgs mass are the top quarks, models which attempt to restore naturalness typically contain *top partners*: particles which provide radiative contributions that cancel that of the top quarks. The key point here is that these partners should not only provide radiative corrections to the Higgs mass but also to the loop-induced couplings of the Higgs to gauge fields. These are vanishing at

tree-level, which means that contributions from higher mass scales are more likely to be significant enough to be detected. The more closely these couplings are seen to adhere to the Standard Model predictions, the more massive the top partners must be, which imply a higher degree of tuning for the theory. The paper presented in Chapter 2 quantitatively demonstrate this point and discusses the degree to which it is independent of the particular model chosen for the top partners.

1.1.5 Supersymmetric Models

A specific choice of new dynamics to restore naturalness to the Standard Model consist of *supersymmetry*, or SUSY[2]. The idea of supersymmetry is to enhance the Poincarré spacetime symmetry of the Standard Model with an additional set of "anti-commuting" generators. It can be shown that this is the only possible way to enlarge the group of spacetime symmetries of a quantum field theory without making it trivial, a result known as the Coleman-Mandula theorem [5]. Because a supersymmetric transformation exchanges fermionic and bosonic degrees of freedom supersymmetry forces the fields of the theory to arrange themselves in "supermultiplets", irreducible representation of the symmetry group which include both fermions and bosons. This has dramatic consequences on naturalness considerations: the masses of fermions are generically protected by chiral symmetries, which means that they can only be *multiplicatively* renormalized. In other words, radiative corrections to these masses vanish if their tree-level values go to zero. Because supersymmetry demands that the fermions and bosons within a supermultiplet have the same mass, it extends this protection to the

[2]See [4] for an excellent introduction.

bosonic degrees of freedom of the theory. This is a result of a more general feature of supersymmetry known as the *non-renormalization theorem*.

If we extend the Standard Model with the degrees of freedom required to make it supersymmetric, then the radiative corrections to the Higgs mass will vanish and naturalness will be restored. Of course, supersymmetry is *not* observed in nature, at least not at the scale at which we have been able to make observations so far! This implies that, if it exists, supersymmetry must be broken in some way. To effectively be a solution to the naturalness problem, this breaking must not happen at a too high scale, otherwise radiative corrections between the breaking scale and the electroweak scale would once again require us to fine-tune the Higgs mass.

1.1.6 The Topic of Chapter 3: Swan Models

The phenomenology of SUSY theories is a rich and extended subject. The most common implementation of supersymmetry is the Minimal Supersymmetric Standard Model (MSSM). In this model, the Standard Model fermions are made to be a part of a supermultiplet which also contains scalar fields, the *squarks*. These *superpartners* also make radiative contributions to the Higgs mass, similar to Figure 1.1, but with the opposite sign, which cancels the quadratic divergences.

In Chapter 3 we present a study of a different kind supersymmetric model, which we dub the *Swan model*[3] [6]. Unlike the MSSM, in Swan models the top

[3] "Swan" is a contraction of "spin-one", which is itself a shorter way of referring to "spin-one top partners". Let History always remember that it was the genius of John Stout who gave us this name; my co-authors and myself merely adopted it.

quark is made to be part of a multiplet that contains the gauge field of an enlarged gauge symmetry. The super partners will then not be scalar fields, but rather the spin-one force carriers for these gauge symmetries. The phenomenology of these models will differ in many ways from that of the MSSM: Chapter 3 studies the constraints and possible signatures of these models at both current and future colliders.

1.2 Dualities in 3D Field Theories

Quantum Chromodynamics (QCD), the theory of the strong interactions of the quarks and gluons which make up the nuclei, is described by an SU(3) gauge theory which has the following Lagrangian:

$$\mathcal{L}_{\text{QCD}} = \overline{\psi}_i(i\not{D}^i_j - m)\psi^j - \frac{1}{4}G^a_{\mu\nu}G^{\mu\nu}_a \,, \tag{1.7}$$

where $G^a_{\mu\nu} = \partial_\mu A^a_\nu - \partial_\nu A^a_\mu + g f^{abc} A^b_\mu A^c_\nu$. The ψ fields are the quark fields, which transform in the fundamental representation of SU(3), and the gauge fields A^a_{mu}, $a = 1, ..., 8$ are the gluons. If one assumes that the gauge coupling g is small, then perturbative computations can be performed as usual using Feynman diagrams. However, the influence of radiative corrections will cause this gauge coupling to *run*, i.e. to effectively take on different values at different scales. At high energies, g runs to zero, which means the interactions in the theory become less and less important: the theory is said to be *asymptotically free*. The flip side of this fact is that, as we go to lower energies, g becomes larger and larger until perturbation theory breaks down and we lose our perturbative handle on the theory.

What happens then? The consensus is that, at lower energies, the theory *con-*

fines: quarks and gluons become tightly bound together by non-perturbative effects which prevent them from ever being observed as free particles. Instead, we observe a wide spectrum of bound states, the hadrons. Because this phenomenon involves strong, non-perturbative dynamics, Feynman diagrams are quite useless when it comes to analyzing QCD at low energy. What are the alternatives? One possibility is to discretize the Lagrangian given in Eq. (1.7) and perform the path integral numerically [7]; another approach, commonly employed for collider physics, is to treat the hadrons as "bags" containing quarks and gluons (which, in this context, are called *partons*). At high energies, the partons are effectively free, so we can treat the collisions of hadrons as collisions between the partons that they contain [8]. It is also possible to try to approach the problem by trying to solve the equations for bound states in quantum field theories, called the Bethe-Salpeter equations [9]. Finally, one can try to apply the idea of *dualities*.

1.2.1 A Duality for QCD

A duality refers to the fact that a particular theory can be expressed in more than one way without changing its physical content. Because certain descriptions are more convenient to use than others in certain contexts, a duality can allow us to effectively study a theory using whichever description works better. In the context of QCD, the duality which allows us to effectively treat the low-energy regime of the theory is called *chiral perturbation theory*: its only assumption is that QCD possesses an approximate continuous symmetry, the chiral symmetry of the quarks, which is spontaneously broken by the non-perturbative effects. The low energy dynamics of the theory should then consist of fluctuations within

the space of possible symmetry-breaking vacua (this space is called the *moduli space* of the theory). These fluctuations are called Nambu-Goldstone bosons (in this context these are often called *pseudo* Nambu-Goldstone bosons, because the chiral symmetry is only approximate). The theory of these pseudo Nambu-Goldstone bosons has the exact opposite behaviour of QCD with respect to energy: it is weakly coupled at low energies, but becomes non-perturbative at higher momentum scales. This means that it can only reliably be used at low-energies[4], and that it does not tell us the full story. Indeed, we know that the spectrum of QCD bound states goes far beyond the pions and also include a whole menagerie of particles and resonances, such as protons, neutrons, rho mesons, etc. In addition, the whole approach relies on an *assumption*: that chiral symmetry is spontaneously broken by QCD. Certainly, both theoretically and experimentally, there are many reasons to believe that this assumption really is realized in nature, so that in practice this isn't a serious challenge to the use of this particular duality. But it will be important to keep these last two points in mind as we discuss dualities further: they are often only valid (or useful) within a limited regime, and they often rely on assumptions on which the strongest statement that we can make is that they have passed all the tests to which we have subjected them.

1.2.2 Seiberg Dualities and S-Confinement

The main tool used to establish chiral perturbation theory as a duality of QCD was its symmetries. We should then not be surprised that theories with larger

[4] "Low energies" here means that we can only reliably compute observables which are small compared to the *QCD scale*, Λ_{QCD}. Λ_{QCD} is actually not a perfectly well defined quantity, but in practice can be taken to be $O(1)$ GeV.

	$SU(N_c)$	$SU(N_F)$	$SU(N_F)$	$U(1)_B$	$U(1)_R$
Q	$\square$	$\square$	1	1	$\frac{1}{N_F}$
$\overline{Q}$	$\overline{\square}$	1	$\overline{\square}$	-1	$\frac{1}{N_F}$

Table 1.1: Matter and symmetry content of SQCD with $N_F = N_c + 1$flavours.

sets of symmetries are even more likely to be approachable using dual representations. Such is the case of the supersymmetric version of QCD, *SQCD* [10]. As discussed in Section 1.1.5, supersymmetry requires that the field content of QCD be augmented by adding a coloured scalar for each coloured fermions; these are the *squarks*. We must also add fermionic superpartners for the gauge fields, called *gauginos*. Typically, we also get rid of the mass terms by imposing a flavour symmetry on the matter superfields (although these can be added back in later as a small deformation of the theory, just like in chiral perturbation theory). If we allow the gauge group to be a generic SU(N_c) rather than the usual SU(3) of QCD, and allow for an arbitrary number N_f of quarks-antiquarks pairs, then the matter content of the theory can be represented as in Table 1.1.

Seiberg [11, 12] made the celebrated proposition that, for $N_F > N_c - 1$, there is a series of dualities that can be used to describe SQCD at low energies. While these are, in a sense, "morally" similar to the case chiral perturbation theory in QCD, they present many novel features which go beyond our purposes here; we will content ourselves with presenting the $N_F = N_c + 1$ case, which exhibits the phenomenon of *S-confinement*. Seiberg's proposal is that SQCD with $N_F = N_c + 1$ is dual, at low energies, to a supersymmetric theory of N_F "baryons" B_i, $i = 1, ..., N_F$, N_F "anti-baryons" $\overline{B}_i$, $i = 1, ..., N_F$, and N_F^2 "mesons" which are usually assembled into an $N_F \times N_F$ matrix M. This matter content is summarized

	$SU(N_c)$	$SU(N_F)$	$SU(N_F)$	$U(1)_B$	$U(1)_R$
M	1	$\square$	$\overline{\square}$	0	$\frac{2}{N_F}$
B	1	$\square$	1	$N_F - 1$	$\frac{N_F - 1}{N_F}$
$\overline{B}$	1	1	$\overline{\square}$	$1 - N_F$	$\frac{N_F - 1}{N_F}$

Table 1.2: Matter and symmetry content of the dual of SQCD with $N_F = N_c + 1$ flavours.

in Table 1.2.

The dual theory also possess a superpotential W which describe the interactions of its fields:

$$W = B_i M^i_j \overline{B}^j - \mathrm{Det}(M) \tag{1.8}$$

This duality might be taken as the supersymmetric equivalent of the duality described in the previous section. Indeed, just like chiral perturbation theory, it gives us a theory of chargeless fields which we expect should correspond to the lowest energy bound states of the confining SQCD theory. There is a new feature here however: unlike chiral perturbation theory, this duality does not require that the chiral symmetry of SQCD be broken. If we look at the superpotential in Eq. (1.8), we can easily see that the point where all the fields are equal to zero, where there is no spontaneous symmetry breaking, is part of the moduli space of the theory. This indicates that in SQCD with $N_F = N_c + 1$, unlike "our" QCD, the strong dynamics of the theory do *not* break the chiral symmetry[5]. Theories such as these, which exhibit confinement without spontaneous breaking of the chiral symmetry, are called *s-confining* [13].

[5]Note, however, that for $N_F = N_c$, SQCD *does* exhibit chiral symmetry breaking; see e.g. [10].

1.2.3 Test of the Duality: Anomaly Matching

The reader may well wonder at this point why exactly we should trust Seiberg's proposal of s-confinement for SQCD with $N_F = N_c + 1$. After all, it's not as if we have an experimental realization of this theory to convince us that this assumption is reasonable, like we do for chiral perturbation theory. One could try to use lattice methods to try to verify the duality, but such means were not available to Seiberg in the mid-nineties; so why did he feel so confident that his conjectured duality was reasonable? The answer is that, while we may not be able to rigorously prove the duality described above, we can expose it to a series of very constraining consistency tests. Anyone is free to conjecture a duality for SQCD, but if this duality can not satisfy of all of these tests then it is dead on arrival. Part of the reason for the appeal of Seiberg's conjecture is that it has survived all of the tests that anyone has ever been able to think to subject it to. The most celebrated and insightful of these is probably *t'Hooft anomaly matching*. The idea is as follow: we imagine taking one of the global continuous symmetry of our theory, and "weakly gauging" it, i.e. gauging it with a very, very small gauge coupling. The key observation is that the **anomaly coefficients**[6] of this new gauge interaction must be the same on both side of the theory. We might convince ourselves this by adding some light fermions to the theory which only interact with the weakly gauged sector and which have exactly the right charge to cancel the anomalies. Then the weakly gauged group is non-anomalous and is a perfectly legitimate deformation of the theory, and the duality can only be valid is this statement is true for both representation of the theory, which implies the equality of their anomaly coefficients. Because dual theories generically have very different fields content, it is a highly non-trivial result for their anomaly

[6] See e.g. [14, 5] for a discussion of anomalies in quantum field theories

coefficients to match: the fact that Seiberg's duality (all of them!) satisfy this constraint is a very strong argument in favour of their validity.

1.2.4 Gauge Theories in Three Dimensions

Let us now leave aside QCD and its supersymmetric cousins and consider field theories which live in three dimensions (that is, two spatial and one time dimension). To motivate the study of this subject (beyond pure curiosity in quantum field theory in itself), consider a $U(1)$ gauge theory in three dimensions, i.e. a three-dimensional analog of quantum electrodynamics. The question we would like to answer is, what would be the potential energy of two static heavy charges (which we can represent as external sources) which are placed some distance R apart? In four dimensions, classical field theory tells us that the answer is given by the well known Coulomb potential, $V(R) \sim -\frac{e_1 e_2}{R}$. This conclusion has to be modified somewhat to account for quantum corrections: if the theory possesses some light fields charged under the $U(1)$ gauge group, quantum fluctuations of these fields will help "shield" the two charges from each other at large distances, so that the potential becomes $V(R) \sim -\frac{e_1 e_2}{R \log R}$. In three dimensions, things are dramatically different already at the classical level: according to classical field theory, a single charge emits a potential of the form $V(R) \sim \log R$: the energy of the two charges diverges logarithmically as we take them farther and farther apart. Strong dynamics, then, are not optional for three-dimensional gauge theory: they are a built-in feature.[7] Whatever the spec-

[7] Another way to see this is to consider the dimension of the gauge coupling in three dimensions. Since the three dimensional gauge field A_μ has canonical dimension $1/2$, and it couples to matter by replacing all ordinary derivative ∂_μ by covariant derivatives $D_\mu = \partial_\mu - g_3 A_\mu$, the gauge coupling g_3 must have dimension $1/2$ too. A positive mass dimension for a coupling indicates that it is *relevant*, that is, that it becomes important at low energies (or, equivalently, at large

trum of theory ends up being, we can feel confident that it will not include any particles which can be straightforwardly associated with the matter fields. This example shows that we should expect three-dimensional gauge theories to be fertile ground for all kinds of non-perturbative phenomena. Beyond the the intrinsic interests of such phenomena, one might hope that, by studying strongly coupled three-dimensional theories, we could gain valuable insight into more directly phenomenologically interesting cases, such as QCD. This program has had tantalizing successes in the past: Polyakov [15] has shown that, for three-dimensional QED, the "logarithmic confinement" discussed above is modified into a full blown, genuine "linear confinement" due the effect of *instantons* (also variously referred to as *pseudo-particles* and *monopoles* in the literature) on the path integral. That is, when the effect of the instantons is accounted for, the energy between two charged particles becomes $V(R) \sim TR$, with T some constant: the energy grows *linearly* with the distance, due to the formation of a string of field lines between the charges. This is exactly the kind of confinement which we expect to see in four dimensional QCD! Unfortunately, this result does not generalize to four dimensions. More recently, [16] studied gaugino condensation in supersymmetric theories that live in one time dimension, two space dimensions, and one "rolled up" periodic space dimension.[8] They have shown that, if the periodic space dimension is small enough, the gaugino condensate can be shown to arise from weakly-coupled effects due to instantons. The periodic space dimension can then be enlarged so that the theory becomes undistinguishable from a four-dimensional field theory: by following this program, the four-dimensional gaugino condensate for a variety of four-dimensional gauge theories can be extracted from weakly-coupled computations on the cylinder.

distances).

[8] Mathematically, such a space can be written $\mathcal{R}^{(2,1)} \times S^1$; in the literature, one often speaks of this kind of space by saying that we are considering the theory "on the cylinder".

1.2.5 An Example: SQED

Let us now consider gauge theories living in three dimensions and possessing a $\mathcal{N} = 2$ supersymmetry[9]. What does the classical low-energy behaviour of such a theory look like? On the one hand, the scalar components of the quark superfields can acquire VEVs, spontaneously breaking the gauge symmetry and leaving only some weakly-interacting singlets in the low-energy spectrum of the theory. The part of the moduli space where the squarks acquire VEVs is called the *Higgs branch* of the theory because of its similarity to the spontaneous symmetry breaking of Standard Model due to the Higgs field. This sort of behaviour is also common in four dimensions, where the squarks fields can acquire VEVs just as well as in three dimensions. However, in three dimensions, there is a new feature which is not present in four dimensions. This is due to the presence of an extra scalar field in the gauge supermultiplet of $\mathcal{N} = 2$ three-dimensional theories: this field, usually referred to as σ, can also acquire VEVs: when it does so, it gives masses to the quark superfields and spontaneously break the gauge theory down to its $U(1)$ subgroups. The low-energy spectrum of the theory then consists of a set of $U(1)$ gauge supermultiplets with no matter fields. Because only $U(1)$ gauge groups are left in the theory at low energies, this part of the moduli space is called the *Coulomb branch*. If we are "far along" either the Higgs branch or the Coulomb branch (by which we mean that the VEVs involved are large compared to the strong coupling scale), then the classical description given above should be accurate. What happens, however, if we take the VEVs to be comparable, or smaller than, the strong coupling scale? Weak-coupling computations cannot help us here, but dualities might. Let's consider an explicit

[9] In three dimensions, $\mathcal{N} = 2$ supersymmetry corresponds to four real supercharges; in that sense, it possesses the same amount of supersymmetry as a $\mathcal{N} = 1$ theory in *four* dimensions.

example: $\mathcal{N} = 2$ SQED with one quark and one antiquark[10]. The potential for the squarks Q and $\overline{Q}$ and real scalar σ is

$$V = e^2\sigma^2\left(|Q|^2 + |\overline{Q}|^2\right) + e^2\left(|Q|^2 - |\overline{Q}|^2\right)^2 \tag{1.9}$$

This can be minimized for

$$\begin{aligned} \sigma &= 0, \\ Q &= ve^{i\phi}, \\ \overline{Q} &= v\ . \end{aligned} \tag{1.10}$$

This corresponds to the Higgs branch of this theory[11]. We can parameterize this region of the moduli space in a gauge-invariant way in terms of the VEV of the gauge single composite field $M \equiv \widetilde{QQ}$.[12] In addition to Eq. (1.10), we can minimize the potential with the field configuration:

$$\begin{aligned} \sigma &= \text{anything}, \\ Q &= 0, \\ \overline{Q} &= 0\ . \end{aligned} \tag{1.11}$$

This which correspond to the Coulomb branch. Actually, the parameterization of this branch is a little more intricate than simply specifying the VEV of σ: in three dimensions, we can re-write the gauge supermultiplet in such a way that we exchange the vector field, A_μ, in favor of a real scalar field, γ, defined by the relationship $\epsilon_{\mu\nu\rho}F^{\mu\nu} = \partial_\rho\gamma$.[13] The point here is that γ can also acquire a VEV on

[10] My favourite presentation of this example is in [17]

[11] In Eq. (1.10), I've used the gauge symmetry of the theory to rotate away the phase of the $\overline{Q}$ field. Since gauge symmetries are *really* symmetries of our theories, but rather a redundancy of our notation, all the vacua which are related to each other by such gauge transformations are really physically equivalent.

[12] It is a general result that the field values which minimize the D-term potential of supersymmetric theory can be parameterized using only such gauge-invariant operators, along with some possible constraints amongst these operators.

[13] One aspect of this duality may at first be troubling: A_μ has three components, while γ only has one. How can this duality be true if it does not preserve the number of degrees of freedom?

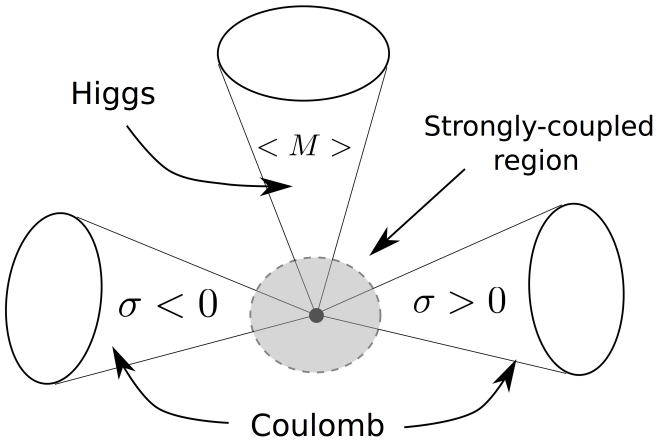

Figure 1.2: Pictorial representation of the moduli space of $\mathcal{N} = 2$, three-dimensional SQED with one flavour. The shaded region cannot be studied using weakly-coupled methods.

the Coulomb branch, so we should include it in our parameterization of this region of moduli space. Putting everything together, and with the benefit of some foresight, we might draw a pictorial representation of this moduli space which looks like Figure 1.2.

The moduli space as drawn in this figure is made up of three "prongs": one prong corresponds to the Higgs branch ($\langle M \rangle \neq 0$), one prong correspond to the part of the Coulomb branch where $\langle \sigma \rangle > 0$, and one prong corresponds to the part of the Coulomb branch where $\langle \sigma \rangle < 0$. All three prongs meet at the point where $\langle M \rangle = \langle \sigma \rangle = 0$: at that point, and in the surrounding region, the VEVs are smaller than the strong coupling scale of the theory, so that our classical analysis becomes unreliable. [14]

The answer is that while the field A_μ may have three components, it only has one *physical* degree of freedom: we can use the equations of motion, along with gauge invariance, to remove two dynamical degrees of freedom, leaving only a single one.

[14]This can also be stated by deriving the Kahler metric controlling the interactions of the moduli fields. Far away from the center of the moduli space, these are nice, smooth functions, which agree with the classical analysis. But as we approach the center, this metric becomes

Can we think of a theory who might be dual to this version of SQED, but which might be easier to study near the center of the moduli space? Clever minds have proposed that the so-called "XYZ theory" might just be such a dual theory. This theory is easily stated: it consists of three chiral supermultiplets, X, Y and Z, with a superpotential

$$W = hXYZ\,, \tag{1.12}$$

where h is some coupling constant. As a first test if this proposed duality, we can derive the moduli space of the XYZ theory and verify that it matches that of three-dimensional SQED. This is easily done: the vacua of the XYZ theory consists of field configurations where at most one of the three fields acquire a VEV. But this is exactly the kind of "three-pronged" moduli space that we drew for SQED! So it is, at least, not completely unreasonable to hope that by studying the dynamics XYZ theory at low energy, we will, through this duality, learn about the dynamics of three-dimensional SQED. But hang on a second! Something fishy is going on here. XYZ theory is a model with three chiral superfields, each acting as a coordinate on one of the prongs of the moduli space. But three-dimensional SQED seems to only possess *two* fields that acts as coordinates on its moduli space: M and the holomorphic combination of σ and γ. In Figure 1.2, we used a bit of a sleight of hand to draw attention away from this fact by separating the $\sigma > 0$ and $\sigma < 0$ regions. But surely, these are both parameterized by the same field? Part of the answer here is that, while the above may be true *classically*, we have no right to expect it to still hold when strongly-coupled quantum dynamics come in play. After all, to cross from the $\sigma > 0$ region to the $\sigma < 0$ region, we must travel through the troubled sea of the small VEVs region, where there be quantum dragons. We can state this another way: consider the

singular, indicating the unreliability of this approach.

chiral supermultiplet Σ whose scalar component is $\sigma + i\gamma$, and then consider the functions e^{Σ} and $e^{-\Sigma}$. Classically, we can think of these two functions as obeying the "classical constraint" $e^{\Sigma}e^{-\Sigma} = 1$. The point is that, while this may seem like a trivial statement, it may no longer be true in the quantum theory: if XYZ theory is indeed dual to SQED, then the quantum version of this constraint becomes $e^{\Sigma}e^{-\Sigma} = 0$. We should then think of e^{Σ} and $e^{-\Sigma}$ as two distinct objects. If we (arbitrarily) decide that the X field is dual to the M field of three-dimensional SQED, then e^{Σ} and $e^{-\Sigma}$ should be dual to the Y and Z fields.[15] But then, how do these e^{Σ} and $e^{-\Sigma}$ manifest themselves in SQED? This is maybe the most interesting part of the story. We can show that, on the part of the moduli space where the matter fields acquire VEVs, there are solutions to the classical equations of motions of SQED where the phase of the Q and $\overline{Q}$ fields change by integer multiples of 2π as we go around the "circle at spatial infinity". These *solitons*[16] have finite energy, and they should be interpreted as massive excitations of the quantum field theory-that is, as particles. It turns out that it is these solitons which should be associated with the Y and Z fields of the XYZ theory![17] In the full quantum theory then, the Coulomb branch consists of the phase of this theory where these vortices condense, i.e. acquire a VEV. We are almost at the end of our (long) story. We have seen that, on all three prongs of the moduli space, the low-energy dynamics of theory correspond to weakly interacting massless singlet fields.[18]

[15] This is skipping ahead a little bit: at this point, we have no reason to think that it should be these functions of Σ that should be dual to Y and Z. Why not $e^{2\Sigma}$, or $1/\Sigma$? But as we will see, we do indeed have a good reason to think that it really are e^{Σ} and $e^{-\Sigma}$ which are dual to Y and Z.

[16] Because the gauge field also winds around at infinity for these field configurations, they are commonly referred to as *vortices*.

[17] There are many arguments for this, but one of the most instructive is that the vortices (resp. anti-vortices) are charged under a global topological charge which correspond to the winding of the gauge field at infinity. This is dual to the global symmetry of the XYZ theory under which Y has charge 1, Z has charge -1, and X (the meson) is uncharged. In SQED, this global symmetry acts on γ, the scalar dual of the gauge field, through $\gamma \to \gamma + c$. So the operators e^{Σ} and $e^{-\Sigma}$ transform as $e^{\Sigma} \to e^{\Sigma}e^{ic}$ and $e^{-\Sigma} \to e^{-\Sigma}e^{-ic}$: that is, they have charge 1 and -1 respectively, just like the operators Y and Z in the XYZ theory.

[18] We still have a $U(1)$ gauge group on the Coulomb branch, but there are no charged fields

What happens at the very center of the moduli space? Do we also have a theory of weakly coupled singlets at low energies? It seems very difficult to answer that question for SQED, but fortunately it is much more tractable in the dual XYZ model. There are various reason to believe that at the origin of the moduli space, the XYZ theory flows to a strongly coupled interacting, and scale invariant theory at low energies. With a slight abuse of language, theories such as these are often called *Conformal Field Theories*, or CFTs. Unlike most of the field field theories that phenomenologists may be used to dealing with, CFTs have no interpretations of terms of particles and S-matrix elements; instead, they have a "spectrum" of operators with well specified scaling dimensions and correlation functions. We've come a long way from our classical description of SQED in terms of charged particles with logarithmic Coulomb potential!

The Lessons of SQED

What have we learned from our rather detailed look at SQED? First, that gauge theories in three dimensions have, at the classical level, moduli spaces which tend to break in different Higgs branches and Coulomb branches. The points where these different branches join each others cannot be treated by weak-coupling methods, and we should expect non-perturbative dynamics to play an important role. Near these singular points, there might be dual descriptions of the theory which allows us to more conveniently describe the dynamics, and which may involve degrees of freedoms, like vortices, which do not appear as fields in the original Lagrangian. With this in mind, we now move on to the more intricate case of non-abelian gauge theories in three-dimensions.

remaining in the low-energy spectrum.

Another Example: SQCD

Let's now consider a three-dimensional $SU(N)$ gauge theory with N_F fields that transform under the fundamental representation and N_F other fields which transform under the anti-fundamental representation. This theory has a $\mathcal{N} = 2$ supersymmetry: it is the three-dimensional version of the SQCD we were considering in Section 1.2.2. What does the classical moduli space of this theory look like? Just as for SQED, it possess a Higgs branch where the squarks acquire VEVs. It also possesses a Coulomb branch where scalar fields acquire VEVs which spontaneously break the gauge group down to its $U(1)$ subgroups; and just like in SQED, we expect that at the points where the Higgs branch and the Coulomb branches meet, the strong-coupling effects become important and the classical description becomes inadequate. For non-abelian groups, however, the moduli space is made somewhat more complicated by the fact that the gauge multiplet contains many different σ fields which can acquire VEVs. Whenever any single of those VEVs vanish, some of the matter fields become (classically) massless, and we can attach a Higgs branch to this point. The result looks schematically like Figure 1.3.

How will this picture be modified by non-perturbative effects? There is a new feature here that arises from the self-interactions of the gauge field which was not present in SQED: it consists of the presence of *instantons*, saddle-points of the Euclidian path integrals. Suppose for a moment that the theory had no matter fields (i.e. that $N_F = 0$); then we can go far along the moduli space and evaluate the instantons semi-classically to show that they will generate effective superpotential terms on the Coulomb branch. If we use the symbols Y_i to indicate the vortices operators which parameterize these branches of the moduli space,

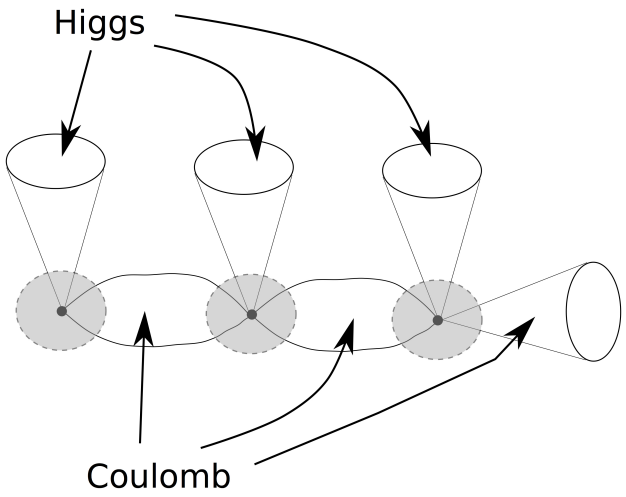

Figure 1.3: Pictorial representation of the *classical* moduli space of $\mathcal{N} = 2$, three-dimensional SQCD with N_F flavours. All of the shaded regions involve strongly-coupled dynamics and cannot be analyzed using perturbative methods.

then the potential generated by the instantons takes the form $\sum_i \frac{1}{Y_i}$[19] This would indicate that the VEVs of the Y_i fields should be dynamically "pushed away" to infinity, so that the theory does not in fact possess a stable supersymmetric vacuum. But if we not put the matter fields back in the theory, we can avoid this conclusion: the fermionic quarks can couple to certain instantons and cancel their contribution to the superpotential! This allows us to save one part of the Coulomb branch from destruction: the one in which the gauge group is spontaneously broken in a $SU(N) \to SU(N-2) \times U(1)^2$ pattern. The vortex coordinate used to parameterize this unlifted branch is called Y (with no subscript). This

[19] In the literature these instantons are commonly called "monopoles", and the Y_i are called "monopole operators" because of the origin of the superpotential term. In my opinion, this is a highly misleading notation: "monopoles" is a name given to *particles* in four dimensional theories, whereas the instantons we are talking about are "just" mathematical saddle-points in the path integral. The Y_i, meanwhile, should be associated with *vortices* configurations, not monopoles. Throwing all of these objects under the umbrella of "monopoles" emphasizes the mathematical resemblance between them but obscures the very real physical differences.

semi-classical analysis has taken us quite far, but that seems to be the end of the road for it. It tells us that the low-energy degrees of freedom of SQCD should, at the most, consist of the gauge-singlets if the Higgs branch (the mesons and baryons, M and B, $\overline{B}$) and the vortex Y. But the strong interactions have yet to have their say, and who knows what their effects might be? Maybe some of these degrees of freedom acquire masses at low energies? Maybe they interact only very weakly, or maybe the low energy theory is an interacting CFT? The full, quantum version of the moduli space could contain different regions where these different results apply. The key to this question, as was the case for SQED, will be to use the power of dualities.

1.2.6 From Four Dimensions to Three Dimensions: Dimensional Reduction

In a recent paper [18], it was proposed that we could use the four-dimensional Seiberg dualities to extract "descendant" dualities in three-dimensional theories. The idea goes as follow: we start with some duality between two theories (call them A and B) in four dimensions. We then imagine "putting the theories on the cylinder"; that is, we compactify one of the space dimensions, so that it is now a periodic circle. While at high energies this should not change either of our theories, we now expect that their low energy behaviour should be dramatically altered. Indeed, low energies imply large distance scales: so no matter how "large" our compact dimension is, at low enough energies it will be small compared to the wavelengths of the field excitations, and so the theories will effectively look like three-dimensional theories. This procedure is called *dimen-*

sional reduction.[20] Let us called the dimensionally reduced theories A' and B'. The assumption is that, just as A and B were dual to each other at low energies, A' and B' will similarly be dual in that same regime. Since, at low-energies, A' and B' look like three-dimensional theories, this process has given a new duality for three-dimensional field theories. But not so fast! There is a twist in the story. It turns out that there remains some effect of the compactified dimension even at low-energies. This is because we can construct instantons where the gauge field winds around the compactified dimension; these are commonly called *KK monopoles*[21] At low energies the compactified dimension is "removed" from the theory, but the effect of these KK monopoles remains and is equivalent to the generation of a term of the form ηY in the superpotential. Since this ηY term is, in a sense, an artefact of the four-dimensional origin of the theories A' and B', we would like to remove it so that we can consider theories which are purely three-dimensional. To do this, we can employ a trick: we give a real mass term to one of the flavours in our theories. This can be done by imagining that we are weakly gauging one of the flavour symmetries and giving a VEV to the scalar component of this new gauge multiplet. It has been argued that the, at energy scales below this mass deformation, the ηY will be decoupled and vanish as desired. The price we have to pay for this is that our duality is no longer between the theory A' and B', but between deformations of these theories which are obtained by decoupling a flavour in this way. We can summarize all of the above like so: **Consider two theories, A and B, which live in four dimensions. Obtain the theories the three-dimensional theories A'' and B'' from these by compactifying a dimension and decoupling a flavour; then if A and B are dual**

[20] Dimensional reduction is ubiquitous in string theory, where it is used to extract the low-energy four dimensional behaviour of "parent" string theories which live in much higher dimensional space.

[21] "KK" stands for "Kaluza-Klein"; Theodor Kaluza and Oscar Klein were pioneers of the methods of dimensional deconstruction, hence the name.

to each other at low energies, so will A'' and B''. This is illustrated in Figure 1.4.

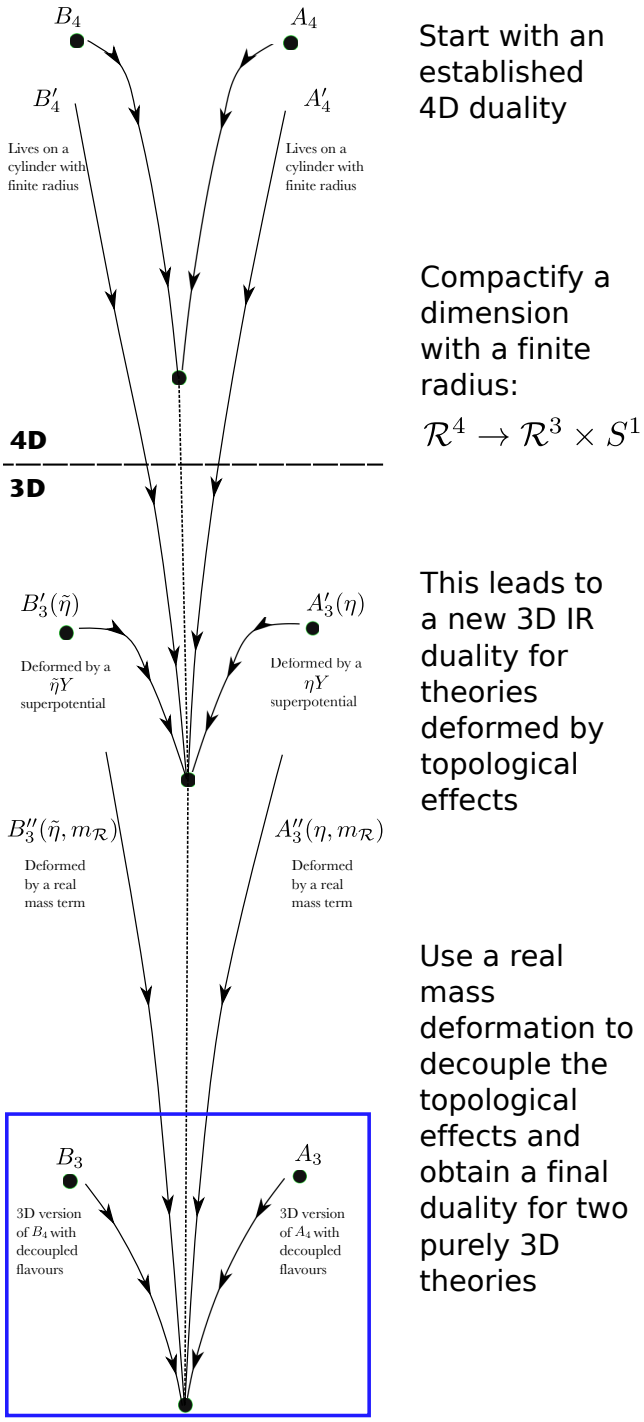

Figure 1.4: Representation of the RG flow of various theories during the process of dimensional reduction.

As an illustrative example, let's apply this program to the Seiberg duality of four-dimensional SQCD with $N_F = N_c + 1$. We have seen in Section 1.2.2 that this theory is s-confining: at low energy it is described by the superpotential $W = B_i M^i_j \overline{B}^j - \mathrm{Det}(M)$. If we dimensonally reduce SQCD and decouple a flavour, then what we have is three-dimensional SQCD with $N_F = N_c$. On the other side of the duality, we need to remove all of the singlets which are charged under the symmetry $Q_{N_f+1} \to Q_{N_F+1} e^{i\phi}$, $\overline{Q}^{N_F+1} \to \overline{Q}^{N_F+1} e^{-i\phi}$. The fields that remain are M^a_b for $a, b < N_F + 1$, the two baryons B_{N_F+1}, $\overline{B}^{N_F+1}$, and the lone field $M^{N_F+1}_{N_F+1}$. For notational convenience, let us rename these fields m^a_b, b, $\overline{b}$, and $\widetilde{M}$. Then we have obtained a new duality: three-dimensional SQCD with $N_F = N_c$ is dual, at low-energy, to a theory of singlets interacting through the superpotential:

$$W = \widetilde{M}\left(b\overline{b} - \mathrm{Det}(m)\right) \tag{1.13}$$

Let's consider this duality for a moment: the fields m, b and $\overline{b}$ are all easy to interpret as the gauge singlets of $N_F = N_c$ SQCD. But what about the $\widetilde{M}$ field? Is there an object in SQCD which we can associate to this field? The answer is yes: the vortex Y! With this association in mind, we can rewrite Eq. (1.13) as:

$$W = Y\left(b\overline{b} - \mathrm{Det}(m)\right) \tag{1.14}$$

We have thus arrived at an answer for the question which we asked at the end of Section 1.2.5, at least for $N_F = N_c$: at low energies, the fields of the Higgs and Coulomb branch interact with each other through the potential given in Eq. (1.14).

1.2.7 The Topic of Chapter 4: Dressed Monopoles Operators

We are now ready to discuss the topic of Chapter 4: dressed monopole in three-dimensional theory. The idea is to apply the method of dimensional reduction to all the known s-confining theories in four-dimension. By analogy with the case of Section 1.2.6, we expect that these should allow us to derive a similar list of theories in three-dimensions which exhibit a similar kind of s-confining behaviour, i.e. theories where the low-energy limit is described by gauge singlets interacting through a superpotential whose origin is accessible. As will be the discussed in the paper, the dimensional reduction itself is straightforward, but the results contain several operators who cannot seem to be matched either to the hadrons or to the monopole operators of the gauge theories. We will show that these operators in fact consist of *dressed monopole operators*: bound states of vortices and matter fields! These new kind of degrees of freedom appear in theories which are *chiral*, i.e. where the number of flavours is different from the number of anti-flavours. This imbalance will cause the appearance of *Chern-Simons* term at the quantum level, which will give electric charges to the vortices and cause them to bind with the matter field. While we only present in detail a single example of a theory which exhibit this behaviour, the tools presented in Chapter 4 can be applied to all S-confining four-dimensional theories to classify all s-confining theories in three-dimensions; this will be done in a future work currently in production.

1.3 Thermal Dark Matter Relics

1.3.1 The Case for Dark Matter

There are many observations, both astronomical and cosmological, which suggest that the vast majority of the matter in our universe is not of the usual, or "baryonic" kind. By this, we mean that it does not consist of particles which arise out of the Standard Model of particle physics. Some of the most convincing arguments which support this conclusion are [19]:

- **Galaxy Rotation Curves**: The velocity at which matter bound to a galaxy rotates around its center can be straightforwardly predicted using classical gravity and newtonian motion. For a satellite a large distance R away from the center of the galaxy, where most of the visible mass is contained within the orbit, the virial theorem, $V = -2K$, implies that the velocity v should go like $v \propto R^{-1/2}$. Observations of these *rotation curves* for various galaxies, however, shows that velocity is roughly constant over large distances away from the galactic center. This could be explained by the fact that most of the matter in a galaxy is *not*, in fact, contained in its visible matter; instead, it could be found in a diffuse, spherical *halo* which would extend far beyond the visible disk. Whatever it is that makes up this halo would be the theorized dark matter particle(s).
- **The Bullet Cluster**: The *bullet cluster* refers to the result of the collision between two clusters of galaxies, some 4 billion light years away from Earth. The significance of this event becomes clear when we look at it using two different sets of "eyes". On the one hand, we can look at the

electromagnetic radiation emitted by the visible, baryonic matter in the clusters to establish where most of their visible mass is concentrated. On the other hand, we can use the method of *gravitational lensing* to map out the entire mass distribution, visible *and* invisible, of those clusters. These results show a net separation between the net enters and mass and the centers of visible mass in the clusters: once again, we are led to conclusion that most of these stellar objects is not contained in the visible matter, but rather in some invisible dark material. In addition, the results of the bullet cluster observation show that the dark matter in the clusters was barely affected by the collisions of the two objects: whereas the visible matter was disturbed, heated up, and slowed down by the impact, the dark matter seems to have just gone right on through with very little effect. As we will discuss later, we can use this to put upper bound on the self-interaction of dark matter.

- **Cosmological Fits**: At large enough scales, the dynamical behaviour of the universe can be well described by specifying the different types of contributions to the average energy densities of the universe: these are non-relativistic (or "cold") matter Ω_m, relativistic (or "warm") matter Ω_{rad}, dark energy (also called the cosmological constant) Ω_Λ, and the curvature of the universe, Ω_k. The *scale factor* a, which control the expansion (or possible contraction) of the universe, is then controlled by the Friedmann equation [20]:

$$\frac{\dot{a}}{a} \equiv H = H_0 \sqrt{\Omega_m a^{-3} + \Omega_{rad} a^{-4} + \Omega_k a^{-2} + \Omega_\Lambda}\,, \tag{1.15}$$

where H_0 is Hubble's constant as measured today, and we set $a = 1$ at the present day, so that the sum of the energy densities must be 1. There are many cosmological and astronomical observables, such as the features of

the Cosmic Microwave Background (CMB), the distributions of galaxies, and the relic abundances of the many elements, which are affected by the behaviour of the scale factor a throughout cosmological history. We can therefore use these measurements to fit for the values of the various energy densities. When this is done, the best fit is for $\Omega_m \approx 0.28$; since the value of Ω_m for visible matter is about 0.05, this fit indicates the presence of an invisible component to Ω_m which is larger than the observed value by about a factor of 5.

These arguments have created a widespread consensus on the existence of dark matter. What should the properties of a dark matter candidate be?

- A dark matter particle should be **stable** over cosmological time scales: its decay rate, if it has any, should be small enough to allow it to maintain its density throughout the age of the universe.
- A dark matter particle must have **tightly constrained self-interactions** to respect the bounds set by the bullet cluster. This bound can approximately in terms of the ratio of the dark matter scattering cross-section to its mass as: $\frac{\sigma}{m} < 2\,\frac{\text{barn}}{\text{GeV}}$ [21, 22, 23].
- A dark matter particle must be approximately **dissipationless**: that is, its interactions, whatever they are, must not allow it to dissipate its kinetic energy away to other forms of matter or radiation. This is because, were it otherwise, the dark matter would not have formed the large, diffuse halos necessary for galaxy formation: it would have radiated way its energy and collapsed into much more compact shapes, the way visible matter does.

In addition to these, the ways in which the dark matter is actually produced in the early universe is also very constrained: not only must this production mechanism give us the correct present day relic density of $\Omega_{DM} \approx 0.23$, but it must also produce a population of dark matter particles which is cold enough to allow for structure formation. If the population of dark matter particles produced is too hot (i.e. too relativistic), then it will tend to "free stream" and avoid forming dense gravitational pits which can be used to accrete visible matter. Let us now examine a common way of explaining the dark matter relic density: the thermal relic paradigm.

1.3.2 Dark Matter as Thermal Relic

A *thermal relic* is a particle which was in thermal equilibrium with the photon bath of the Standard Model in the early universe. However, as the universe expanded, this particle eventually decoupled from the photon bath, at which point its energy density evolved independently of the dynamics of the Standard Model sector. The relic neutrinos are a known example of such a particle.

The "advantage" of such a paradigm, from a phenomenological point of view, is that it directly relates the microscopic properties of the thermal relic (such as its mass and couplings) to its cosmological properties: by computing the various collision and annihilation rates of a thermal relic and comparing them to the rate of the expansion of the universe we can compute the relic abundance for this particle, i.e. the amount of particles left over.

Let us be a little more specific. If a particle species is thermalized "with itself" its distribution will be characterized by only two quantities: its chemical potential μ and its temperature T' (we reserve the use of T for the temperature of the

Standard Model photon bath). We will find it a little more convenient to use the quantities y and r, defined through

$$n_\chi(T) = y(T) n_\chi^{eq}(rT) \,, \tag{1.16}$$

where

$$n_\chi^{eq}(T') = \frac{g_\chi}{2\pi^2} m^2 T' K_2(m/T') \,. \tag{1.17}$$

In other words, $y = e^{\mu/T'}$ and $r = T'/T$. Again, assuming that the dark matter remains thermally coupled to itself, the parameters y and r can be obtained by solving the *Boltzmann equations* which control its thermal evolution. Since we have two unknowns, we need two equations to uniquely determine them. For all cases, one of these will be the Boltzmann equation for the energy density [20]:

$$\frac{\partial \rho_\chi}{\partial t} + 3H(\rho_\chi + P_\chi) = \langle \sigma v \cdot \delta E \rangle_{\rm kin} n_\chi n_\gamma^{\rm eq}, \tag{1.18}$$

where $\langle \sigma v \cdot \delta E \rangle_{\rm kin}$ is the rate of energy transfer from the photon bath to the χ particles, which can be computed from its couplings; ρ_χ and P_χ are the energy and the pressure density of the dark matter particles, respectively, and are simply related to its equilibrium distribution. The second equation we need to use is the Boltzmann equation for the number density. Its exact form will depend on the dominant number-changing process for the particle. A common example is the Weakly Interacting Massive Particle (WIMP) [24], which tends to annihilate into Standard Model particles through interactions of the form $\chi + \chi \to \text{SM} + \text{SM}$. For this case, the number-changing Boltzmann equation would be:

$$\frac{\partial n_\chi}{\partial t} + 3H n_\chi = -\langle \sigma v \rangle_{2\to 2} (n_\chi^2 - n_\chi^{2\,\rm eq}) \,. \tag{1.19}$$

Another example which has been studied more recently consists of the Strongly Interacting Massive Particle (SIMP) [25, 26]: this dark matter candidate has only

negligible annihilations to the Standard Model. Instead, its dominant number-changing process is *self-annihilation*, e.g. $\chi + \chi + \chi \to \chi + \chi$. In this case the number-changing Boltzmann equation is:

$$\frac{\partial n_\chi}{\partial t} + 3Hn_\chi = -\langle \sigma v^2 \rangle_{3\to 2}(n_\chi^3 - n_\chi^2 n_\chi^{\rm eq}) \,. \tag{1.20}$$

For any given microscopic model describing the dark matter particles (i.e. a Lagrangian describing its masses and couplings) we can compute the transition rates $\langle \sigma v \cdot \delta E \rangle_{\rm kin}$, $\langle \sigma v \rangle_{2\to 2}$ (or $\langle \sigma v^2 \rangle_{3\to 2}$, as is appropriate) and use them to numerically solve the Boltzmann equations. In all cases, however, the story of a (valid) dark matter relic is similar: at high temperatures it is in thermal equilibrium with the photon bath and in chemical equilibrium: that is say, it has $r = y = 1$. As the universe expands and cools down, however, it becomes harder and harder for the thermal relic to maintain both of these equilibriums. Eventually, the dark matter particle will reach a density low enough that they will become unable to "find themselves" and will effectively stop interacting at all, both with the Standard Model and with each other.[22] When this happens, the co-moving energy density of the dark matter particles is fixed and does not change anymore. This story is illustrated in Figs. 1.5 and 1.6.

[22] As we will soon discuss, it makes a crucial difference whether the χ particles stop interacting with themselves or with the Standard Model first.

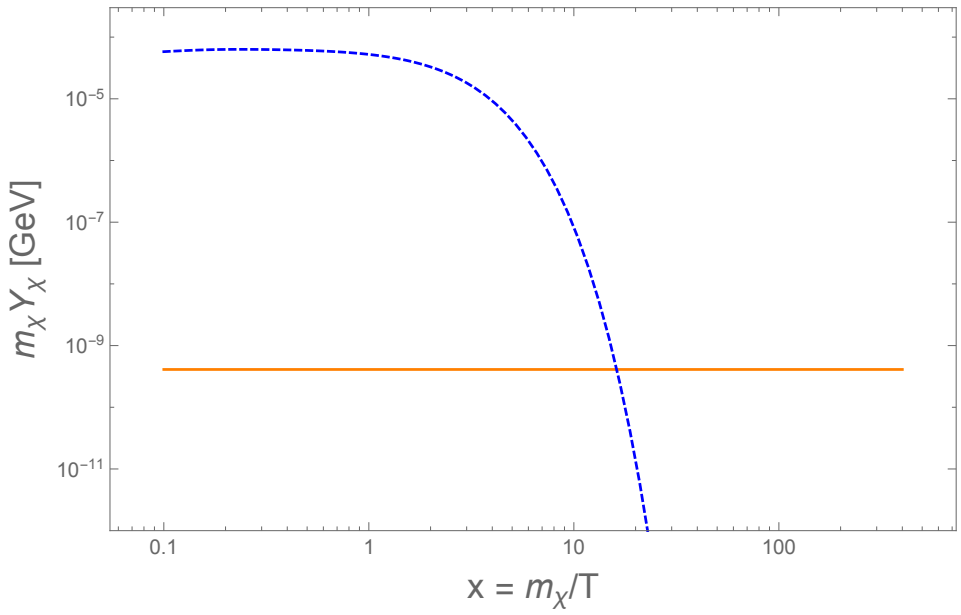

Figure 1.5: The life of a thermal relic, part 1. The dashed blue line represent the yield, or energy density of a thermal relic normalized by the entropy density of the photon bath, if it stayed in thermal and chemical equilibrium throughout its life. The solid orange line corresponds to the observed yield of dark matter in our universe. When $T \lesssim m$, the number density becomes exponentially suppressed and plummets downward to zero.

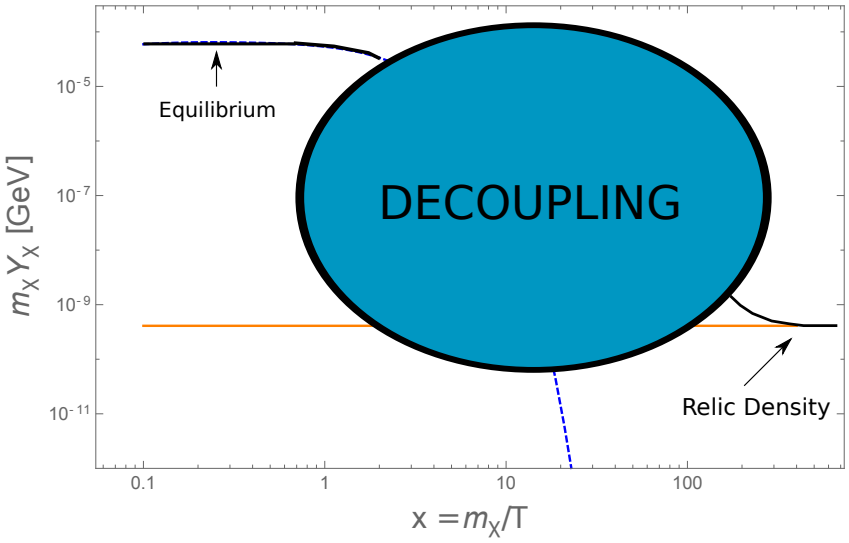

Figure 1.6: The life of a thermal relic, part 2. For a real thermal relic (solid black line), the interactions that keep the particle in thermal and chemical equilibrium stop being effective when $T \lesssim m$, and the yield stops following the equilibrium distribution. After decoupling, the yield is constant.

1.3.3 The Topic of Chapter 5: ELDERs

Chapter 5 is a paper which present a new kind of thermal relic dark matter, the Elastically Decoupling Relic (ELDER). This dark matter candidate is similar to a SIMP in that its dominant number-changing interactions consist of self-annihilations. However, the ELDER has a larger self-annihilation rate and a smaller coupling with the Standard Model compared to the SIMP: this means that, for the ELDER, the first process to turn off will be the exchange of energy with the Standard Model. This is quite unlike both the SIMP and the WIMP, which both remain in thermal contact with the SM throughout the important part of their decoupling process. After the ELDER has decoupled from the pho-

ton bath, it will begin a *cannibalization*[23] phase [27]: the self-annihilations will start converting mass energy into kinetic energy, keeping the temperature of the ELDER far above that of the Standard Model. Eventually, self-annihilations too will decouple, and the co-moving energy density of the ELDER will reach its final value. The key point, however, is that the final relic density depends very little on the self-annihilation rate: the relic density changes very slowly during the cannibalization phase, so it doesn't matter that much when exactly the self-annihilation decouple. As a result of this, the ELDER relic density is controlled almost completely by its elastic scattering rate with the Standard Model. Remarkably, the final number density is controlled by a process which is not number-changing!

A more detailed presentation of the ELDER scenario, which include its expected couplings, mass range, exclusion bounds, and discovery prospect, is the subject of Chapter 5.

[23]While I think that the term "cannibalization" is both witty and appropriate, the editorial staff of PRL disagreed; sadly, the term has been changed to "self-heating" in the published version of the paper presented on Chapter 5.

CHAPTER 2

HIGGS COUPLINGS AND NATURALNESS

Many extensions of the Standard Model postulate the existence of new weakly coupled particles, the top partners, at or below the TeV scale. The role of the top partners is to cancel the quadratic divergence in the Higgs mass parameter due to top loops. We point out the generic correlation between naturalness (the degree of fine-tuning required to obtain the observed electroweak scale), and the size of top partner loop contributions to Higgs couplings to photons and gluons. If the fine-tuning is required to be at or below a certain level, a model-independent lower bound on the deviations of these Higgs couplings from the Standard Model can be placed (assuming no cancellations between contributions from various sources). Conversely, if a precise measurement of the Higgs couplings shows no deviation from the Standard Model, a certain amount of fine-tuning would be required. We quantify this connection, and argue that a measurement of the Higgs couplings at the per-cent level would provide a serious and robust test of naturalness.[1]

2.1 Introduction

The recent discovery of a new particle, roughly consistent with the Standard Model (SM) Higgs boson, has opened a new window into physics at the electroweak scale. In the next decade, the Higgs physics will enter the precision era,

[1] This paper was co-authored with Marco Farina and Maxim Perelstein; it was published in July 2014 by Physical Review D. [28]

in which the goal will be to measure the properties of this particle, in particular its couplings, with the highest possible accuracy. Besides the continuing experiments at the LHC, the idea of a next-generation electron-positron collider such as the International Linear Collider (ILC) is currently under active discussion, with precise measurements of the Higgs couplings as its prime motivation [1]. Such a facility would be capable of measuring several couplings at a per cent level. It is important to understand the implications that these measurements could have on our ideas about physics beyond the Standard Model.

Predictions of many SM extensions for the Higgs couplings have already been extensively studied. In this paper, we point out a very general, and important, feature of such predictions. In any model which stabilizes the Higgs mass against radiative corrections by postulating weakly-coupled new physics, the amount of fine-tuning required to obtain the observed electroweak scale is *inversely correlated* with the size of certain non-SM contributions to the Higgs couplings to photons and gluons. In other words, if the fine-tuning is required to be at or below a certain level, a model-independent *lower bound* on the deviations of these Higgs couplings from the SM can be placed (assuming no cancellations between contributions from various sources). Conversely, if a precise measurement of the Higgs couplings shows no deviation from the SM, a certain amount of fine-tuning would be required. We will quantify these statements, and show that per-cent level Higgs coupling measurements, expected to be achievable at the next-generation experimental facilities, would provide a serious test of naturalness of the electroweak scale. This gives a clear and compelling physics motivation for such measurements.[2]

The paper is organized as follows. In Section 2.2, we present the gen-

[2]For earlier work along these lines, see Refs. [29, 30, 31].

eral argument for the correlation between naturalness and loop-induced Higgs couplings to gluons and photons. The key observation is that the same object, the Higgs-dependent mass of the top partner (or partners), determines the dominant radiative corrections to the Higgs mass parameter, via the Coleman-Weinberg (CW) potential, and the top partner contributions to the Higgs couplings to gluons and photons, via the well-known "low-energy theorems" [32]. In Section 2.3, we study the correlation between fine-tuning and Higgs couplings quantitatively, using a simple toy model with a single top partner (scalar or fermion) as the benchmark. In Section 2.4, we explore how the picture may be affected by the presence of a second top partner, and find that excepting small regions of parameter space where accidental cancellations occur, the conclusions of the benchmark one-partner analysis remain valid. We discuss our findings and conclude in Section 2.5.

2.2 General Argument: Top Partners, Naturalness, and the Higgs Couplings

The starting point of our analysis is a single Higgs doublet H with the SM tree-level potential

$$V(H) = -\mu^2|H|^2 + \lambda|H|^4. \tag{2.1}$$

This hypothesis is the simplest interpretation of the LHC discovery consistent with all other experimental data. In particular, there is no evidence in the data of H mixing with other scalar fields, and the constraints on such mixing are now quite stringent. In the SM, the measurements of the Higgs vacuum expectation

value (vev) and mass provide precise values for the parameters in the potential:

$$\mu = 90 \text{ GeV}, \lambda = 0.13. \tag{2.2}$$

How natural are these parameters? To address this question, we need to consider quantum corrections to the potential (2.1). At the one-loop order, these corrections are conveniently given by the Coleman-Weinberg (CW) formula

$$V_{\text{CW}}(h) \;=\; \frac{1}{2}\sum_k g_k(-1)^{F_k}\int \frac{d^4\ell}{(2\pi)^4}\,\log\left(\ell^2 + m_k^2(h)\right), \tag{2.3}$$

where the sum runs over all particles in the model, and g_k and F_k is the multiplicity and fermion number of each particle, respectively. For example, for a gauge-singlet complex scalar, $g = 2$ and $F = 0$; for a gauge-singlet Dirac fermion, $g = 4$ and $F = 1$. Here $h/\sqrt{2}$ is the real part of the $U(1)_{\text{em}}$-neutral component of H; in the SM vacuum, $\langle h\rangle = 246$ GeV. The one-loop correction to the Higgs mass parameter is given by

$$\delta\mu^2 \equiv \frac{\delta^2 V_{\text{CW}}}{\delta h^2}|_{h=0}. \tag{2.4}$$

In the SM, the largest contribution to the CW potential comes from the top quark, since the top Yukawa is the strongest coupling of the Higgs:

$$\delta\mu^2 \;=\; -\frac{3y_t^2}{8\pi^2}\Lambda^2 + \ldots, \tag{2.5}$$

where Λ is the scale at which all loop integrals in V_{CW} are cut off. Since we expect $\Lambda \gg M_{\text{EW}}$, the quantum correction to μ from the top loop is unreasonably large, and would require fine-tuning if no new physics is present. If the theory is weakly coupled at the TeV scale, the only way to avoid fine-tuning is to introduce a new particle, the *top partner*, with mass at or below the TeV scale. (Multiple top partners may be involved in the divergence cancellation.) Such partners can be spin-0 scalars, as in supersymmetric (SUSY) models[3], or vector-

[3]The special role played by the stops, the partners of the top quarks, in determining the degree of naturalness of the electroweak scale in SUSY models was emphasized in Refs. [33], and more recently in Refs. [34, 35, 36, 37, 38].

like spin-1/2 fermions, as in Little Higgs [**?**, 39, 40] or 5-dimensional composite Higgs models [41, 42, 43].[4] In either case, the top partner mass has the form

$$m^2(T_i) = m_{0,i}^2 + c_i h^2 + \cdots \tag{2.6}$$

where we allow for the possibility of multiple top partners labeled by T_i, and drop the terms of higher order in h. By dimensional analysis, such higher-order terms need to be suppressed by powers of a mass scale; our approximation is valid if this mass scale is $\gg v$. The absence of a term linear in h in the mass is a consequence of the top partners' vector-like $SU(2)$ charges. The combined top sector contribution to the quadratic terms in the Higgs potential is

$$\delta\mu^2 \;=\; \frac{1}{16\pi^2}\left[\left(\sum_i g_i(-1)^{F_i}c_i - 6y_t^2\right)\Lambda^2 + \sum_i g_i(-1)^{F_i}c_i m_{0,i}^2 \log\frac{\Lambda^2}{m_{0,i}^2} - 6y_t^2 m_t^2 \log\frac{\Lambda^2}{m_t^2} + \ldots\right]. \tag{2.7}$$

Cancellation of the quadratic divergence yields the sum rule

$$6y_t^2 = \sum_i g_i(-1)^{F_i}c_i\,. \tag{2.8}$$

This sum rule is imposed by the symmetry of the theory in both SUSY and Little Higgs. The remaining fine-tuning can be quantified by taking the ratio of the quantum correction to μ^2 to its measured value:

$$\Delta = \frac{\delta\mu^2}{\mu^2} \approx 0.78\left(\sum_i g_i(-1)^{F_i}c_i\left(\frac{m_{0,i}}{1\text{ TeV}}\right)^2 \log\frac{\Lambda^2}{m_{0,i}^2} - 6y_t^2\left(\frac{m_t}{1\text{ TeV}}\right)^2 \log\frac{\Lambda^2}{m_t^2}\right). \tag{2.9}$$

If $\Delta \gg 1$, the theory must be fine-tuned to accommodate the observed EWSB. Note that Δ only measures fine-tuning in the Higgs mass parameter; we assume that the observed quartic coupling can be generated with no additional fine-tuning. In certain specific models, such as the minimal supersymmetric standard model (MSSM), a significant loop contribution to the quartic is required,

[4] In principle, a spin-1 top partner is also a possibility [44]; we will not consider this case here.

which in turn implies strong constraints on the top sector and associated fine-tuning in the Higgs mass parameter. However, such correlations between the quartic and the mass are very model-dependent, and we will not take them into account in this analysis.

The effects of the top partners on the Higgs couplings first appear at the one-loop level. The best place to look for such effects is in the couplings which vanish in the SM at the tree level. We focus on the couplings of the Higgs to gluons and photons. At the one-loop order, the contributions of particles with masses $\gg m_h$ to these couplings are described by effective operators,

$$\mathcal{L}_{h\gamma\gamma} = \frac{2\alpha}{9\pi v} C_\gamma h F_{\mu\nu} F^{\mu\nu}, \quad \mathcal{L}_{hgg} = \frac{\alpha_s}{12\pi v} C_g h G_{\mu\nu} G^{\mu\nu}. \tag{2.10}$$

The Wilson coefficients can be found using the well-known "low-energy theorems" [32]:

$$\begin{aligned} C_\gamma &= 1 + \frac{3}{8} \sum_f^{Dirac\ fermions} N_{c,f} Q_f^2 \frac{\partial \ln m_f^2(v)}{\partial \ln v} + \frac{3}{32} \sum_s^{scalars} N_{c,s} Q_s^2 \frac{\partial \ln m_s^2(v)}{\partial \ln v}, \\ C_g &= 1 + \sum_f^{Dirac\ fermions} C(r_f) \frac{\partial \ln m_f^2(v)}{\partial \ln v} + \frac{1}{4} \sum_s^{scalars} C(r_s) \frac{\partial \ln m_s^2(v)}{\partial \ln v}, \end{aligned} \tag{2.11}$$

where the first term is the contribution of the SM top loops, the sum runs over the top partners, and $N_{c,i}$ and Q_i are the dimension of the $SU(3)_c$ representation and the electric charge (in units of electron charge) of the particle i. Note that the exact same objects, the Higgs-dependent masses of top partners $m_i(h)$, enter the CW potential and the Higgs couplings, providing a very general and robust connection between these quantities. In the approximation of Eq. (2.6), we

obtain

$$
\begin{aligned}
C_\gamma &\approx 1 + \frac{3}{4}\sum_f \frac{N_{c,f} Q_f^2 c_f v^2}{m_{0,f}^2 + c_f v^2} + \frac{3}{16}\sum_s \frac{N_{c,s} Q_s^2 c_s v^2}{m_{0,s}^2 + c_s v^2}\,, \\
C_g &\approx 1 + 2\sum_f \frac{C(r_f) c_f v^2}{m_{0,f}^2 + c_f v^2} + \frac{1}{2}\sum_s \frac{C(r_s) c_s v^2}{m_{0,s}^2 + c_s v^2}\,.
\end{aligned} \tag{2.12}
$$

The set of coefficients $\{m_{0,i}, c_i\}$ determines both the fine-tuning Δ and the Wilson coefficients, generically resulting in a correlation between these quantities. Assuming that there are no other non-SM contributions to the Higgs couplings to photons and gluons, the deviations of these couplings from the SM in the presence of top partners are given by

$$
R_g \equiv \frac{g(hgg)}{g(hgg)|_{\rm SM}} = C_g, \quad R_\gamma \equiv \frac{g(h\gamma\gamma)}{g(h\gamma\gamma)|_{\rm SM}} \approx 1 - 0.27\left(C_\gamma - 1\right), \tag{2.13}
$$

where the contribution of the W loop has been taken into account in the photon coupling.

It should be noted that in the above discussion, we assumed that the top loop contribution to the Higgs couplings is exactly equal to its value in the SM. In some relevant models of new physics, this assumption is not valid, due to deviations of the top Yukawa from its SM value. Models in which the Higgs is a pseudo-Goldstone boson, such as Little Higgs models, provide an example. In these models, the shift in the top loop contribution to hgg and $h\gamma\gamma$ couplings is of the same order as the top partner loop contributions to these couplings [45, 46, 47]. The effect of the additional shift is model-dependent. In some cases, a cancellation between the top-Yukawa and top partner loop effects may occur, due to the specific structure of the top mass matrix [48]. In this case, our analysis would not apply. Note, however, that in all theoretically motivated examples that we are aware of, the shift in the top Yukawa is due to Higgs compositeness, at a scale not far above the electroweak scale. Such models also predict large,

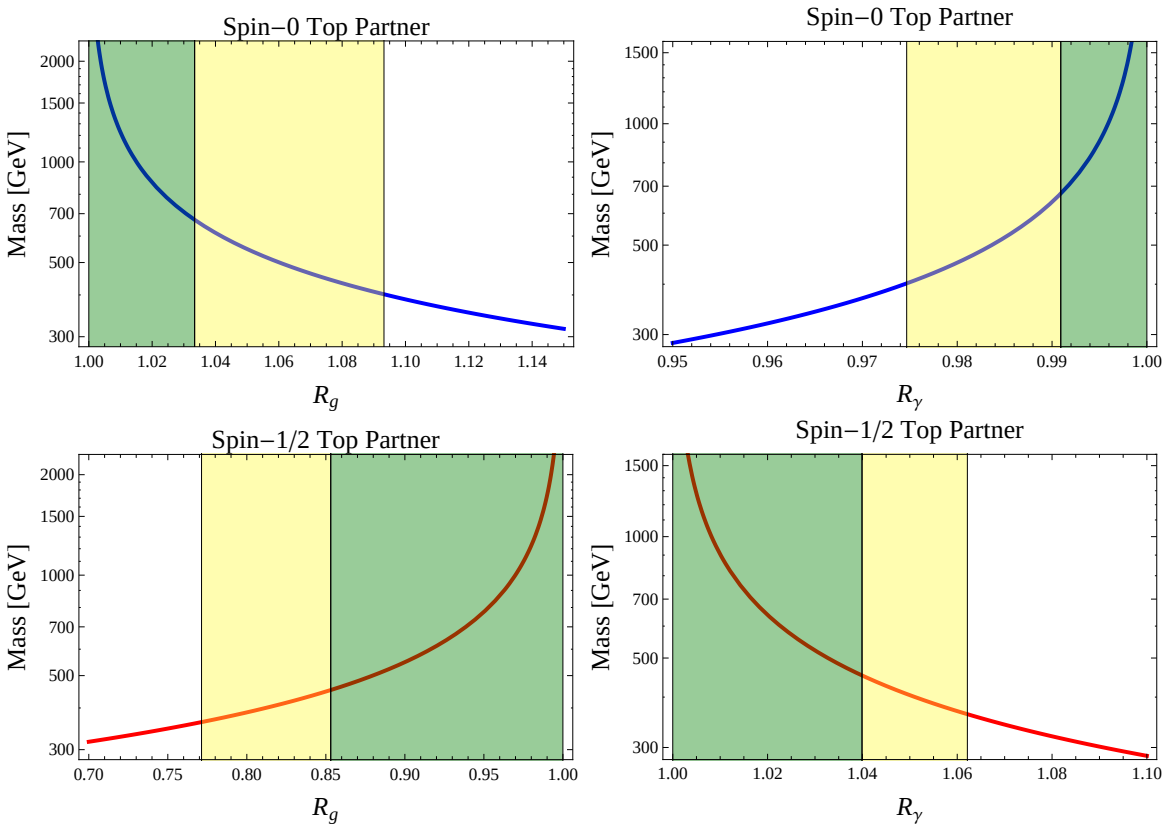

Figure 2.1: Fractional deviation of the Higgs coupling to gluons (left panel) and photons (right panel) from the SM value, as a function of the top partner mass. Top row: Spin-0 top partner. Bottom row: Spin-1/2 top partner. Regions currently allowed by the LHC and Tevatron data are shown in green (68 % c.l.) and yellow (95 % c.l.).

tree-level deviations of the Higgs couplings to W and Z bosons, which will be probed with high precision by any experiment capable of precise measurements of gluon and photon couplings.

2.3 Benchmark Model: a Single Top Partner

The simplest possibility is that there is a single top partner, in fundamental rep of $SU(3)$ and with electric charge 2/3, just like the SM top. (The single partner model is applicable to models with multiple top partners if they have the same $m_{0,i}$ parameters: for example, the MSSM with two degenerate stops.) This simple model can be used as a benchmark for evaluating the potential of precision Higgs couplings to probe naturalness. In this case, c_1 is fixed by the sum rule (2.8), and $m_{0,1}$ is the only free parameter in the predictions:

$$\begin{aligned} C_\gamma &= C_g = 1 + \frac{1}{4}\frac{y_t^2 v^2}{m_{0,1}^2 + y_t^2 v^2} \quad \text{(spin 0 partner);} \\ C_\gamma &= C_g = 1 - \frac{y_t^2 v^2}{2m_{0,1}^2 - y_t^2 v^2} \quad \text{(spin 1/2 partner).} \end{aligned} \tag{2.14}$$

The correlation between the Higgs coupling deviations from the SM and the mass of the top partner is shown in Fig. 2.1. For reference, we also show constraints obtained from a fit to the current LHC-7, LHC-8 [49, 50, 51, 52, 53] and Tevatron [54] data, assuming that top-partner loops are the only non-SM contribution to Higgs couplings. To obtain these constraints, we fit to the published Higgs event rates observed in various channels, assuming no correlation between any of the data points, and include the theoretical uncertainties provided by the Higgs cross section working group [55, 56]. Our results are roughly consistent with the more detailed fits performed by the LHC collaborations [57, 58]: for example, our one-sigma error bar on R_g is about ± 0.1, compared to 0.14 reported by the ATLAS collaboration [57] in a two-parameter fit where R_g and R_γ were assumed to be the only non-SM contributions to the Higgs rates. A broad range of top partner masses in the region motivated by naturalness are currently allowed by data: the 95% c.l. limit on the top partner mass is about 320 GeV for a spin-0 top partner, and 400 GeV for a spin-1/2 partner. (Note that our best-fit

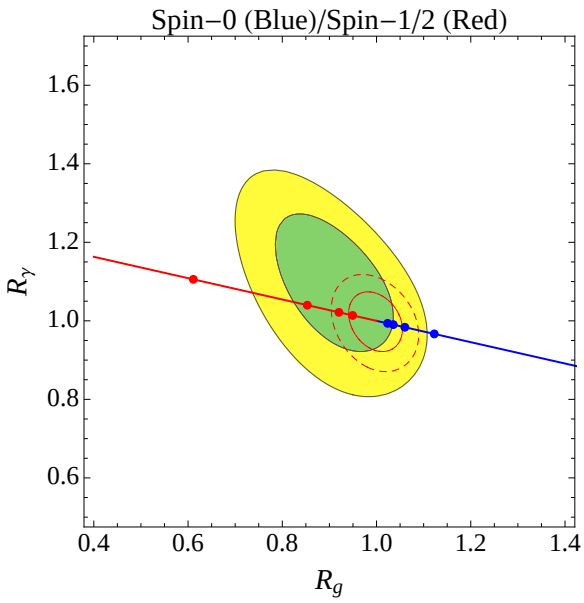

Figure 2.2: Regions allowed by the LHC and Tevatron measurements of the Higgs rates in the $R_\gamma - R_g$ plane, at the 68 % c.l. (green) and 95 % c.l. (yellow). The spin-0 top partner model predicts deviations along the blue line, while the spin-1/2 top partner induces deviations along the red line. The points on both lines correspond to the partner masses of 350, 500, 650, and 800 GeV. For comparison, projected constraints from the LHC-14 [1] are shown by red lines.

value for R_g is about 0.7σ below the SM expectation of 1.0, resulting in a slightly stronger bound on the spin-0 partners and a slightly weaker bound on the spin-1/2 case.) However, future precise measurements of the Higgs coupling at the LHC-14 and a future e^+e^- facility would probe much of the interesting parameter space. For example, a 1% measurement of the gluon coupling will probe the top partner masses in excess of 1 TeV, for both spin-0 and spin-1/2 top partners.

Since the one-partner model has only one free parameter, the deviations in gluon and photon couplings are correlated. This is shown in Fig. 2.2, along with the current and future LHC constraints on the two couplings. (We used the information provided in Ref. [1] to estimate the LHC-14 contours.) It is

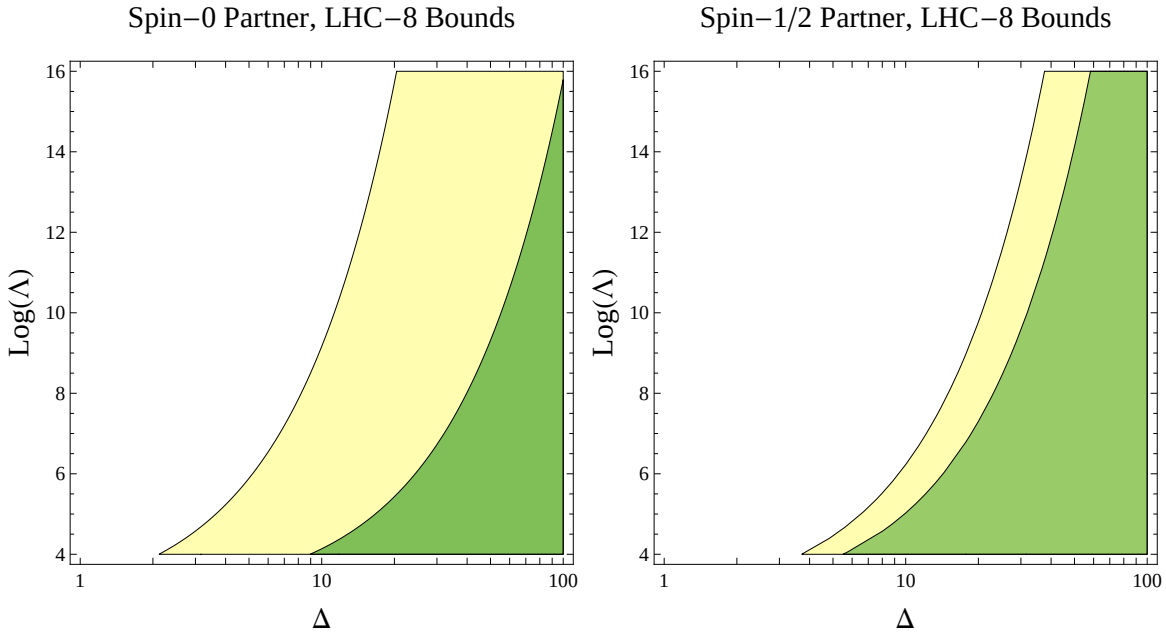

Figure 2.3: Regions allowed by the LHC and Tevatron data in the $\Delta - \log \Lambda$ plane, at the 68 % c.l. (green) and 95 % c.l. (yellow). Here, Λ is the scale (in GeV) where the logarithmic divergence in the Higgs mass renormalization is cut off. Left panel: Spin-0 top partner. Right panel: Spin-1/2 top partner.

clear that the constraints are strongly dominated by the gluon coupling measurement, due to both the slope of the trajectory and the stronger experimental bound on R_g. If a deviation from the SM is observed, it would be straightforward to check whether it can be interpreted within the one-partner framework by simply checking whether the trajectories shown here intersect with the experimentally determined region. If the answer is positive, these measurements will also allow to unambiguously determine the top partner spin.

The connection between Higgs couplings and fine-tuning is illustrated more directly in Figs. 2.3 and 2.4. Since the top partners only cut off the quadratic divergence in the top loop, leaving the logarithmic divergence uncanceled, the value of the fine-tuning measure Δ depends logarithmically on the scale Λ

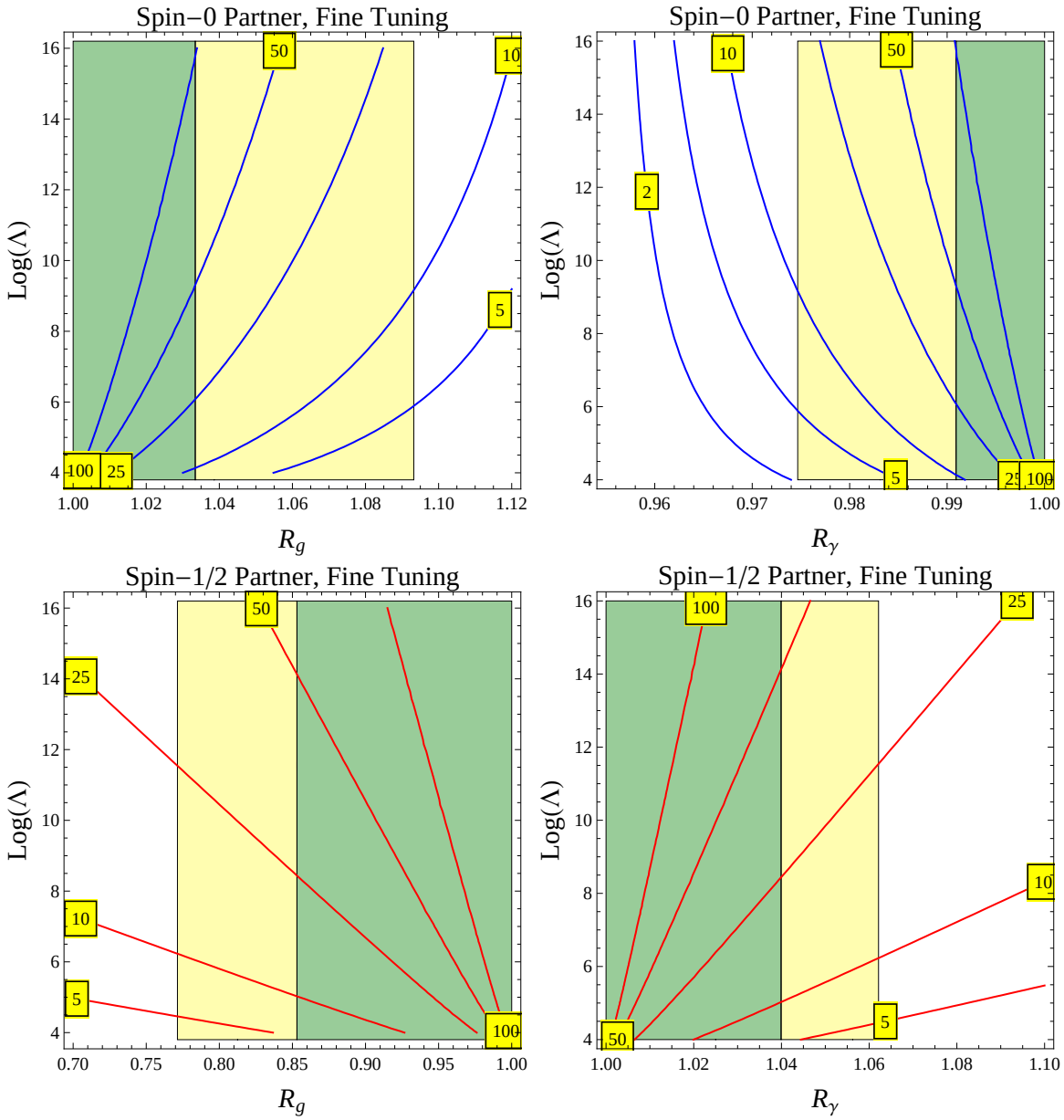

Figure 2.4: Fine-tuning as a function of the fractional deviation of the Higgs coupling to gluons (left panel) and photons (right panel) from the SM value, and the energy scale Λ (in GeV) where the logarithmic divergence in the Higgs mass renormalization is cut off. Top row: Spin-0 top partner. Bottom row: Spin-1/2 top partner. Regions currently allowed by the LHC and Tevatron data are shown in green (68 % c.l.) and yellow (95 % c.l.).

where the logarithmic divergence is cut off. The value of Λ is very model-dependent. To demonstrate its effect, we vary Λ between the "low" 10 TeV scale, representing a rough lower bound on this scale in realistic models, and the "high" 10^{16} GeV, motivated by grand unification. In the case of a spin-0 partner, the 95% c.l. lower bound on the fine-tuning from the current Higgs data varies between $\sim 1/2$ for a low-scale model and $\sim 1/20$ for a high-scale model. The bounds for the spin-1/2 partner are slightly stronger, between $\sim 1/3$ and $\sim 1/30$. Of course, these bounds can be dramatically improved by the future precise measurements of Higgs couplings. For example, if the gluon coupling is found to agree with the SM at a 1% level, the minimal amount of fine-tuning required would be $\sim 1/25$ for the low-scale model, and $\sim 1/400$ for a high-scale model.

We emphasize that the probe of naturalness advocated here is complementary to direct searches for top partners. Sensitivity of the direct searches, especially at hadron colliders such as the LHC, depends on details of the spectrum and the decay patterns of the produced top partners. For example, while the LHC "headline" direct bounds on stops are already about 600 – 700 GeV [**?**], these bounds can be evaded in a variety of ways, *e.g.* "stealthy" [59] or compressed stop spectra, or R-parity violation. In contrast, the nature of the Higgs coupling deviations discussed here is very tightly connected to the restoration of naturalness, and the connection is essentially model-independent. Of course, the simple correlation exhibited in the benchmark one-partner models may be violated in more complicated setups, where for example cancellation among various loop contributions is in principle possible. We will investigate an example of this in the next section. Still, it is worth emphasizing that the "loopholes" inherent in the test of naturalness proposed here are completely different from

the ones plaguing direct searches. Together, these techniques should provide an extremely powerful and robust test of naturalness.

2.4 Two Top Partners

Cancellation of the top loop divergence does not have to be achieved with a single new particle. For example, in the MSSM, there are two spin-0 top partners, $\widetilde{t}_1$ and $\widetilde{t}_2$, generically with different masses, both of which participate in divergence cancellation. Models with multiple top partners are characterized by multi-dimensional parameter spaces, even after the divergence cancellation sum rule is imposed. We expect that throughout most of the parameter space of a given model, the correlation between Higgs couplings and fine-tuning studied in Section 2.3 continues to hold. However, there could be special regions of parameter space where it can fail, due to cancellations between contributions of the two top partners, either to the CW potential or to the Higgs couplings. To illustrate this, in this section we will consider a toy model with two spin-0 partners, both in fundamental rep of $SU(3)$ and with electric charge $2/3$. (These are the quantum number assignments of the MSSM stops, so the results of this section will approximately apply in that model; the correspondence becomes exact in the limit of soft masses large compared to v.[5]) The model has four free parameters, $\{m_{0,i}, c_i\}$, $i = 1, 2$; after the sum rule (2.8) is imposed, the number is reduced to 3. We choose to work in terms of

$$m_1; \;\; \mu = \frac{m_2}{m_1}; \;\; \theta = \tan^{-1} \frac{c_2}{c_1}, \tag{2.15}$$

[5]Many authors examined the stop loop contributions to Higgs couplings in the MSSM; see, for example, Refs. [60, 61, 62, 63].

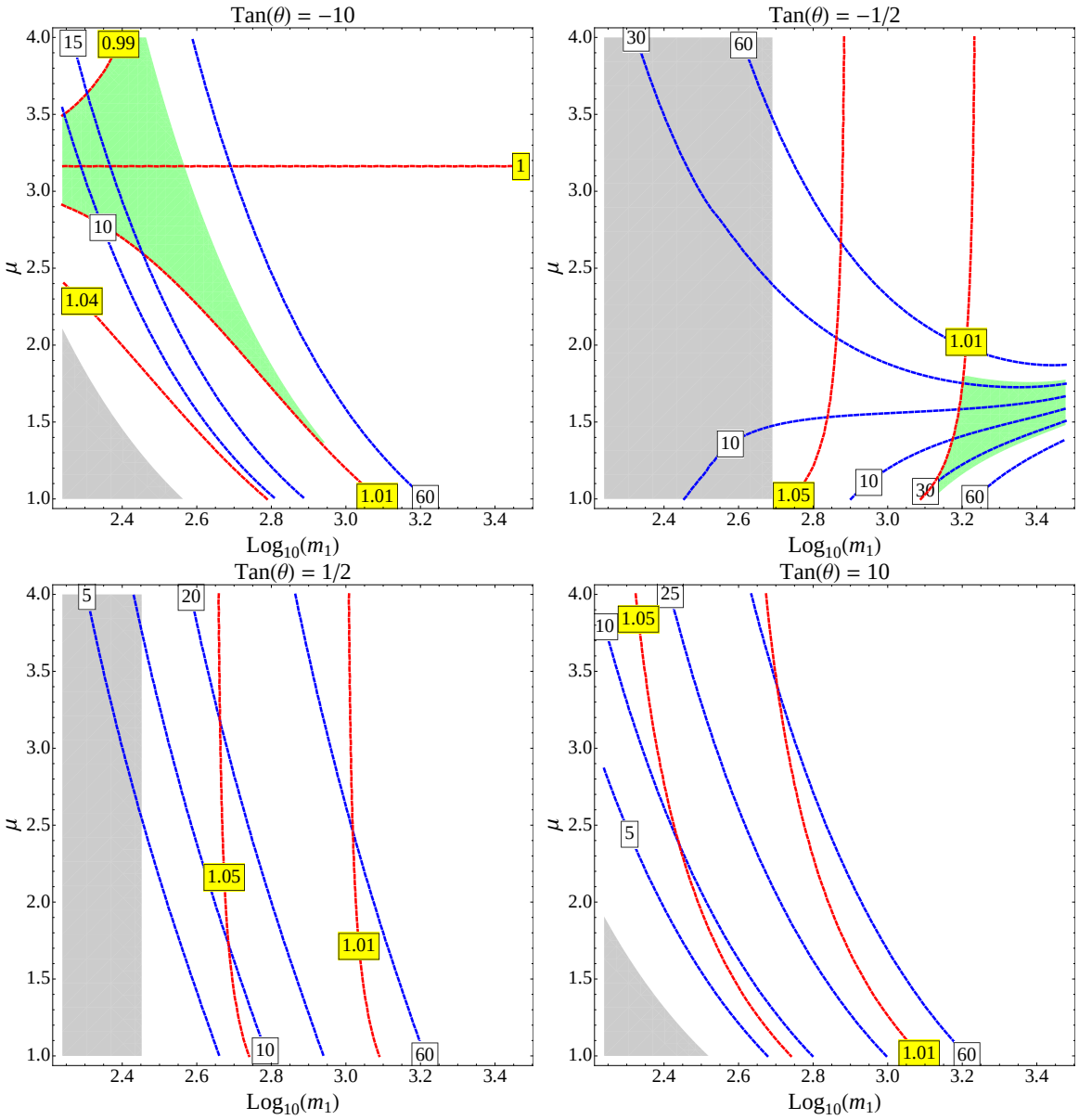

Figure 2.5: Contours of fine tuning (in blue) and R_g (in red) for fixed values of θ, with $\Lambda = 20$ TeV. The regions shaded in green correspond to points where $|R_g - 1| < 0.01$ but for which the amount of fine tuning is less than what is predicted for a one scalar partner model with $R_g = 0.01$. The regions shaded in gray corresponds to points where $|c_i v^2/m_{0,i}^2| > 1$. The top partner mass m_1 is in units of GeV.

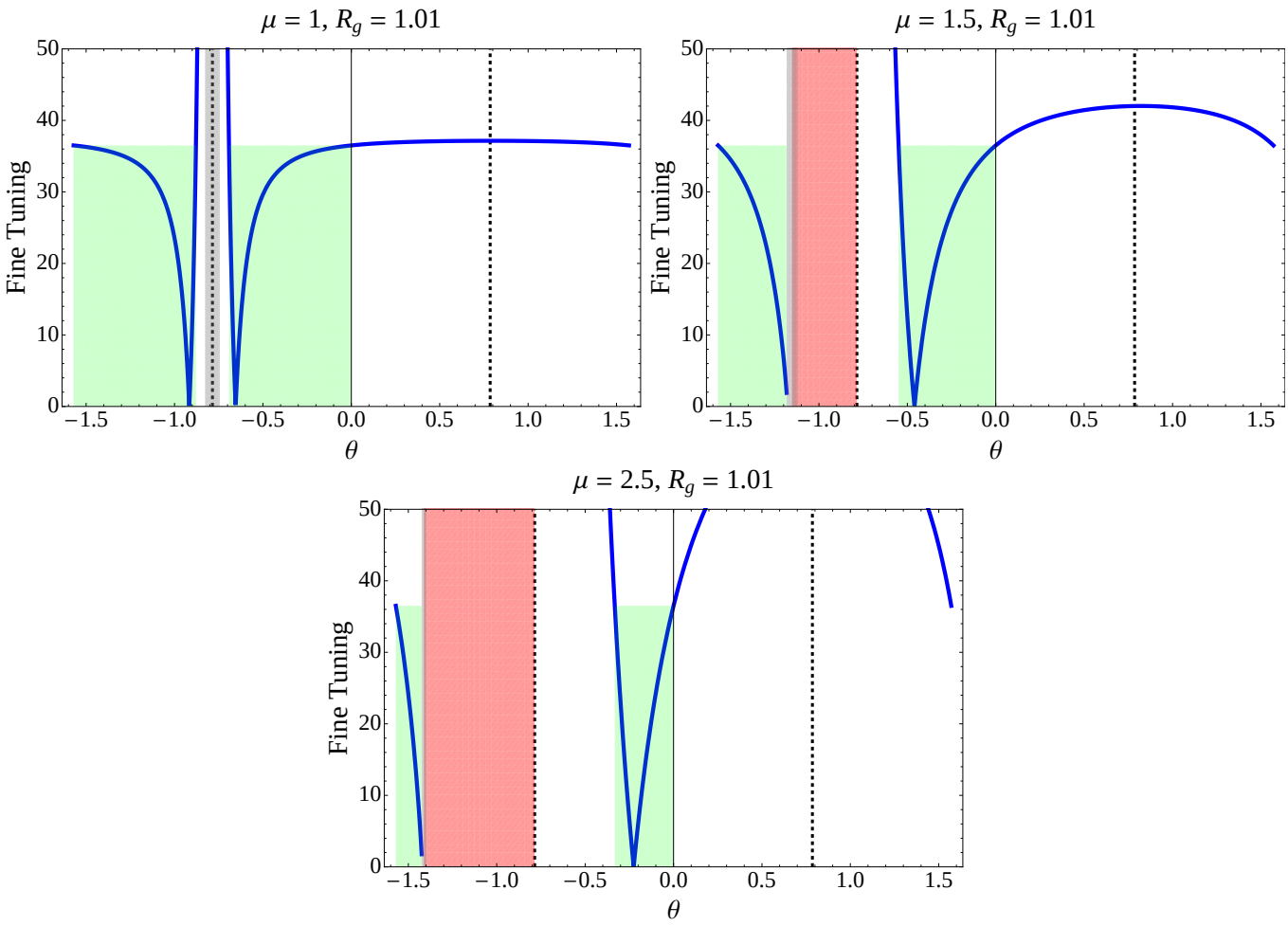

Figure 2.6: Fine tuning (in blue) as a function of θ for fixed values of μ and R_g, with $\Lambda = 20$ TeV. The regions shaded in in gray indicate values of θ where $|c_i v^2/m_{0,i}^2| > 1$; the regions shaded in red are unphysical due to $m_1^2 < 0$. Green regions indicate values of θ for which the fine tuning is less than what is predicted for a one scalar partner model with $R_g = 0.01$.

where $m_i = \sqrt{m_{0,i}^2 + c_i v^2}$ are the physical masses of the top partners, and $m_1 < m_2$. Note that in the limits ($\mu \to 1$, any θ) and ($\theta \to 0$, any μ), the model reduces to the one-partner model with the same $m_{0,1}$, considered in Section 2.3 above.

The main conclusion of our analysis of this model is that the correlation of the Higgs coupling deviations and fine-tuning, observed in the benchmark one-

partner models of Section 2.3, is rather robust. This is illustrated in Fig. 2.5. For example, suppose that the gluon coupling is found experimentally to agree with the SM prediction at a level of 1%. Interpreting this bound within a one-partner model places a lower bound on fine tuning of about 1/35 assuming $\Lambda =$ 20 TeV. The two-partner model *can* produce the gluon coupling within 1% of the SM value with *smaller* fine-tuning; however, the regions of parameter space where this occurs (shaded in green in Fig. 2.5) are rather small, so an accidental cancellation is clearly involved. Note also that such accidental reduction in fine-tuning can only occur when c_1 and c_2 have opposite signs ($\theta < 0$). The accidental nature of the fine-tuning reduction is further illustrated in Fig. 2.6: once the masses are fixed, fine-tuning drops significantly below the value inferred from the one-partner model only for a narrow range of the couplings.

In principle, cancellation of the top quadratic divergence may involve > 2 new particles, although we are not aware of any explicit model in which this is the case. It seems reasonable to conjecture that if this were the case, the correlation of Higgs coupling deviation and fine-tunings would persist, modulo possible accidental cancellations.

2.5 Conclusions

In this paper, we pointed out and quantified a correlation between the level of fine-tuning of electroweak symmetry breaking and the deviations of the Higgs couplings to photons and gluons from their SM values. The connection holds in a very large class of well-motivated models: the basic assumptions are that the physics at the weak/TeV scale is weakly coupled, and that the quadratic di-

vergence in the Higgs mass from the SM top loop is canceled by loops of new particles, the top partners. The top partners' contributions to the Higgs mass parameter and to the Higgs couplings to photons and gluons are determined by the same objects, their Higgs-dependent masses, resulting in a simple relationship between them. Thus, measuring Higgs couplings precisely provides a robust, model-independent test of naturalness. We showed that a measurement of Higgs couplings to gluons and photons at a per-cent level will either result in a discovery of a deviation from the SM, or imply that electroweak symmetry breaking is significantly tuned. This test of naturalness should be within the power of the proposed next-generation electron-positron collider such as the ILC.

A potential "loophole" in our argument is that the top partner contributions to the hgg and $h\gamma\gamma$ couplings may be canceled by other non-SM contributions to these vertices. In the case of multiple top partners, there is also the possibility of cancellations of the top partners' contributions to hgg and $h\gamma\gamma$ couplings among themselves. Typically, such cancellations should be regarded as accidental, and therefore unlikely. This was illustrated with an example of a two top partner model in Section 2.4. The only example that we are aware of where the cancellation of the top partner contributions to hgg and $h\gamma\gamma$ happens for a reason that seems inherent to the structure of the theory and not accidental is the model studied in Ref. [48, 64, 65]. However, the composite nature of the Higgs in that model implies large tree-level deviations of the Higgs couplings to W and Z bosons, and therefore it will still not escape detection via measurements of Higgs couplings.

So far, naturalness of the electroweak scale has been mainly probed through

direct searches for the top partners, which will of course continue in the next decade. We emphasize the complementarity between this program and the test of naturalness proposed here. The Higgs couplings test does not suffer from the well-known loopholes which plague direct searches (*e.g.* special spectra or R-parity violation). At the same time, there seems to be no reason for models where the deviations of hgg and $h\gamma\gamma$ are suppressed, for whatever reason, to pose unusual difficulties for direct searches. Taken together, the two programs will provide a powerful and robust test of naturalness.

In summary, we believe that the test of naturalness proposed here provides a compelling motivation for the future program of precision Higgs coupling measurements. We hope that this program will be realized in the coming years.

Acknowledgments

We would like to thank Christophe Grojean and Alfredo Urbano for useful discussions. This research is supported by the U.S. National Science Foundation through grant PHY-0757868 and CAREER grant PHY-0844667. NRL is supported by NSERC of Canada. MF would like to thank GGI for their hospitality during the completion of this work.

Note Added:

As we were completing this manuscript, Ref. [66] appeared on the `arXiv.org` in which similar ideas were explored.

CHAPTER 3

SPIN-ONE TOP PARTNER: PHENOMENOLOGY

Cai, Cheng, and Terning (CCT) suggested a model in which the left-handed top quark is identified with a gaugino of an extended gauge group, and its superpartner is a spin-1 particle. We perform a phenomenological analysis of this model, with a focus on the spin-1 top partner, which we dub the "swan". We find that precision electroweak fits, together with direct searches for Z' bosons at the LHC, place a lower bound of at least about 4.5 TeV on the swan mass. An even stronger bound, 10 TeV or above, applies in most of the parameter space, mainly due to the fact that the swan is typically predicted to be significantly heavier than the Z'. We find that the 125 GeV Higgs can be easily accommodated in this model with non-decoupling D-terms. In spite of the strong lower bound on the swan mass, we find that corrections to Higgs couplings to photons and gluons induced by swan loops are potentially observable at future Higgs factories. We also briefly discuss the prospects for discovering a swan at the proposed 100 TeV pp collider. [1]

3.1 Introduction

Discovery of the Higgs boson brought into sharp focus the long-standing theoretical problem of the Standard Model (SM), the hierarchy problem. If the SM is the complete description of physics up to scale Λ, radiative corrections generate

[1] This paper was co-authored with Jack Collins, Bithika Jain and Maxim Perelstein; it was published in August 2014 by the Journal of High Energy Physics [67]

a contribution to the Higgs mass parameter of order $\Lambda/(4\pi)$. The Higgs mass parameter is now precisely known, $\mu = (126\text{ GeV})/\sqrt{2} \approx 90$ GeV. Unless unrelated contributions to μ cancel, we expect the scale of SM break-down Λ to be of order 1 TeV. This argument strongly motivates experimental searches for non-SM physics at the LHC energies, and an extensive program of such searches is ongoing.

The hierarchy argument does not uniquely fix the nature of new physics at scale Λ, but it does provide some important clues. Precision electroweak measurements constrain the scale at which generic strong-coupling extensions of the SM may become relevant to ~ 10 TeV or above. This indicates that the solution to the hierarchy problem must rely on weakly-coupled physics, unless significant fine-tuning is involved. All known weakly-coupled solutions to the hierarchy problem involve new particles at the scale $\Lambda \lesssim$ TeV. Loops of these particles introduce additional contributions to the Higgs mass parameter, which cancel the leading contribution of SM loops. Such cancellations can occur naturally due to symmetries; known examples are supersymmetry, shift symmetry, and gauge symmetry extended to models with extra compact dimensions of space. Each of these symmetries can be implemented in a variety of ways, leading to a large zoo of possible explicit models for non-SM physics at the TeV scale. Most of these models have a rich spectrum of new states, and their masses are typically extremely model-dependent, making it difficult to choose optimal targets for experimental searches. However, in all models, the particles canceling the loops of SM tops, the "top partners", play a special role. The large value of the top Yukawa in the SM implies that the top partners must be quite light, below a few hundred GeV, for the model to be natural, independent of model-building details. This makes top partners a particularly well-motivated target for the

LHC searches.

The conventional wisdom says that top partners fall into one of two classes: spin-0 partners, or "stops", if the hierarchy problem is solved by supersymmetry; and spin-1/2 partners, if it is solved by shift symmetry or higher-dimensional gauge symmetry. Both these possibilities are extensively covered by experimental searches. There is, however, an alternative possibility, which has so far received far less attention: a spin-1 top partner. An explicit model realizing this scenario was constructed by Cai, Cheng and Terning (CCT) in 2008 [6]. However, to date, no comprehensive study of phenomenology of this model has been performed. The goal of this paper is to rectify this omission.

The paper is organized as follows. We review the CCT model, emphasizing the aspects that will be germane for the discussion of phenomenology, in Section 3.2. We then discuss the two main sources of current constraints on the model, precision electroweak fits (Section 3.3) and direct searches for Z' bosons at the LHC (Section 3.4). In Section 3.5, we discuss how the 125 GeV Higgs boson can be accommodated in this model, and briefly discuss the degree of fine-tuning implied by the constraints. Section 3.6 discusses the deviations in the Higgs couplings to gluons and photons induced by the new particles of the CCT model, while Section 3.7 contains a brief sketch of the possible signatures of the model at a 100 TeV hadron collider. We conclude in Section 3.8, and relegate some of the details of the analysis to the Appendix.

	$SU(5)$	$SU(3)$	$SU(2)$	$U(1)_H$	$U(1)_V$	$U(1)_Y$
Q_i	$\mathbf{1}$	$\square$	$\square$	$\frac{1}{6}$	0	$\frac{1}{6}$
$\overline{u}_i$	$\mathbf{1}$	$\overline{\square}$	$\mathbf{1}$	$-\frac{2}{3}$	0	$-\frac{2}{3}$
$\overline{d}_i$	$\mathbf{1}$	$\overline{\square}$	$\mathbf{1}$	$\frac{1}{3}$	0	$\frac{1}{3}$
L_i	$\mathbf{1}$	$\mathbf{1}$	$\square$	$-\frac{1}{2}$	0	$-\frac{1}{2}$
$\overline{e}_i$	$\mathbf{1}$	$\mathbf{1}$	$\mathbf{1}$	1	0	1
H	$\square$	$\mathbf{1}$	$\mathbf{1}$	$\frac{1}{2}$	$\frac{1}{10}$	$\left(\frac{2}{3},\frac{1}{2}\right)$
$\overline{H}$	$\overline{\square}$	$\mathbf{1}$	$\mathbf{1}$	$-\frac{1}{2}$	$-\frac{1}{10}$	$\left(-\frac{2}{3},-\frac{1}{2}\right)$
Φ_3	$\square$	$\overline{\square}$	$\mathbf{1}$	$-\frac{1}{6}$	$\frac{1}{10}$	$\left(0,-\frac{1}{6}\right)$
Φ_2	$\square$	$\mathbf{1}$	$\overline{\square}$	0	$\frac{1}{10}$	$\left(\frac{1}{6},0\right)$
$\overline{\Phi}_3$	$\overline{\square}$	$\square$	$\mathbf{1}$	$\frac{1}{6}$	$-\frac{1}{10}$	$\left(0,\frac{1}{6}\right)$
$\overline{\Phi}_2$	$\overline{\square}$	$\mathbf{1}$	$\square$	0	$-\frac{1}{10}$	$\left(-\frac{1}{6},0\right)$

Table 3.1: Chiral superfields of the model, and their gauge quantum numbers. Here, $i = 1\ldots3$ is the flavor index.

3.2 Review of the Model

The model studied in this paper was proposed by Cai, Cheng and Terning (CCT) in [6]. In this section we will review the model.

3.2.1 Structure and Particle Content

The CCT model is a supersymmetric gauge theory, based on a gauge group $G = SU(5)\times SU(3)\times SU(2)\times U(1)_H\times U(1)_V$. The matter superfields of the model, and their gauge quantum numbers, are listed in Table 1.The superpotential has the form

$$\begin{aligned} W &= y_1 Q_3\Phi_3\overline{\Phi}_2 + \mu_3\Phi_3\overline{\Phi}_3 + \mu_2\Phi_2\overline{\Phi}_2 + y_2\overline{u}_3 H\overline{\Phi}_3 + \mu_H H\overline{H} \\ &+ \frac{Y_{Uij}}{M_F}Q_i\overline{u}_j\overline{\Phi}_2 H + \frac{Y_{Dij}}{M_F}Q_i\overline{d}_j\Phi_2\overline{H} + \frac{Y_{Eij}}{M_F}L_i\overline{e}_j\Phi_2\overline{H}, \end{aligned} \tag{3.1}$$

where $i, j = 1\ldots3$ are flavor indices. In addition, one must also add soft SUSY-breaking terms generated at some messenger scale Λ. With the usual motiva-

tion of the hierarchy problem, we assume that all soft masses are around the TeV scale; their precise values will not be important for most of our discussion. As will be described in more detail below, SUSY breaking triggers gauge symmetry breaking by causing the four link fields, $\Phi_{2,3}$ and $\overline{\Phi}_{2,3}$, to acquire vacuum expectation values (vevs) of the form

$$\langle\Phi_3\rangle = \begin{pmatrix} f_3 & 0 & 0 & 0 & 0 \\ 0 & f_3 & 0 & 0 & 0 \\ 0 & 0 & f_3 & 0 & 0 \end{pmatrix}, \qquad \langle\overline{\Phi}_3\rangle^T = \begin{pmatrix} \overline{f}_3 & 0 & 0 & 0 & 0 \\ 0 & \overline{f}_3 & 0 & 0 & 0 \\ 0 & 0 & \overline{f}_3 & 0 & 0 \end{pmatrix},$$
$$\langle\Phi_2\rangle = \begin{pmatrix} 0 & 0 & 0 & f_2 & 0 \\ 0 & 0 & 0 & 0 & f_2 \end{pmatrix}, \qquad \langle\overline{\Phi}_2\rangle^T = \begin{pmatrix} 0 & 0 & 0 & \overline{f}_2 & 0 \\ 0 & 0 & 0 & 0 & \overline{f}_2 \end{pmatrix}. \tag{3.2}$$

Given their connection with SUSY breaking, we assume that all f's are at roughly the same scale, $f \sim$ TeV; we will discuss experimental constraints on f's in detail later in this paper. This pattern of vevs breaks G to $G_{\rm SM} = SU(3)_c \times SU(2)_L \times U(1)_Y$, with the $SU(3)_c \times SU(2)_L$ identified with the diagonal linear combination of the $SU(3) \times SU(2)$ subgroup of $SU(5)$, and the additional $SU(3) \times SU(2)$ factor in G. The unbroken hypercharge $U(1)_Y$ is given by the linear combination of the diagonal generator T_{24} of $SU(5)$ and the two explicit $U(1)$ factors in G: $Y = \frac{1}{\sqrt{15}}T_{24} + H + V$. The SM gauge couplings at the scale f are related to the G couplings (denoted by hats):

$$\frac{1}{g_{2,3}^2} = \frac{1}{\hat{g}_{2,3}^2} + \frac{1}{\hat{g}_5^2}, \qquad \frac{1}{g_Y^2} = \frac{1}{\hat{g}_H^2} + \frac{1}{\hat{g}_V^2} + \frac{1}{15\hat{g}_5^2}. \tag{3.3}$$

Examining the matter field quantum numbers under $G_{\rm SM}$, it is easily seen that the model contains all of the familiar matter content of the MSSM. In particular, the fields Q_i, $\bar{u}_i$, $\bar{d}_i$, L_i and $\bar{e}_i$ are directly identified with the corresponding MSSM fields, with the exception of the third-generation quarks which require special treatment. The two Higgs fields of the MSSM, H_d and H_u, are embedded in the

H and $\overline{H}$ fields, along with the (non-MSSM) color triplets and anti-triplets $\overline{T}^c$ and $\overline{T}$:

$$H = \begin{pmatrix} \overline{T}^c \\ H_u \end{pmatrix}, \qquad \overline{H} = \begin{pmatrix} \overline{T} \\ H_d \end{pmatrix}. \tag{3.4}$$

The last four terms of the superpotential (3.1) then reproduce the full MSSM superpotential. In particular, SM quark and lepton Yukawa couplings are of order f/M_F, and can naturally be small if there is a hierarchy between these scales.

The model also has a rich spectrum of non-MSSM fields. These are listed in Table 2, along with their $G_{\rm SM}$ quantum numbers and R parity. Since SUSY breaking and $G \to G_{\rm SM}$ breaking occur at roughly the same scale, in this case we list each field and its superpartner separately. Note that the conserved R parity in the CCT model, which plays the same role as the usual R parity in the MSSM, is a convolution of a "global" R parity which commutes with all gauge transformations, and a "twist" transformation, which acts on the $SU(5)$ multiplets as $P_{\rm twist} = {\rm diag}(-1,-1,-1,1,1)$. The twist is required because the scalar components of the H and $\bar{H}$ multiplets must be assigned opposite R-parities, $+1$ for the Higgs and -1 for the $\overline{T}$ and $\overline{T}^c$.

Interestingly, some of the fields in Table 2 have the same quantum numbers as MSSM fields, allowing them to mix. In particular, there are three fields with the quantum numbers of the left-handed quark doublet Q, $(\mathbf{3},\mathbf{2},1/6)$: the "off-diagonal" $SU(5)$ gaugino λ, and the link field "inos" Φ_{2t} and $\bar{\Phi}_{3t}$. There are also three fields in the conjugate representation, $(\bar{\mathbf{3}},\mathbf{2},-1/6)$: $\bar{\lambda}$, $\bar{\Phi}_{3t}$ and Φ_{2t}. The mass matrix for these fields, before electroweak symmetry breaking (EWSB), is given in Table 3.3. Note that only Q_3 participates in the mixing due to the structure of the superpotential; more generally, we can always relabel the linear

Field	Spin	$SU(3)_c$	$SU(2)_L$	$U(1)_Y$	R-Parity	UV Multiplet	Mass Scale
$\Phi_{3S}, \overline{\Phi}_{3S}$ $\Phi_{2S}, \overline{\Phi}_{2S}$	0	**1**	**1**	0	+1	$\Phi_i, \overline{\Phi}_i$	f
$\Phi_{3A}, \overline{\Phi}_{3A}$	0	**Adj**	**1**	0	+1	$\Phi_3, \overline{\Phi}_3$	f
$\Phi_{2A}, \overline{\Phi}_{2A}$	0	**1**	**Adj**	0	+1	$\Phi_2, \overline{\Phi}_2$	f
$\widetilde{\overline{\Phi}}_{3t}, \widetilde{\Phi}_{2t}$	0	**3**	**2**	1/6	-1	$\Phi_2, \overline{\Phi}_3$	f
$\widetilde{\Phi}_{3t}, \widetilde{\overline{\Phi}}_{2t}$	0	$\overline{\mathbf{3}}$	**2**	-1/6	-1	$\Phi_3, \overline{\Phi}_2$	f
$\widetilde{\Phi}_{3S}, \widetilde{\overline{\Phi}}_{3S}$ $\widetilde{\Phi}_{2S}, \widetilde{\overline{\Phi}}_{2S}$	1/2	**1**	**1**	0	-1	$\Phi_i, \overline{\Phi}_i$	f
$\widetilde{\Phi}_{3A}, \widetilde{\overline{\Phi}}_{3A}$	1/2	**Adj**	**1**	0	-1	$\Phi_3, \overline{\Phi}_3$	f
$\widetilde{\Phi}_{2A}, \widetilde{\overline{\Phi}}_{2A}$	1/2	**1**	**Adj**	0	-1	$\Phi_2, \overline{\Phi}_2$	f
$\overline{\Phi}_{3t}, \Phi_{2t}$	1/2	**3**	**2**	1/6	+1	$\Phi_2, \overline{\Phi}_3$	f
$\Phi_{3t}, \overline{\Phi}_{2t}$	1/2	$\overline{\mathbf{3}}$	**2**	-1/6	+1	$\Phi_3, \overline{\Phi}_2$	f
$\widetilde{\overline{T}}$	0	$\overline{\mathbf{3}}$	**1**	-2/3	-1	$\overline{H}$	f
$\widetilde{\overline{T}^c}$	0	**3**	**1**	2/3	-1	H	f
$\overline{T}$	1/2	$\overline{\mathbf{3}}$	**1**	-2/3	+1	$\overline{H}$	v
$\overline{T}^c$	1/2	**3**	**1**	2/3	+1	H	f
λ	1/2	**3**	**2**	1/6	+1	$SU(5)$ gauginos	v
$\overline{\lambda}$	1/2	$\overline{\mathbf{3}}$	**2**	-1/6	+1	$SU(5)$ gauginos	f
$\widetilde{W}'$	1/2	**1**	**Adj**	0	-1	$SU(2)$, $SU(5)$ gauginos	f
$\widetilde{G}'$	1/2	**Adj**	**1**	0	-1	$SU(3)$, $SU(5)$ gauginos	f
$\widetilde{B}', \widetilde{B}''$	1/2	**1**	**1**	0	-1	$U(1)_H$, $U(1)_V$, $SU(5)$ gauginos	f
W'	1	**1**	**Adj**	0	+1	$SU(2)$, $SU(5)$ gauge fields	f
G'	1	**Adj**	**1**	0	+1	$SU(3)$, $SU(5)$ gauge fields	f
Z', Z''	1	**1**	**1**	0	+1	$U(1)_H$, $U(1)_V$, $SU(5)$ gauge fields	f
$\vec{Q}$	1	**3**	**2**	1/6	-1	$SU(5)$ gauge fields	f

Table 3.2: Field content after the UV symmetry breaking; all entries with spin 0 correspond to complex scalar fields. The MSSM fields are not included in this table.

combination of the quark doublet fields which couples to $\Phi_3\bar{\Phi}_2$ as Q_3. Because the mass matrix has four columns but only three rows, there will always be a linear combination of Q-like fields which will be massless at this level, acquiring a mass through ESWB only. We identify this field with the third generation quark doublet of the SM, Q_3^{SM}. The key idea of the CCT model is that for a certain

	λ	Φ_{2t}	$\overline{\Phi_{3t}}$	Q_3
$\overline{\lambda}$	M_5	$\hat{g}_5 f_2$	$\hat{g}_5 \overline{f}_3$	0
Φ_{3t}	$\hat{g}_5 f_3$	0	μ_3	$y_1 \overline{f}_2$
$\overline{\Phi}_{2t}$	$\hat{g}_5 \overline{f}_2$	μ_2	0	$y_1 f_3$

Table 3.3: Mass matrix for fermions in the $(\mathbf{3}, \mathbf{2}, 1/6)$ (and conjugate) sector.

range of parameters, Q_3^{SM} is predominantly the gaugino λ. If that's the case, top-loop contribution to the Higgs mass must be canceled by its superpartner, a spin-1 ("swan") gauge boson $\vec{Q}$. This occurs if [6]

$$\begin{aligned} M_5 &\ll \hat{g}_5 f_2, \quad \hat{g}_5 f_3 \ll \mu_3, \quad \hat{g}_5 f_3 \ll \hat{g}_5 \overline{f}_2, \\ \hat{g}_5 \overline{f}_2 &\ll \mu_2, \quad \hat{g}_5^2 \frac{f_2 \overline{f}_2}{M_5 \mu_2} \approx 1, \quad \hat{g}_5 \lesssim y_1. \end{aligned} \tag{3.5}$$

We will assume throughout this paper that these conditions are realized. Another sector in which mixing occurs is the fields with the quantum numbers $(\bar{\mathbf{3}}, \mathbf{1}, -2/3)$: $\bar{u}$ and $\bar{T}$. One of their linear combinations gets a mass of order f, while the other remains massless until EWSB, and is identified with the SM right-handed top. Generating an order-one top Yukawa requires that the massless combination be predominantly $\overline{T}$; the condition for this is

$$\mu_H \ll y_2 \overline{f}_3. \tag{3.6}$$

The dominant coupling of the SM top to the Higgs comes from the $SU(5)$ gaugino-sfermion-fermion interaction of the field $\overline{H}$:

$$- \sqrt{2} \hat{g}_5 \overline{H}^* \left(-T^{a*} \lambda_5^a\right) \widetilde{\overline{H}} \supset \hat{g}_5 H_d^* \lambda \overline{T}. \tag{3.7}$$

Since $\hat{g}_5$ can be $O(1)$ while the other Yukawa couplings in Eq. (3.1) are suppressed by the ratio f/M_F, this explains the mass splitting between the top and the other quarks. The down-type third generation singlet is still $\overline{d}_3$, just like in the MSSM, so the bottom quark still gets its mass from the superpotential

Yukawas. From now on we will assume that the gaugino fraction of the third generation doublet is very close to unity, i.e. $\langle Q_3^{SM}|\lambda\rangle \approx 1$. Note that this equality cannot be exact without forcing the bottom quark's mass to vanish since it is proportional to $\left|\langle Q_3^{SM}|Q_3\rangle\right| \leq \sqrt{1-\left|\langle Q_3^{SM}|\lambda\rangle\right|^2}$. Still, assuming that the deviation of $\langle Q_3^{SM}|\lambda\rangle$ from unity is small, the gauge coupling $\hat{g}_5$ must satisfy

$$\hat{g}_5 = \frac{\sqrt{2}m_t}{v\cos\beta} \approx \sqrt{1+\tan^2\beta}\,, \tag{3.8}$$

where m_t is the top mass, $v = \sqrt{v_u^2+v_d^2} = 246$ GeV, and β is defined through the usual MSSM relationship $\tan\beta \equiv v_u/v_d$. With this result, the first of Eqs. (3.3) uniquely fixes $\hat{g}_2$ and $\hat{g}_3$ in terms of $\tan\beta$, while the second one reduces to

$$\frac{1}{g_Y^2}(1-\epsilon) = \frac{1}{\hat{g}_H^2} + \frac{1}{\hat{g}_V^2}, \tag{3.9}$$

where

$$\epsilon = \frac{g_Y^2}{15\hat{g}_5^2} \approx \frac{8\cdot 10^{-3}}{1+\tan^2\beta}. \tag{3.10}$$

Thus, requiring that the model reproduce the SM gauge couplings and the top Yukawa leaves only two independent parameters in the gauge sector: $\tan\beta$ and the $U(1)$-sector mixing angle

$$\theta = \arctan\left(\frac{\hat{g}_V}{\hat{g}_H}\right). \tag{3.11}$$

3.2.2 Gauge Boson Spectrum

The model contains several additional gauge bosons, which will be especially important for the analysis of this paper for two reasons. First, as already mentioned, one of them, the swan $\vec{Q}$, is largely responsible for canceling the quadratically divergent contribution of the SM top loop to the Higgs mass. Second,

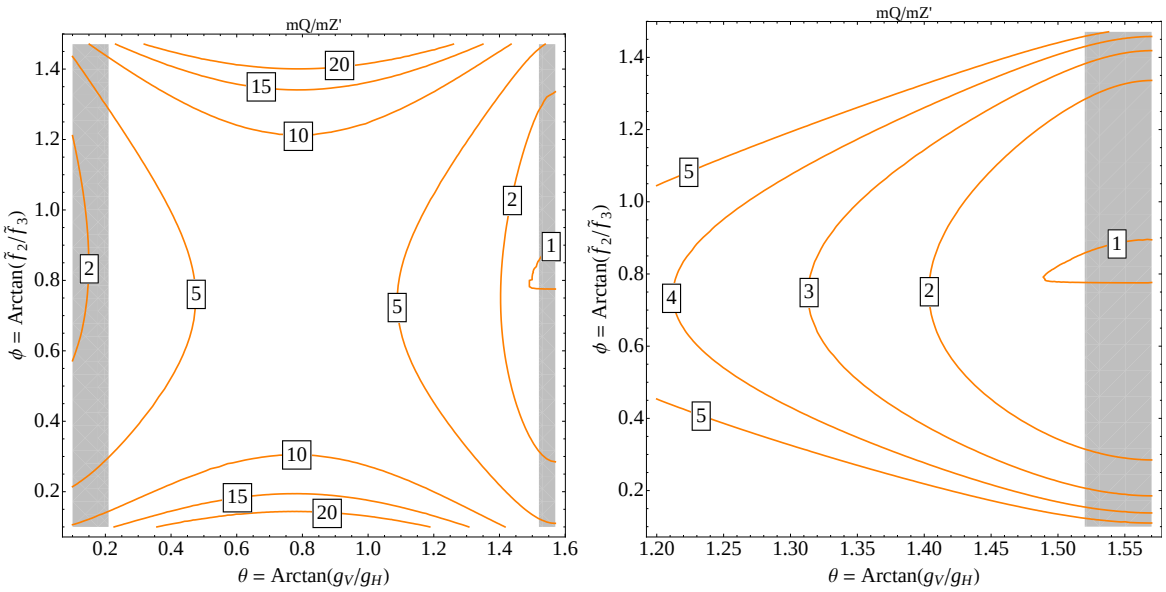

Figure 3.1: Ratio of the masses of the spin-1 top partner ("swan") and the lightest Z'. Left panel: full parameter space (gray regions indicate regions where one of the gauge couplings becomes non-perturbative). Right panel: the region where the ratio is minimized. In both plots, $\tan\beta = 0.95$; the ratio scales as $\sqrt{1+\tan^2\beta}$.

the extra $U(1)$ gauge bosons are responsible for the strongest experimental constraints on the model parameter space. The swan mass is given by

$$m_{\vec{Q}}^2 = \hat{g}_5^2\left(\widetilde{f}_2^2 + \widetilde{f}_3^2\right), \tag{3.12}$$

where we defined

$$\widetilde{f}_{2,3} = \frac{f_{2,3}^2 + \bar{f}_{2,3}^2}{2}. \tag{3.13}$$

Requiring that the left-handed top quark is predominantly a gaugino requires $f_3 \ll \bar{f}_2$, as mentioned above; however, no particular hierarchy between $\bar{f}_3$ and f_2 is required, so the scales $\widetilde{f}_2$ and $\widetilde{f}_3$ are essentially independent parameters. We find it convenient to define

$$\widetilde{f} = \sqrt{\widetilde{f}_2^2 + \widetilde{f}_3^2}, \quad \phi = \arctan\frac{\widetilde{f}_2}{\widetilde{f}_3}. \tag{3.14}$$

With this notation, the swan mass is simply

$$m_{\vec{Q}}^2 = \hat{g}_5^2 \widetilde{f}^2 \approx (1 + \tan^2\beta)\widetilde{f}^2. \tag{3.15}$$

The mass of the lightest extra $U(1)$ gauge boson, the Z', is given by

$$m_{Z'}^2 \approx 2g_Y^2 \frac{\csc^2 2\theta \sin^2 2\phi}{5 - \cos 2\phi}\, \widetilde{f}^2, \tag{3.16}$$

where corrections of order ϵ and $v^2/\widetilde{f}^2$ have been dropped. (The complete spectrum of the $U(1)$ gauge bosons is given in Appendix A.) Since $g_Y \approx 0.3$, the swan is generally significantly heavier that the Z'; see Fig. 3.1. We will see below that this results in very strong experimental lower bounds on the swan mass.

For completeness, we also list the masses of the heavy partners of the gluon and the charged W bosons:

$$m_{G'}^2 = 2\left(\hat{g}_3^2 + \hat{g}_5^2\right)\widetilde{f}_3^2 \approx \frac{2g_3^2(1 + \tan^2\beta)\cos^2\phi}{1 + \tan^2\beta - g_3^3}\, \widetilde{f}^2, \tag{3.17}$$

$$m_{W'}^2 = 2\left(\hat{g}_2^2 + \hat{g}_5^2\right)\widetilde{f}_2^2 \approx \frac{2g_2^2(1 + \tan^2\beta)\sin^2\phi}{1 + \tan^2\beta - g_2^3}\, \widetilde{f}^2. \tag{3.18}$$

3.2.3 Beta Functions and the Strong-Coupling Scale

The CCT model is an effective theory, since some of its gauge groups are not asymptotically free and their gauge couplings hit a Landau pole at a finite energy scale. At that scale, the model has to be either embedded into a larger structure, providing a UV completion, or else a non-perturbative description of the dynamics is required. Defining the one-loop beta function as

$$\beta_i \equiv \mu \frac{dg_i}{d\mu} = -\frac{g_i^3}{16\pi^2} b_i, \tag{3.19}$$

we find the coefficients

$$b_5 = 9\,, b_3 = -2\,, b_2 = -5\,, b_H = -\frac{40}{3}\,, b_V = -\frac{3}{5}\,. \tag{3.20}$$

With the exception of $SU(5)$, all other factors in G are not asymptotically free. We estimate the strong-coupling scale Λ_i for each group with the condition $g_i(\Lambda_i) = \beta_i$, or equivalently $b_i g_i^2/(16\pi^2) = 1$; this yields

$$\Lambda_i = f_i \exp\left[\frac{2\pi}{|b_i|\alpha_i(f)} - \frac{1}{2}\right], \tag{3.21}$$

where f_i is the scale where the gauge group associated with each gauge coupling is broken.

The parameters in the gauge sector of the theory are restricted by perturbativity requirements. For the asymptotically free $SU(5)$ coupling, we demand $b_5\hat{g}_5^2/(16\pi^2) \leq 1$ at the symmetry-breaking scale f; for the other couplings, we require $\Lambda_i/f \gtrsim 5$. This yields

$$0.8 \lesssim \tan\beta \lesssim 4.0, \quad 0.2 \lesssim \sin\theta \lesssim 0.99. \tag{3.22}$$

The bounds on $\tan\beta$ should be compared to the case of the MSSM, where the relationship analogous to Eq. (3.8) is $y_t = \frac{\sqrt{2}m_t}{v\sin\beta}$ and imposes only the much weaker constraints $0.3 \lesssim \tan\beta \lesssim 150$. The fact that $\tan\beta$ is constrained to lie close to 1 will tend to suppress the Higgs mass, since at tree-level and in the decoupling limit it is proportional to $\cos 2\beta$; this will be discussed in Section 3.5.

3.3 Precision Electroweak Constraints

As described in the previous section, the CCT model extends the SM gauge group and introduces additional R-even gauge bosons, W' and Z'. These gauge bosons generically mix with the SM Z and W, leading to deviations of their properties from the SM predictions. In addition, tree-level exchanges of W' and Z' induce effective four-fermion interactions not present in the SM. Such effects

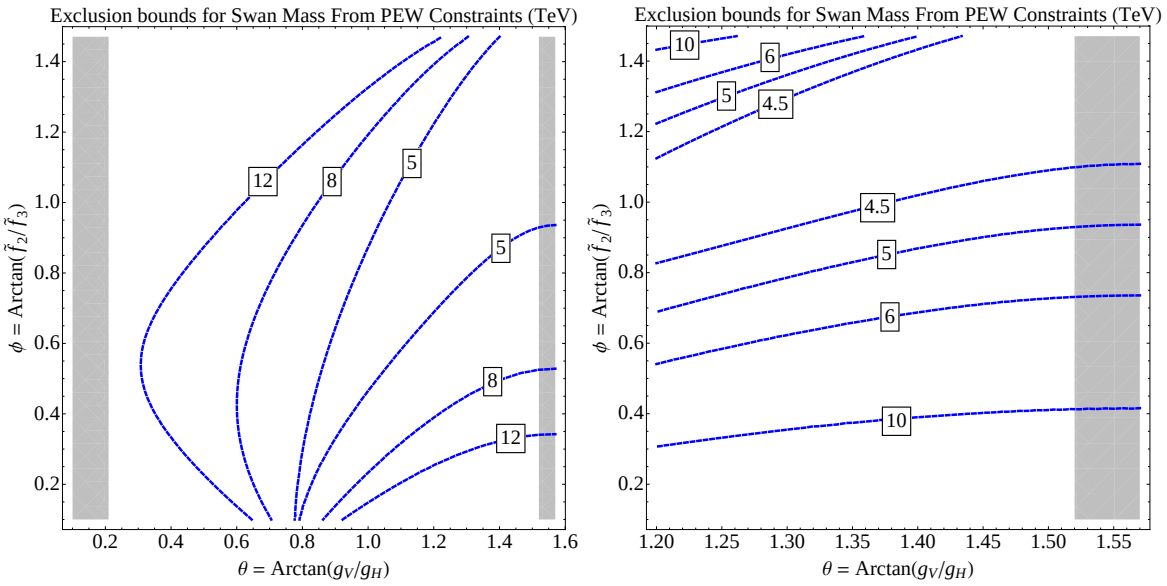

Figure 3.2: Lower bound on the swan mass (in TeV) from precision electroweak constraints. Left panel: full parameter space (gray regions indicate regions where one of the gauge couplings becomes non-perturbative). Right panel: the region where the constraint is minimized. In both plots, $\tan\beta = 0.95$; the bounds scale as $\sqrt{1+\tan^2\beta}$.

are tightly constrained by precision electroweak (PEW) measurements, which can be translated into restrictions on the parameter space of the CCT model. Before proceeding, let us note that while the CCT model predicts many new states at the TeV scale (see Table 3.2.1), it is easy to see that the PEW constraints are dominated by the W' and Z'. Most of the other fields do not contribute to PEW observables at tree level at all, either due to negative R-parity or, as in the case of vector-like fermions in the top sector and the heavy partner of the gluon, due to the structure of their couplings to the SM. The only states that do make a tree-level contribution are the scalars from link fields, which however only have suppressed couplings to light fermions of order v/M_F. We will ignore such contributions.

It is well known that the effect of Z' and W' bosons on PEW observables can be cast in terms of the oblique parameters S, T and U [68, 69, 70, 71]. Evaluating the T parameter in the CCT model yields[2]

$$\alpha T = \left[\frac{3}{4} \frac{\left((1-\epsilon)\cos^2\theta + \epsilon\right)^2}{\cos^2\phi} + \frac{1}{8} \frac{((1-\epsilon)\cos 2\theta - 4\epsilon)^2}{\sin^2\phi} \right] \left(\frac{v}{\widetilde{f}}\right)^2 . \tag{3.23}$$

Both S and U parameters are not generated at order $(v/\widetilde{f})^2$. The leading contributions to these parameters, up to $O(\epsilon)$ corrections, are given by

$$\begin{aligned} U &= \left(\frac{\cos^2\theta_W}{2\alpha}\right)\left(\frac{9\sin^2\theta\cos^6\theta}{2\cos^4\phi} + \frac{\sin^2 4\theta}{32\sin^4\phi} + \frac{3\sin^2\theta\cos 2\theta\cos^4\theta}{\sin^2\phi\cos^2\phi}\right)\left(\frac{v}{\widetilde{f}}\right)^4 ; \\ S &= -U - \frac{\sin^2\theta_W}{16\alpha}\,\frac{1}{\sin^4\phi}\,x(1+x)^{-3}\left(\frac{v}{\widetilde{f}}\right)^4 , \end{aligned} \tag{3.24}$$

where $x = (g_2/\hat{g}_5)^2 \approx g_2^2(1+\tan^2\beta)^{-1}$.

The 95% c.l. PEW lower bound on the swan mass is shown in Figure 3.2. As expected, the bound is strongly dominated by the T parameter. (The current 95% c.l. bound on T, for $S \approx 0$, is $T \lesssim 0.12$ [73].) Here we fixed $\tan\beta = 0.95$, close to the low end of the allowed range; the bound is stronger for larger values of $\tan\beta$, scaling as $\sqrt{1+\tan^2\beta}$. We find that the lowest possible bound occurs when $\widetilde{f_2} > \widetilde{f_3}$ and $\hat{g}_V \gg \hat{g}_H$, and it is roughly given by

$$m_{\vec{Q}} \gtrsim 4.5 \text{ TeV}. \tag{3.25}$$

Since swans need to be pair-produced in proton collisions due to their negative R-parity, this bound effectively puts them out of reach of the direct LHC searches. It also implies significant fine-tuning in the EWSB, as will be discussed in section 3.5.

Additional contributions to PEW observables may be generated by strongly-coupled physics in the ultraviolet (UV), and in a generic UV completion, the

[2]Oblique parameters in the CCT model have been previously computed in Ref. [72].

strong-coupling scale must be above ~ 10 TeV to avoid conflict with experiment. Bounds on the perturbative contribution to the T parameter, together with the parameter space constraints (3.22), ensure that such non-perturbative contributions are negligible throughout the viable parameter space, with the possible exception of the far upper-right corner of the plots in Fig. 3.2, where the $SU(3)$ gauge group may become strongly coupled below 10 TeV. Since $SU(3)$ is not part of the electroweak gauge group, this by itself does not imply additional contributions to PEW observables at the same scale; they may or may not be induced, depending on the nature of the UV completion. In any case, this caveat only affects a small corner of the parameter space, and the basic conclusions of the perturbative analysis remain valid.

3.4 Direct Searches at the LHC

Further bounds on the model parameter space come from direct searches at the LHC. Conventional SUSY searches place bounds on many of the R-odd states, which are also present in the MSSM spectrum. In the MSSM, assuming a spectrum with a weakly interacting lightest R-odd particle, and large mass gaps between this particle and colored R-odd states, current LHC bounds require $m_{\widetilde{G}} \gtrsim 1.2 - 1.4$ TeV for gluinos, $m_{\widetilde{Q}} \gtrsim 0.8$ TeV for squarks of first two generations, and $m_{\widetilde{t}} \gtrsim 0.7$ TeV for stops/sbottoms. The bounds in the CCT model can be modified due to the presence of additional states with the quantum numbers of gluinos and stops, $\widetilde{G}'$, $\widetilde{\bar{T}}$, and $\widetilde{\bar{T}}'$. These can induce additional cascade decays, strengthening the bounds somewhat; however, we do not expect a major qualitative change. It should also be noted that while the superpartner masses are generally expected to be at the scale f, the precise relation between them is

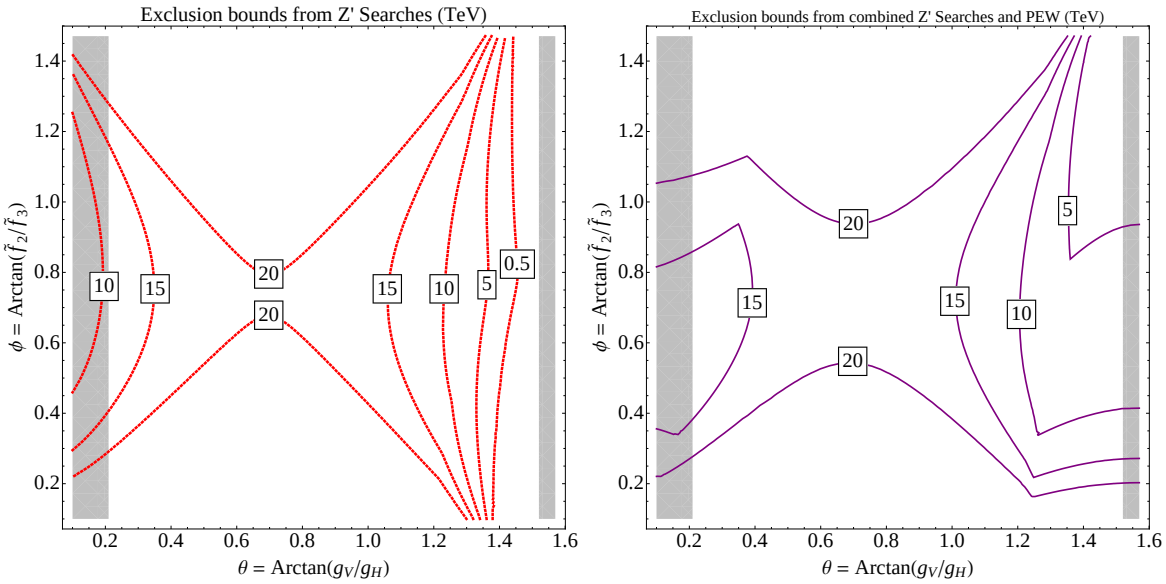

Figure 3.3: Lower bounds on the swan mass (in TeV) from direct searches for the Z' at the LHC (left panel) and the combination of direct search and precision electroweak constraint (right panel). In both plots, $\tan\beta = 0.95$; the bounds scale as $\sqrt{1 + \tan^2\beta}$.

model-dependent, since the details of SUSY breaking come into play. On the other hand, searches for the R-even states, in particular extra gauge bosons, in many cases have higher reach, since these states can be produced singly, and can be described in terms of just a small number of parameters, as explained in Section 3.2. With this motivation, we investigate these bounds in detail in this section.

The strongest bounds come from searches for Z' gauge bosons, in particular in the $Z' \to \mu^+\mu^-$ channel. We incorporated the relevant couplings of the CCT model (listed in Appendix 3.9) into the `MadGraph/MadEvent 5` event generator [74], and computed the cross section of the process $pp \to Z' \to \mu^+\mu^-$ at the $\sqrt{s} = 8$ TeV LHC as a function of the Z' mass. We then used the cross section bound presented by the CMS collaboration [75], based on the full 20 fb^{-1} data

set collected at LHC-8, to constrain the model parameter space. The resulting bound on the swan mass, for $\tan\beta = 0.95$, is shown in Fig. 3.3 (left panel). (As for precision electroweak, the direct search bound on the swan mass scales as $\sqrt{1+\tan^2\beta}$, so the bounds in Fig. 3.3 become stronger for larger $\tan\beta$.) Generically, the bounds on the swan mass are quite high, above 10 TeV in most of the parameter space. This is stronger than the PEW bound. However, the direct search bound is weakened significantly in the region $g_V \gg g_H$, where the Z' couplings to fermions are suppressed. In this region, the PEW constraint dominates; the combined bound from PEW and direct searches is presented in Fig. 3.3 (right panel). Overall, the lowest bound on $m_{\vec{Q}}$ found in the PEW analysis, about 4.5 TeV, remains unchanged.

In addition to Z', the model contains two more electrically neutral gauge bosons: Z'', the heaviest of the mass eigenstates composed of $U(1)_H$, $U(1)_V$ and T_{24} gauge bosons; and W'^3, the heavy mass eigenstate composed of the diagonal $SU(2)$ and $SU(2)' \in SU(5)$ gauge bosons. Since $\hat{g}_5$ is larger than the other gauge couplings, both Z'' and W'^3 are significantly heavier than the Z' throughout the parameter space. Furthermore, for the same reason, both Z'' and W'^3 are dominated by their $SU(5)$ components, and since light fermions are not charged under the $SU(5)$, their production cross sections are suppressed. As a result, we find that including these states in the analysis does not improve the bounds derived by considering only the lightest Z'. Likewise, massive electrically charged gauge bosons W' and color-octet gauge bosons G' do not yield relevant bounds.

3.5 Higgs Mass and EWSB Fine-Tuning

Just as in the MSSM, the superpotential of the CCT model, Eq. (3.1), does not contribute to the Higgs quartic coupling, and the D-term contribution by itself is far too small for compatibility with a 125 GeV Higgs. The quartic is enhanced by the RG evolution between the SUSY breaking scale $\Lambda_{\rm susy}$, and the electroweak scale. To understand whether this enhancement is sufficient to produce a viable Higgs mass, we evolve the weak-scale Higgs quartic $\lambda(M_t)$, inferred from the data, up to the scale $\Lambda_{\rm susy}$, and compare it with the SUSY prediction at that scale:[3]

$$\lambda_{\rm susy} = \frac{g_2^2(\Lambda_{\rm susy}) + g_Y^2(\Lambda_{\rm susy})}{8} \cos^2 2\beta. \tag{3.26}$$

Assuming that all non-SM particles have masses at or above $\Lambda_{\rm susy}$, we use the SM beta functions at two-loop order, and the values of SM couplings at the weak scale given in Ref. [76], to obtain $\lambda_{\rm SM}(\Lambda_{\rm susy})$. We find that accommodating the 125 GeV Higgs in the minimal CCT model, with no additional contributions to the quartic, requires

$$\Lambda_{\rm susy} \gtrsim 100 \text{ TeV}. \tag{3.27}$$

This is clearly a much stronger constraint than the experimental bounds considered above, and a model with such a high SUSY-breaking scale would require a very significant amount of fine-tuning: very roughly, fine-tuning can be estimated as $(v/\Lambda_{\rm susy})^2 \sim 10^{-6}$. Moreover, for $\tan\beta \approx 1.0$, which is preferred from the point of view of the PEW and direct constraints, a much higher SUSY-breaking scale is required, since $\lambda_{\rm susy}$ is suppressed.

However, simple extensions of the minimal setup can easily alleviate this tension. For example, consider the scenario in which the gauge symmetry

[3]Our normalization for λ is such that the Higgs scalar potential in $V = -m^2 H^\dagger H + \lambda (H^\dagger H)^2$, where H is the Higgs doublet field. In this normalization, $\lambda_{\rm SM}(M_t) \approx 0.127$.

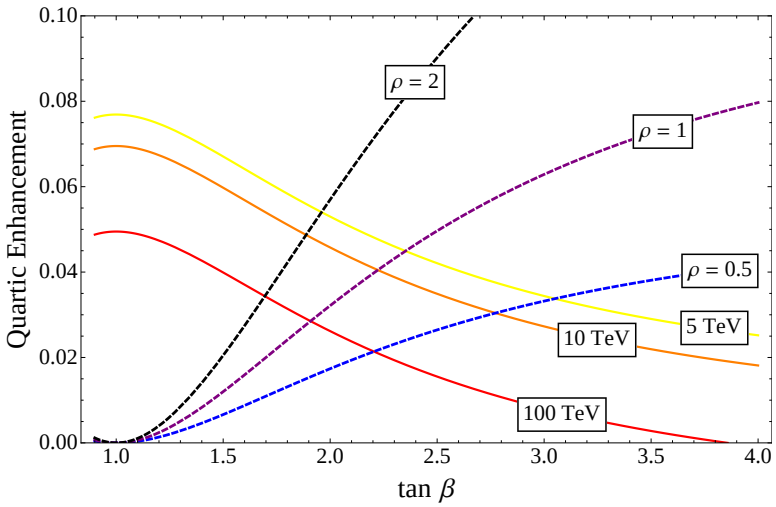

Figure 3.4: Solid lines: The difference δ between the value of the Higgs quartic $\lambda_{\rm SM}(\Lambda_{\rm susy})$ needed to accommodate the 125 GeV Higgs, and the value predicted by a SUSY theory with the SM gauge group. Top to bottom: $\Lambda_{\rm susy} = 5, 10, 100$ TeV. Dashed lines: The additional contribution to λ from non-decoupling D-terms possibly present in the CCT model. Top to bottom: $\rho = 2.0, 1.0, 0.5$. (For definition of ρ and other details, see Appendix 3.10.)

breaking occurs below the SUSY-breaking scale, $f_i < \Lambda_{\rm susy}$. In this case, $\lambda_{\rm susy}$ receives additional contributions from the D-terms associated with non-SM gauge generators, the "non-decoupling D-terms" [77, 78]. The non-decoupling D-terms in the CCT model were considered in Ref. [72]. They can be obtained as follows. Introduce additional superfields $A_{2,3}$ (in the adjoint representations of $SU(2)$ and $SU(3)$, respectively) and $S_{2,3}$ (both singlets under G), with a superpotential[4]

$$W_{\rm new} = \lambda_{S2} S_2 \Phi_2 \overline{\Phi}_2 + \lambda_{S3} S_3 \Phi_3 \overline{\Phi}_3 + \lambda_{A2} \overline{\Phi}_2 A_2^a \frac{\sigma^a}{2} \Phi_2 + \lambda_{A3} \overline{\Phi}_3 A_3^m G^m \Phi_3. \tag{3.28}$$

When the link fields Φ and $\bar{\Phi}$ acquire vacuum expectation values, F-terms for S are generated, inducing "hard" F-term SUSY-breaking and prevent the complete

[4]Our model of the non-decoupling D-terms differs slightly from Ref. [72] in that we include soft mass terms in the scalar potential, allowing for a simpler field content and superpotential. For details, see Appendix 3.10.

decoupling of the ultraviolet D-terms. The UV value of the Higgs quartic is modified as follows:

$$\lambda_{\rm susy}^{\rm NDDT} = \frac{\Delta_2 g_2^2(\Lambda_{\rm susy}) + \Delta_Y g_Y^2(\Lambda_{\rm susy})}{8} \cos^2 2\beta\,, \tag{3.29}$$

where Δ_2 and Δ_Y are order-one coefficients which can be calculated in terms of the superpotential couplings and soft SUSY-breaking terms. (For details, see Appendix 3.10.) In Fig. 3.4, we compare the size of the quartic correction required to accommodate a 125 GeV Higgs, defined as $\delta\lambda = \lambda_{\rm SM}(\Lambda_{\rm susy}) - \lambda_{\rm susy}$, with the non-decoupling D-term contribution for reasonable model parameters. It is clear that the D-term contribution can easily be large enough to provide a viable model with $\Lambda_{\rm susy}$ in the $5 - 10$ TeV range. Thus, we conclude that in the presence of non-decoupling D-terms, the 125 GeV Higgs does not place constraints beyond those already known from PEW fits and direct searches. The required fine-tuning is roughly of order 10^{-3}. The only problematic region is around $\tan\beta = 1$, where all D-term contributions to quartic vanish as $\cos^2 2\beta$. In this region, either a much higher value of $\Lambda_{\rm susy}$, or an alternative mechanism for raising the quartic (*e.g.* large threshold corrections), is required.

Note that the A fields introduced in this section will affect the β function coefficients, potentially shifting the location of Landau poles and modifying the constraints on the parameter space in Eq. (3.22). We find that the only effect this has is on the lower bound on $\tan\beta$, which is raised from 0.8 to 0.95. This does not have a significant effect on the precision electroweak and direct constraints on the model.

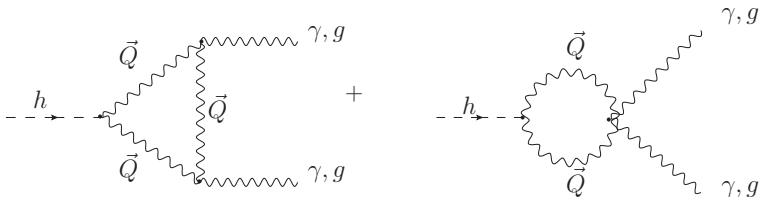

Figure 3.5: Swan contribution to Higgs couplings to gluons and photons, at the one-loop level.

3.6 Higgs Couplings to Photons and Gluons

Following the discovery of the Higgs boson, a multi-year program to precisely measure the Higgs couplings is envisioned [79]. The upcoming LHC experiments as well as, hopefully, experiments at a next-generation electron-positron Higgs factory [80, 81], will be able to measure many Higgs couplings with precision of $\sim 1\%$ or better. It is therefore worthwhile to study deviations from the SM predicted by models of new physics at the TeV scale.

In the CCT model, the corrections to Higgs couplings are of two types. First, since the full structure of the MSSM is reproduced, the Higgs sector is extended to a two-Higgs doublet model, leading to tree-level shifts in the Higgs couplings to gauge bosons and fermions. These effects have been already comprehensively studied in the MSSM [82]. More interesting are the corrections from new particles running in loops. In particular, it has been argued in Ref. [83, 84, 85, 28] that very generally, loops of top quark partners (*i.e.*, particles whose loops cancel the quadratic divergence in m_h^2 induced by the SM top loop) induce potentially observable shifts in the hgg and $h\gamma\gamma$ couplings.[5] The corrections from spin-0

[5]These two couplings are singled out because they are absent at tree level in the SM, making the new physics effects relatively more significant. Top partner loops may have other potentially observable effects, *e.g.* wavefunction renormalization corrections which may be measured in the $e^+e^- \to hZ$ process at Higgs factories [86].

and spin-1/2 top partners have been previously calculated. Here, we focus on the effect of the spin-1 top partner loops, shown in Fig. 3.5. We performed the calculation using the `Mathematica` implementation of the $h \to VV$ decay amplitudes for a generic gauge extension of the SM, described in [87] and available on the website `http://www.phy.syr.edu/ jhubisz/HIGGSDECAYS/`. To leading order in $(m_h/M_{\vec{Q}})^2$, we obtain the effective Lagrangian

$$\mathcal{L}_{h\gamma\gamma} = \frac{2\alpha}{9\pi v} C_\gamma h F_{\mu\nu} F^{\mu\nu}, \quad \mathcal{L}_{hgg} = \frac{\alpha_s}{12\pi v} C_g h G^a_{\mu\nu} G^{a\mu\nu}, \tag{3.30}$$

where F and G^a ($a = 1 \ldots 8$) are the SM $U(1)$ and $SU(3)$ field strength tensors, respectively, and the Wilson coefficients are

$$C_g = C_\gamma = \frac{21}{4} \frac{\hat{g}_5^2 v^2}{m_{\vec{Q}}^2}. \tag{3.31}$$

Here the normalization of C_g and C_γ is such that the SM top loop contribution, in the low-m_h limit, is 1. Note that, due to a large numerical coefficient, the swan induces a much larger deviation of the $hgg/h\gamma\gamma$ couplings from their SM values than either a spin-0 stop or a spin-1/2 top partner of the same mass. We find that even very strong bounds on the swan mass discussed above do not completely preclude a potentially observable deviation: a 5 TeV swan, at $\tan\beta = 1.0$, induces a fractional shift in the $hgg/h\gamma\gamma$ couplings of about 3%, which may be within a 3-sigma detection reach at the proposed e^+e^- Higgs factories.

The CCT model contains a large number of colored and/or electrically charged states at the same mass scale as the swan, and loops of those particles will in general contribute to the coefficients C_g and C_γ, modifying the predictions (3.31). The contributions of scalars and fermions can be computed using the Higgs low energy theorems [88, 89], while the spin-1 states other than the swan can be treated using the results of [87]. A comprehensive analysis of these effects is complicated by the large dimensionality of the parameter space. We

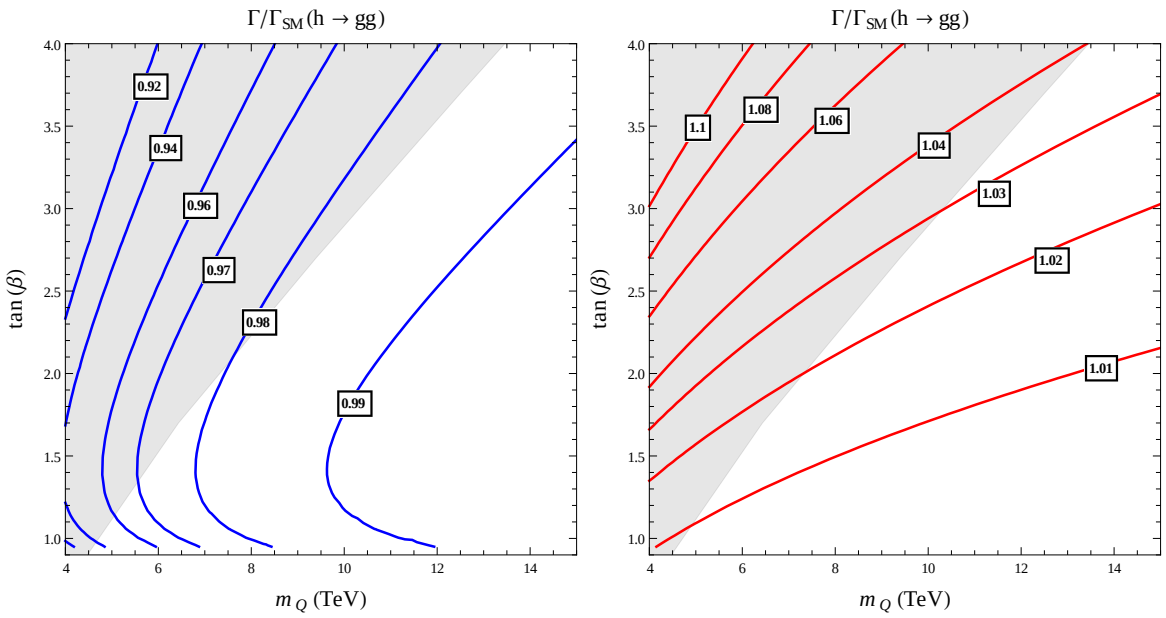

Figure 3.6: Fractional deviation in the hgg (left panel) and $h\gamma\gamma$ (right panel) couplings from the SM in the CCT model, as a function of the swan mass and $\tan\beta$. (See text for details on the values of other model parameters.) The shaded region is disfavored by precision electroweak constraints and direct LHC searches for a Z'.

will not attempt such an analysis here; instead, we illustrate the typical size of the overall contribution to C_g and C_γ with a two-dimensional plot, Fig. 3.6, where we vary the swan mass and $\tan\beta$ and fix all other parameters. (All parameters with dimension of mass are fixed at the scale $m_{\vec{Q}}$, with mild hierarchies imposed in some cases to ensure that the conditions (3.5) are satisfied and an acceptable Higgs mass is generated through non-decoupling D-terms.) In this slice of the parameter space, we find that deviations in the hgg coupling of about 5% are possible, while the maximum deviation in $h\gamma\gamma$ is about 4%. Such shifts may be within reach of the proposed e^+e^- Higgs factories.

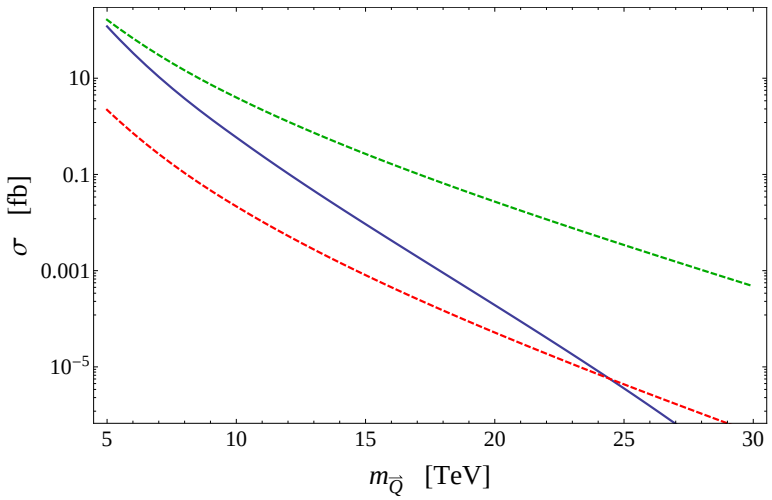

Figure 3.7: Swan production cross sections at a 100 TeV pp collider: $pp \to \vec{Q}\vec{Q}$ (blue), $\vec{Q}\widetilde{g}$ (green dashed), $\vec{Q}\widetilde{\chi}_1^0$ (red dashed).

3.7 Future Prospects for Direct Searches

Existing bounds on the swan mass, and the fact that swans must be pair-produced, preclude the possibility of direct swan production at the LHC. Of course, it may well happen that other particles in the CCT model, such as a Z' or some of the MSSM-like states, will be within the reach of the LHC-14. However, without a direct observation of the swan, it would be difficult to distinguish between this model and more conventional realizations of weak-scale supersymmetry. If a Z' is discovered, some indirect evidence can perhaps be obtained by measuring its couplings, which are predicted in the CCT model with few free parameters (see Appendix A). A much more direct and convincing test would have to await the direct discovery of the swan, and measurement of its spin. A next-generation pp collider with $\sqrt{s} = 100$ TeV, which is currently under discussion in the high-energy physics community, would provide an opportunity for such a direct discovery. As a first step to an estimate of the po-

tential of such a collider to search for swans, we computed the cross sections of swan pair-production, along with associated production with a gluino $\widetilde{g}$ and a neutralino $\widetilde{\chi}_1^0$. The analytic formulas for parton-level cross sections are collected in Appendix C. The cross sections for 100 TeV pp collisions are plotted in Fig. 3.7. Here we assumed $m_{\widetilde{g}} = 1$ TeV and $m_{\widetilde{\chi}_1^0} = 0.5$ TeV; the plotted associated production cross sections represent the maximum possible values, and would decrease if $m_{\widetilde{g}}/m_{\widetilde{\chi}_1^0}$ are increased. We used the `NNPDF2.3` NNLO parton distribution functions [90], including top quark pdf's for associated production, and set the renormalization/factorization scale to $Q^2 = (10 \text{ TeV})^2$. It is interesting to note that the large associated production cross sections are due to appreciable b and t content in the proton at this scale.

Swans within a broad mass range will be copiously produced in 100 TeV pp collisions. For example, if 3000 fb^{-1} of data is collected (the integrated luminosity assumed in the Snowmass study [91]), we expect that $\gtrsim O(100)$ swans would be produced in pair-production up to $m_{\vec{Q}} \approx 15$ TeV, and in association with gluinos up to $m_{\vec{Q}} \approx 25$ TeV (assuming $m_{\widetilde{g}} \ll m_{\vec{Q}}$). This suggests that direct reach of such an experiment for swan discovery can potentially extend into 10 – 20 TeV domain, although the actual reach depends on the swan decay chains, which will determine relevant backgrounds, kinematic cuts, *etc.* Once a swan is produced, its spin could be determined using the techniques proposed for top partner spin determination at the LHC, see e.g. [92]. Thus, a 100 TeV collider may be capable of directly demonstrating the existence of a spin-1 top partner.

3.8 Conclusions and Outlook

In this paper, we considered the phenomenology of the Cai-Cheng-Terning (CCT) model, in which the superpartner of the (left-handed) SM top quark is the spin-1 particle, the "swan". Our main result is that existing constraints from precision electroweak fits and direct LHC searches for a Z' place a very strong bound on the swan mass, which is required to be above at least 4.5 TeV, and in fact above 10 TeV in most of the parameter space. The primary reason for this bound is the tight relation between the swan mass and the mass of a neutral, R-even Z' boson, which is tightly constrained. The masses of the two bosons arise from the same symmetry breaking, and the structure of the gauge couplings of the CCT model induces an additional hierarchy, typically of a factor 5 – 10, between the swan and Z' masses.

The tight bounds on the swan mass imply that the models of this type would need to be quite fine-tuned if realized in nature, making them less appealing. It also precludes the possibility of a direct swan discovery at the LHC. It is interesting to note, however, that neither conclusion would hold in a model with a spin-1 top partner *not* accompanied a Z' whose mass arises from the same symmetry breaking, or in a model where a Z' is odd under an R parity. It would be interesting to construct such models. Even if a complete model proves hard to build, a phenomenological model with these features, analogous to minimal set-ups used for the spin-0 top partner ("natural SUSY" [93, 94]) and the spin-1/2 top partner (see *e.g.* [95]), would be potentially quite useful.

Acknowledgments

We would like to thank Christophe Grojean, Jay Hubisz, and especially Haiying Cai, for useful discussions. J.C., M.P. and N.R.L. are supported by the U.S. National Science Foundation through grant PHY-0757868. M.P. is also supported by CAREER grant PHY-0844667. B.J. thanks Cornell University for hospitality throughout the course of this work. B.J. is supported by the Department Of Energy under grant DE-FG02-85ER40237.

3.9 Appendix A: Masses and Couplings of Z' States

Compared to the MSSM, this model possesses three additional neutral, massive gauge bosons. Two of them are linear combinations of the UV gauge fields B_H, B_V, B_{24} obtained by diagonalizing the following quadratic terms:

$$6\widetilde{f_3^2}\left(\frac{\hat{g}_H}{6}B_H - \frac{\hat{g}_V}{10}B_V - \frac{\hat{g}_5}{\sqrt{15}}B_{24}\right)^2 + 4\widetilde{f_2^2}\left(\frac{\hat{g}_V}{10}B_V - \frac{\sqrt{15}}{10}\hat{g}_5 B_{24}\right)^2 . \tag{3.32}$$

The massless linear combination $B \equiv \frac{g_Y}{\hat{g}_H}B_H + \frac{g_Y}{\hat{g}_V}B_V + \frac{g_Y}{\sqrt{15}\hat{g}_5}B_{24}$ will be the gauge boson of the SM $U(1)_Y$ group; we refer to the other two eigenstates with non-vanishing masses as the Z' and Z'', in ascending order of masses. As discussed in section 3.2, it is convenient to re-express the parameters $\hat{g}_H$, $\hat{g}_V$, $\hat{g}_5$, $\widetilde{f_2}$, and $\widetilde{f_3}$ in terms of $\epsilon \equiv g_Y^2/15\hat{g}_5^2$, $\theta \equiv \arctan(\hat{g}_V/\hat{g}_H)$, $\widetilde{f^2} \equiv \widetilde{f_2^2} + \widetilde{f_3^2}$ and $\phi \equiv \arctan\left(\widetilde{f_2}/\widetilde{f_3}\right)$. In this parameterization, the mass of the Z' and Z'' can be written as:

$$m^2_{Z',Z''} = \frac{m^2_{\vec{Q}}}{20\,(1-\epsilon)}\left(A(\epsilon,\theta,\phi) \mp \sqrt{B(\epsilon,\theta,\phi)}\right) , \tag{3.33}$$

where $m^2_{\vec{Q}}$ is the squared mass of the swan and the A, B functions are given by:

$$A(\epsilon,\theta,\phi) \equiv 50\epsilon\csc^2\theta\cos^2\phi + 3\epsilon\sec^2\theta(\cos 2\phi + 5) - 2\,(1-\epsilon)(\cos 2\phi - 5) , \tag{3.34}$$

and,

$$\begin{aligned} B(\epsilon,\theta,\phi) &\equiv 2500\epsilon^2 \csc^4\theta\cos^4\phi + 9\epsilon^2\sec^4\theta\,(\cos 2\phi+5)^2 \\ &+ 100\epsilon\csc^2\theta\cos^2\phi\,(5\,(\epsilon+2)\cos 2\phi + 5\epsilon - 2) \\ &+ 3\epsilon\sec^2\theta\,(300\epsilon\cos 2\phi + (27\epsilon+98)\cos 4\phi + 177\epsilon - 2)\ . \end{aligned} \tag{3.35}$$

Since ϵ is typically $O(5)\times 10^{-3}$ (see Eq. (3.10)), we can obtain much simpler formulas by expanding to $O(\epsilon)$, in which case we can write the Z' mass as:

$$m_{Z'}^2 \approx 30 m_{\vec{Q}}^2 \epsilon \frac{\csc^2 2\theta \sin^2 2\phi}{5-\cos 2\phi} = 2 g_Y^2 \frac{\csc^2 2\theta \sin^2 2\phi}{5-\cos 2\phi}\,\widetilde{f^2}, \tag{3.36}$$

where the second equality was obtained by using $m_{\vec{Q}}^2 = \hat{g}_5^2\widetilde{f^2}$ and the definition of ϵ. For the Z'', we have:

$$m_{Z''}^2 \approx m_{\vec{Q}}^2\left(\frac{5-\cos 2\phi}{5}\right) + O(\epsilon)\ . \tag{3.37}$$

The couplings of the Z' to the light fermions of the SM will be given by

$$g_{Z'\bar{f}f} = \hat{g}_H \langle Z'|B_H\rangle\,(Q - T_3)\ , \tag{3.38}$$

where $\langle Z'|B_H\rangle$ is the amount of B_H contained in the Z' mass eigenstates. The couplings of the Z'' follows an analogous formula, with the replacement of $\langle Z'|B_H\rangle$ by $\langle Z''|B_H\rangle$. While explicit formulas for these coefficients are straightforward to compute, they are cumbersome and unenlightening. We note, however, that $\hat{g}_H\langle Z'|B_H\rangle = \dfrac{|g_Y \tan^{-1}\theta|}{\sqrt{15}} + O(\epsilon)$, which indicates that the Z' decouples from the light SM fermions in the large $\tan\theta$ region; this explains why the bounds on the Z' mass are weakest in this region of Fig. 3.3. The couplings of the Z' and Z'' to the third generation quarks will be different from Eq. (3.38) because these fermions are charged differently under the UV gauge group[6]. The coupling to

[6]The exception is the right-handed bottom quark b_R, whose coupling to the Z' follows Eq. (3.38)

the right-handed top is

$$g_{Z'\bar{t}_R t_R} = \frac{1}{2}\hat{g}_H\langle Z'|B_H\rangle - \frac{1}{10}\hat{g}_V\langle Z'|B_V\rangle - \frac{1}{\sqrt{15}}\hat{g}_5\langle Z'|B_{24}\rangle\,, \tag{3.39}$$

while the coupling to the third generation doublet of the SM, $Q_L^3 = (t_L, b_L)$ is

$$g_{Z'\bar{Q}_L^3 Q_L^3} = \sqrt{\frac{5}{12}}\hat{g}_5\langle Z'|B_{24}\rangle\,. \tag{3.40}$$

The couplings of the Z'' can once again be obtained by replacing $\langle Z'|B_i\rangle$ by $\langle Z''|B_i\rangle$ in the above.

3.10 Appendix B: Non-Decoupling D-Terms

The non-decoupling D-terms coefficients Δ_2 and Δ_Y were introduced in Section 3.5 as a way of enhancing the tree-level quartic of the Higgs at the scale Λ_{susy} to obtain the observed Higgs mass. Here we outline the derivation of these coefficients.

Combining the superpotential terms of Eqs. 3.1 and 3.28 to the usual soft SUSY breaking terms, we obtain the following potential for the link fields:

$$\begin{aligned} V_{link} &= \left(\mu_2^2 + m_2^2\right)\Phi_2\Phi_2^* + \left(\mu_2^2 + \overline{m}_2^2\right)\overline{\Phi}_2\overline{\Phi}_2^* + \left(\mu_3^2 + m_3^2\right)\Phi_3\Phi_3^* + \left(\mu_3^2 + \overline{m}_3^2\right)\overline{\Phi}_3\overline{\Phi}_3^* \\ &- b_2\left(\Phi_2\overline{\Phi}_2 + c.c.\right) - b_3\left(\Phi_3\overline{\Phi}_3 + c.c.\right) + y_1^2|\Phi_3\overline{\Phi}_2|^2 + \lambda_{S2}^2|\Phi_2\overline{\Phi}_2|^2 + \lambda_{S3}^2|\Phi_3\overline{\Phi}_3|^2 \\ &+ \lambda_{A2}^2|\overline{\Phi}_2^a\frac{\sigma^a}{2}\Phi_2|^2 + \lambda_{A3}^2|\overline{\Phi}_3^m G^m\Phi_3|^2 + (\text{D}-\text{terms})\,. \end{aligned} \tag{3.41}$$

Though the soft SUSY-breaking masses m_i^2 and $\overline{m}_i^2$ can in principle be independent from one another, we will make the simplifying assumption that they are identical. Note however that while this assumption greatly simplifies the following analysis, the theory possesses no symmetry that could make this equal-

ity exact and stable under radiative corrections, even if it is approximately realized at the messenger scale. Under this assumption then, we can derive simple formulas for the vevs from Eq. (3.41):

$$f_2^2 = \overline{f}_2^2 = \frac{b_2 - \left(\mu_2^2 + m_2^2\right)}{2\lambda_{S2}^2} ,$$
$$f_3^2 = \overline{f}_3^2 = \frac{b_3 - \left(\mu_3^2 + m_3^2\right)}{3\lambda_{S3}^2} . \tag{3.42}$$

We can shift the link fields by these vevs in Eq. (3.41) and compute the mass spectrum for the scalar components of the link sector. It is convenient to invert the formulas for the masses to express the parameters of the potential in terms of more physical quantities: the vevs f_2 and f_3, the masses of the two CP-odd singlets $m_{O_{2,3}}^2$, and the masses of the two CP-even singlets $m_{E_{2,3}}^2$. The relationship between the masses and the parameters of the potential in Eq. (3.41) is:

$$m_{O_{2,3}}^2 = 2b_{2,3} , \tag{3.43}$$
$$m_{E_2}^2 = 4f_2^2\lambda_{S2}^2 , \tag{3.44}$$
$$m_{E_3}^2 = 6f_3^2\lambda_{S3}^2 . \tag{3.45}$$

The effect of the aforementioned non-decoupling D-terms on the low-energy Higgs potential can be obtained by integrating out at tree-level the scalar fields that possess trilinear coupling to the Higgs bilinears. This will effectively modify the low-energy Higgs potential through the substitutions $g_Y \to \Delta_Y g_Y$, $g_2 \to \Delta_2 g_2$, where:

[7]

$$\Delta_2 = \left(1 + \frac{\rho_2}{2\hat{g}_2^2}\right) \times \left(1 + \frac{\rho_2}{2\left(\hat{g}_5^2 + \hat{g}_2^2\right)}\right)^{-1} ,$$
$$\Delta_Y = \frac{1 + N_2\rho_2 + N_3\rho_3 + N_{23}\rho_2\rho_3}{1 + D_2\rho_2 + D_3\rho_3 + D_{23}\rho_2\rho_3} , \tag{3.46}$$

[7] The coefficients Δ_2 and Δ_Y were previously computed in Ref. [72]. Our results are not fully in agreement, but the discrepancies would not affect the qualitative conclusions of Section 3.5.

with

$$\rho_2 \equiv \frac{m_{O2}^2 - m_{E2}^2}{f_2^2} = 2\left(\frac{m_2^2 + \mu_2^2}{f_2^2}\right), \qquad \rho_3 \equiv \frac{m_{O3}^2 - m_{E3}^2}{f_3^2} = 2\left(\frac{m_3^2 + \mu_3^2}{f_3^2}\right), \tag{3.47}$$

and the various $N_i(\theta, \epsilon)$, $D_i(\theta, \epsilon)$ coefficient functions are:

$$\begin{aligned}
N_2(\theta,\epsilon) &\equiv \left(\frac{1+15\epsilon}{2g_Y^2}\right), \\
N_3(\theta,\epsilon) &\equiv 3\left(\frac{\epsilon\sin^2\theta + \cos^2\theta}{g_Y^2}\right), \\
N_{23}(\theta,\epsilon) &\equiv 3\left(\frac{(1-\epsilon)\sin^2\theta\cos^2\theta\left(1+\epsilon\tan^2\theta+25\epsilon\csc^2\theta\right)}{2g_Y^4}\right), \\
D_2(\theta,\epsilon) &\equiv \left(\frac{(1-\epsilon)(1+33\epsilon+16\epsilon\cos 2\theta-(1-\epsilon)\cos 4\theta)}{4g_Y^2}\right), \\
D_3(\theta,\epsilon) &\equiv \left(\frac{3(1-\epsilon)\sin^2 2\theta\left(1+\epsilon\tan^2\theta\right)}{4g_Y^2}\right), \\
D_{23}(\theta,\epsilon) &\equiv \left(\frac{75(1-\epsilon)^2\epsilon\sin^2 2\theta}{8g_Y^4}\right).
\end{aligned} \tag{3.48}$$

3.11 Appendix C: Parton-Level Cross Sections for Swan Production

In this Appendix, we list the formulas for parton-level cross sections of swan production in pp collisions. For swan pair-production, we find

$$\begin{aligned}
\frac{d\sigma(gg\to\vec{Q}\bar{\vec{Q}})}{d\cos(\theta)} &= \frac{g_3^4}{16\pi s}\sqrt{1-\frac{4m_{\vec{Q}}^2}{s}}\Bigg[4+\frac{9\left(m_{\vec{Q}}^4+m_{\vec{Q}}^2 s-tu\right)}{4s^2}+\frac{6m_{\vec{Q}}^4+2s^2}{3\left(t-m_{\vec{Q}}^2\right)^2} \\
&\quad +\frac{6m_{\vec{Q}}^4+2s^2}{3\left(u-m_{\vec{Q}}^2\right)^2}-\frac{\left(m_{\vec{Q}}^2+s\right)\left(m_{\vec{Q}}^2+3s\right)}{2s\left(m_{\vec{Q}}^2-u\right)}-\frac{\left(m_{\vec{Q}}^2+s\right)\left(m_{\vec{Q}}^2+3s\right)}{2s\left(t-m_{\vec{Q}}^2\right)}\Bigg].
\end{aligned} \tag{3.49}$$

The quark-initiated contribution to swan pair-production is negligibly small in the relevant swan mass range. The associated swan-gluino production cross

section is

$$\begin{aligned}\frac{d\sigma(gt_L \to \vec{Q}\widetilde{G})}{d\cos(\theta)} &= \frac{g_3^2\hat{g}_5^2\cos(\theta_{\widetilde{G}})^2}{16\pi s^2}\sqrt{\left(s-m_{\widetilde{G}}^2-m_{\vec{Q}}^2\right)^2-4m_{\widetilde{G}}^2m_{\vec{Q}}^2}\Bigg[\frac{4m_{\vec{Q}}^4-m_{\widetilde{G}}^4-u\left(m_{\widetilde{G}}^2+2m_{\vec{Q}}^2\right)}{9m_{\vec{Q}}^2 s} \\ &+ \frac{4s^2+4m_{\vec{Q}}^4-2m_{\widetilde{G}}^4-2m_{\widetilde{G}}^2m_{\vec{Q}}^2}{9\left(t-m_{\vec{Q}}^2\right)^2}+\frac{2m_{\widetilde{G}}^2m_{\vec{Q}}^4-m_{\widetilde{G}}^6-m_{\widetilde{G}}^4m_{\vec{Q}}^2}{2m_{\vec{Q}}^2\left(u-m_{\widetilde{G}}^2\right)^2}-\frac{1}{18}-\frac{m_{\widetilde{G}}^2}{4m_{\vec{Q}}^2} \\ &- \frac{2m_{\vec{Q}}^2s^2-4s\left(2m_{\vec{Q}}^4-m_{\widetilde{G}}^4-m_{\widetilde{G}}^2m_{\vec{Q}}^2\right)-4m_{\widetilde{G}}^6-9m_{\widetilde{G}}^4m_{\vec{Q}}^2+3m_{\widetilde{G}}^2m_{\vec{Q}}^4+10m_{\vec{Q}}^6}{18m_{\vec{Q}}^2s\left(t-m_{\vec{Q}}^2\right)} \\ &+ \frac{\left(m_{\widetilde{G}}^2+2m_{\vec{Q}}^2\right)\left(s^2-2s\left(m_{\vec{Q}}^2-m_{\widetilde{G}}^2\right)-2m_{\widetilde{G}}^2m_{\vec{Q}}^2+2m_{\vec{Q}}^4\right)}{4m_{\vec{Q}}^2s\left(m_{\widetilde{G}}^2-u\right)}\Bigg], \end{aligned} \tag{3.50}$$

where $\cos(\theta_{\widetilde{G}})$ is the overlap of the gaugino being produced with the $SU(5)$ gaugino. (In Fig. 3.7, we assumed that the mixing angle for gauginos and corresponding gauge bosons are aligned.) Finally, the associated swan-neutralino production cross section is

$$\begin{aligned}\frac{d\sigma(gt_L \to \vec{Q}\widetilde{N})}{d\cos(\theta)} &= \frac{g_3^2\hat{g}_5^2\cos(\theta_{\widetilde{N}})^2}{16\pi s^2}\sqrt{\left(s-m_{\widetilde{N}}^2-m_{\vec{Q}}^2\right)^2-4m_{\widetilde{N}}^2m_{\vec{Q}}^2}\Bigg[\frac{1}{4}+\frac{m_{\widetilde{N}}^2}{24m_{\vec{Q}}^2}+ \\ &+ \frac{t\left(m_{\widetilde{N}}^2+2m_{\vec{Q}}^2\right)-3m_{\widetilde{N}}^2m_{\vec{Q}}^2+2m_{\vec{Q}}^4-2m_{\widetilde{N}}^4}{24m_{\vec{Q}}^2s}+\frac{2s^2+2m_{\vec{Q}}^4-m_{\widetilde{N}}^4-m_{\widetilde{N}}^2m_{\vec{Q}}^2}{12\left(t-m_{\vec{Q}}^2\right)^2} \\ &+ \frac{4m_{\vec{Q}}^2s^2+s\left(2m_{\vec{Q}}^4-m_{\widetilde{N}}^4-m_{\widetilde{N}}^2m_{\vec{Q}}^2\right)-3m_{\widetilde{N}}^2m_{\vec{Q}}^4+2m_{\vec{Q}}^6+m_{\widetilde{N}}^6}{12m_{\vec{Q}}^2s\left(t-m_{\vec{Q}}^2\right)}\Bigg]. \end{aligned} \tag{3.51}$$

CHAPTER 4

FROM S-CONFINEMENT TO 3D CHIRAL THEORIES: DRESSING THE MONOPOLES

Monopole operators play a central role in 3 dimensional supersymmetric dualities: a careful understanding of their spectrum is necessary to match chiral operators on either sides of a conjectured duality. In Chern-Simons theories ($k \neq 0$), monopole operators acquire an electric charge, thus they need to be "dressed" by chiral matter superfields to be made gauge-invariant. Here we present strong evidence that "dressed" monopoles appear in $SU(N)$ chiral theories even for $k = 0$ because of mixed CS terms generated along certain Coulomb branch directions. Our analysis is based on the dimensional reduction of 4-dimensional dualities which, for the simplest s-confining case, allows us to easily identify the spectrum of the electric chiral operators. [1]

4.1 Introduction

Supersymmetry has had many important applications over the years: it is the leading candidate for solving the hierarchy problem, it allows a successful unification of gauge couplings, it predicts a potential dark matter candidate, and it is a necessary ingredient of string theories at high energy. However the arguably most successful application of supersymmetry has been its use as a laboratory for testing non-perturbative physics effects and guessing dualities in various dimensions.

[1] This paper was co-authored with Antonio Amarity, Csaba Csáki and Mario Martone; at the time of this writing, it was being prepared for publication by Physical Review D. [96]

Supersymmetric dualities in 3D have been studied since the late 90s [97, 98, 99, 100, 101, 102, 103, 104, 105]. One of their distinctive features is the role played by monopole operators which are non-trivially mapped across the dualities. Monopole operators are local disorder operators defined by requiring that the gauge field approaches a certain singular profile close to the point where the operator is inserted [106, 107]. These operators are commonly referred to as monopole operators because in Euclidean signature the gauge field singularity looks like that of a Dirac monopole or its non-Abelian generalization.

In theories with Chern-Simons (CS) terms ($k \neq 0$), magnetically charged objects acquire an electric charge, generically implying that a pure monopole operator Y is no longer gauge invariant. Hence the right (chiral) operator that has to be matched across the duality is "dressed" by some matter fields φ such that $Y_{\text{dress}} \equiv Y_{\text{bare}}\varphi^{|k|}$, where φ is an electrically charged operator. Dressed monopoles are generic features of both $U(1)_k$ [108, 109] and $U(N)_k$ [18, 110] theories.

Monopole operators have recently been systematically studied (e.g. [111, 112, 108, 18, 109, 110, 113]). In particular in [110] the super-conformal index was used to identify the chiral monopoles of generic $U(N)_k$ theories (with chiral and non-chiral matter) finding, surprisingly, that monopole operators are not always chiral. Furthermore the authors of [108, 109] have carefully investigated the relations between monopole operators and Coulomb branch (CB) operators. Many of their results will be used here.

The study of monopole operators in $U(1)$ and $U(N)$ theories is made feasible by the extra *topological* global $U(1)_J$ symmetry [97]. Monopole operators are always charged under the $U(1)_J$, and are the only matter fields carrying such a charge, making them clearly identifiable. Simple gauge groups however don't

have this extra global symmetry, making the study of the monopole operators much harder in $SU(N)$ theories. This is the task that we will attempt to address here by investigating a concrete chiral 3D $\mathcal{N} = 2$ $SU(N)$ model.

Using dimensional reduction [18] of 4D s-confining dualities [114, 115] we are able to obtain the low-energy description of 3D s-confining theories. These theories are described in the IR by very basic "confined" dynamics from which we can readily obtain the spectrum of the chiral operators of the UV theory and in particular study its monopole operators. By using this technique we can present evidence for the existence of "dressed" monopole operators in chiral $SU(N)$ theories at zero CS level. Such dressed monopoles have previously appeared [108, 109, 18, 110] in models with non-vanishing CS terms, but this is the first example of such objects mixing the Coulomb and Higgs branches without tree-level CS terms. A crucial ingredient necessitating the dressed monopoles is the presence of matter in the antisymmetric representation of $SU(N)$. These will generate mixed CS terms at one-loop along a particular unlifted $U(1)$ direction, which in turn induces the dressing of the monopole operator associated to that $U(1)$.

This effect appears to be a generic feature of chiral theories with matter fields in tensor representations, and is the last ingredient needed to find a complete classification and description of all 3D s-confining theories, which will be discussed in an upcoming more comprehensive publication [116]. The purpose of this paper is to present the complete and detailed analysis of one such s-confining theory: the simplest one which exhibits all the dynamical effects necessary to understand the full set of s-confining theories [116].

4.2 3D IR Duality in a Chiral $SU(6)$ Gauge Theory

To make our discussion more concrete we perform the explicit analysis for a specific s-confining 3D theory. At high energies the theory (referred to as the "electric" theory) is a (2 + 1) dimensional $\mathcal{N} = 2$ $SU(6)$ gauge theory with four fields in the antifundamental representation of the gauge group ($\bar{Q}$), two fields in the antisymmetric representation of the gauge group (A), and a vanishing superpotential. As mentioned above this is the simplest s-confining theory that contains all the ingredients necessary to eventually completely classify all 3D s-confining theories, and thus perfectly suited for our purposes. At low energies, this theory is described by a "magnetic theory", with several gauge singlet "meson-like" fields and an s-confining superpotential. The matter and symmetry content of this theory is presented in Table 4.1.

The low energy properties of this theory are derived from a similar (3 + 1) dimensional s-confining theory through dimensional reduction. This procedure is by now fairly standard. It involves compactifying a dimension on both sides of a 4D duality to obtain a duality between theories which live on $R^3 \times S^1$ and integrate out a flavor through a real mass deformation to decouple the extra super-potential term generated by a monopole configuration (KK monopole [117, 118, 119, 120, 121, 122]) wrapping around the compactified dimension [18]. The s-confining superpotential for the 3D theory can be obtained by removing from the superpotential of the 4D s-confining theory those fields which gain a mass when the flavor is decoupled [123].

Carrying out this procedure the 3D s-confining super-potential becomes (ig-

	$SU(6)$	$SU(2)$	$SU(4)$	$U(1)_3$	$U(1)_4$	$U(1)_{R'}$
$\bar{Q}$	$\overline{\square}$	1	$\square$	-6	1	0
A	$\square\!\square$	$\square$	1	3	0	0
$b_1 \equiv A\bar{Q}^2$		$\square$	$\square\!\square$	-9	2	0
$b_3 \equiv A^3$		$\square\!\square\!\square$	1	9	0	0
$b_4 \equiv A^4\bar{Q}^2$		1	$\square\!\square$	0	2	0
$\widetilde{M}_0 \equiv Y$		1	1	0	-4	2
$\widetilde{M}_3 \equiv A\widetilde{Y}$		$\square$	1	9	-4	2

Table 4.1: Matter content of the 3D duality obtained from the 4D theory by applying the dimensional reduction procedure.

noring the overall scale):

$$W^{3D} = \widetilde{M}_0 \left(b_4^2 + b_3^2 b_1^2\right) + \widetilde{M}_3 \left(b_4 b_1 + b_3 b_1^2\right) . \tag{4.1}$$

The details of the real mass deformation can be found in Appendix 4.3.1.

From Table 4.1 we can read off the chiral operators of the electric theory. The b_i's are easily mapped to the gauge invariant meson-like operator of the electric theory and it is tempting to associate $\widetilde{M}_0$ and $\widetilde{M}_3$ to unlifted CB directions parametrized by monopole operators. In the next section we will argue that while this is indeed the correct interpretation, the matching of the $\widetilde{M}_3$ field presents features **NRLL which had not been observed in previous analyses of 3D s-confining models [123]; this is due to the chiral nature of this theory.**

4.2.1 The Coulomb Branch Operators

As was discussed in [123], and will be discussed in more details in [116], for an $SU(6)$ theory with a non-chiral field content of fundamental and antisymmetric fields the unlifted CB of the theory is described by three monopole operators,

Y, $\widetilde{Y}$, and $\hat{Y}$, associated with three unlifted $U(1)$ directions. These operators can be written explicitly in terms of the five "fundamental" monopole operators Y_i, $i = 1, ..., 5$, as $Y \equiv Y_1 Y_2 Y_3 Y_4 Y_5$, $\widetilde{Y} \equiv \sqrt{Y_1 Y_2^2 Y_3^2 Y_4^2 Y_5}$ and $\hat{Y} \equiv \left(Y_1 Y_2^2 Y_3^3 Y_4^2 Y_5\right)^{1/3}$. In a chiral theory, however, we must be more careful. Alongside these directions, some matter fields acquire real masses and must be integrated out of the theory. The chiral nature of the theory allows the possibility that this could generate CS terms for the unbroken $U(1)$ gauge groups. These could in turn affect the equations of motions and change the structure of the moduli space. We examine all three CB operators in details. We will find that the Y operator remains unlifted while $\hat{Y}$ is lifted. The operator Y is readily associated to $\widetilde{M}_0$. However the matching of the remaining $\widetilde{Y}$ operator is less trivial. In fact, a CS term is generated along the $\widetilde{Y}$ direction. This causes this operator to acquire an electric charge and to be "dressed up" into the correct gauge invariant operator, $A\widetilde{Y}$. We will show with an explicit calculation that this is indeed the correct operator to describe the flat direction of the electric theory. Furthermore we will show that this operator has exactly the right abelian and non-abelian global quantum numbers to match the $\widetilde{M}_3$ chiral operator leading to the association in Table 4.1.

Generalities

Here we present the essential ingredients to understand the CB dynamics of 3D $\mathcal{N} = 2$ gauge theories. For reviews and more details see [97, 98, 18, 123].

A generic point of the CB of a $\mathcal{N} = 2$ 3D $SU(N)$ gauge theory is parametrized by the VEV of the scalar component of the vector multiplet which, using gauge transformations, can be diagonalized. Thus a generic point of the CB can be parametrized by N parameters: σ_i's, $i = 1, ..., N$, satisfying $\sigma_1 \geq \sigma_2 \geq ... \geq \sigma_N$

and $\sum_i \sigma_i = 0$:

$$\varphi = \begin{pmatrix} \sigma_1 & 0 & ... & 0 \\ 0 & \sigma_2 & ... & 0 \\ 0 & 0 & \ddots & 0 \\ 0 & 0 & ... & \sigma_N \end{pmatrix}, \qquad \sum_{i=1}^{N} \sigma_i = 0 \tag{4.2}$$

For generic values of the σ's $SU(N) \to U(1)^{N-1}$. Each unlifted $U(1)$ direction is parametrized by an operator Y_i, $i = 1, .., N-1$, and thus semi-classically the theory has a $N-1$ dimensional CB. Each Y_i is associated to one of the $N-1$ fundamental monopoles.

At the quantum level, 3D instantons generate contributions to the superpotential [124] which, in absence of matter, fully lift the CB. In the presence of matter, however, the analysis becomes considerably more elaborate as the CB splits in different regions in which some of the quantum corrections are not generated because of the presence of fermionic zero-modes [97, 98, 18, 123].

After accounting for non-perturbative corrections, we are left at most with operators describing unlifted $U(1)$ directions. For a Coulomb vacuum associated to a particular $U(1)_a$ to be allowed, it needs to satisfy[2]:

$$\sum_i 2\pi n_i^{(a)} \left|\Phi_i\right|^2 = \xi_{eff}^{(a)} + \sum_b k_{eff}^{(a,b)} \sigma^{(b)}, \tag{4.3}$$

$$\left(m_{\mathcal{R},i} + n_i^{(a)} \sigma^{(a)}\right) \Phi_i^{(a)} = 0\,, \tag{4.4}$$

where $n_i^{(a)}$ and $\sigma^{(a)}$ are, respectively, the charge of the ith field under and the scalar VEV for the unbroken $U(1)_a$, while Φ_i is the VEV of the ith matter field. The $k_{eff}^{(a,b)}$ are the CS terms generated at one-loop [108, 109]:

$$k_{eff}^{(a,b)} = \frac{1}{2} \sum_i n_i^{(a)} n_i^{(b)} \text{sign}(m_{\mathcal{R},i})\,, \tag{4.5}$$

[2]Here we assuming that both the tree level CS and FI terms vanish, $k = \xi = 0$.

where $m_{\mathcal{R},i}$ is the real mass of the field i. Note that in all the cases we are interested in here, $m_{\mathcal{R},i}$ will be induced by a given $U(1)_{\bar{a}}$ VEVs, thus $m_{\mathcal{R},i} = n_i^{(\bar{a})}\sigma^{(\bar{a})}$. These formulae allows for both "pure", $a = b$, and "mixed", $a \neq b$, CS terms. A similar formula applies for the effective Fayet-Iliopoulos (FI) term

$$\xi_{eff}^{(a)} = \frac{1}{2}\sum_i n_i^{(a)} m_{\mathcal{R},i}\text{sign}(m_{\mathcal{R},i}) \,. \tag{4.6}$$

Furthermore, CS terms will induce electric charges for the fields which are charged under the topological $U(1)_J$'s associated with the various $U(1)$ gauge factors:

$$q_i^{(a)} = -\sum_b k_{eff}^{(a,b)} q_{J,i}^{(b)} \,, \tag{4.7}$$

where $q_i^{(a)}$ is the electric charge under $U(1)_a$ generated for the ith field.

One loop CS terms can also be generated for non-abelian groups. Eq. (4.5) then generalizes to:

$$k_{eff}^{G} = \frac{1}{2}\sum_{\mathbf{r}_i} T_2(\mathbf{r}_i)\text{sign}(m_{\mathcal{R},\mathbf{r}_i}) \,. \tag{4.8}$$

where the real masses $m_{\mathcal{R},\mathbf{r}_i}$ will again be induced by $U(1)$ VEVs.

The Y Direction

Far along on the moduli space, the Y operator describes the direction $\text{diag}(\sigma, 0, 0, 0, 0, -\sigma)$. This field configuration spontaneously breaks $SU(6)$ to $SU(4) \times U(1)_1 \times U(1)_2$ where, up to an irrelevant normalization, the $U(1)_1$ and $U(1)_2$ factors are respectively associated with the generators $\text{diag}(1, 0, 0, 0, 0, -1)$ and $\text{diag}(2, -1, -1, -1, -1, 2)$. Under the unbroken gauge group the matter con-

tent of the theory decomposes as follows :

$$\begin{aligned}\overline{\square} &\to \overline{\square}_{(0,1)} + \mathbb{1}_{(-1,-2)} + \mathbb{1}_{(1,-2)} \,, \\ \begin{smallmatrix}\square\\\square\end{smallmatrix} &\to \begin{smallmatrix}\square\\\square\end{smallmatrix}_{(0,-2)} + \square_{(1,1)} + \square_{(-1,1)} + \mathbb{1}_{(0,4)} \,. \end{aligned} \tag{4.9}$$

We can now compute the possible CS terms generated by integrating out the heavy matter fields. From Eq. (4.9) we see that that all fields charged under $n^{(1)}$ come in pairs of fields whose contributions to the pure CS terms are equal and opposite: hence, all pure CS terms vanish. This argument does not apply to the mixed CS term however, which must be computed:

$$k_{eff}^{(1,2)} = \frac{1}{2}(-8 - 8 + 8 + 8) = 0 \,. \tag{4.10}$$

So the mixed CS term also vanishes, but this is not a generic result and only occurs because of a non-trivial cancellation between the different contributions from the matter fields in the theory. All FI terms also vanish. It follows that this CB direction remains unlifted and unmodified by the chiral effects.

The $\widetilde{Y}$ Direction and the Dressed Monopole

Far along on the moduli space, the $\widetilde{Y}$ direction describes the direction $\mathrm{diag}(\sigma, \sigma, 0, 0, -\sigma, -\sigma)$. This field configuration spontaneously breaks $SU(6)$ to $SU(2)_t \times SU(2)_m \times SU(2)_b \times U(1)_1 \times U(1)_2$. The subscripts "$t$", "$m$" and "$b$" stand for "top", "middle" and "bottom", and refer to the embedding of the $SU(2)$ subgroup of $SU(6)$ in the matrix representation of the group. Up to an irrelevant normalization, the $U(1)_1$ and $U(1)_2$ factors are respectively associated with the generators $\mathrm{diag}(1, 1, 0, 0, -1, -1)$ and $\mathrm{diag}(1, 1, -2, -2, 1, 1)$. Under the unbroken

gauge group the matter content of the theory decomposes as follows:

$$\begin{aligned}
\overline{\square} &\to \overline{\square}^{t}_{(-1,-1)} + \overline{\square}^{m}_{(0,2)} + \overline{\square}^{b}_{(1,-1)}, \\
\square &\to \mathbb{1}_{(2,2)} + \mathbb{1}_{(0,-4)} + \mathbb{1}_{(-2,2)} \\
&\quad + (\square^{t}, \square^{m})_{(1,-1)} + \left(\square^{t}, \square^{b}\right)_{(0,2)} + \left(\square^{m}, \square^{b}\right)_{(-1,-1)} \ .
\end{aligned} \tag{4.11}$$

Once again, all pure CS terms will necessarily cancel because fields with non-vanishing $n^{(1)}$ terms necessarily come in pairs with opposite-sign real masses. This time, however, there is a non-vanishing mixed CS term:

$$k^{(1,2)}_{eff} = \frac{1}{2}\left(-8 - 8 + 8 + 8 - 8 - 8\right) = -8 \ . \tag{4.12}$$

From Eq. (4.6), we see that there should also be an effective FI term generated for the $U(1)_2$ group, $\xi^{(2)}_{eff} = -8\sigma$. Hence (4.3) and (4.4) are modified to:

$$\sum_i 2\pi n^{(1)}_i |\Phi_i|^2 = k^{(1,2)}_{eff}\sigma^{(2)} = -8\sigma^{(2)} \ , \tag{4.13}$$

$$\sum_i 2\pi n^{(2)}_i |\Phi_i|^2 = k^{(1,2)}_{eff}\sigma^{(1)} + \xi^{(2)}_{eff} = -16\sigma^{(1)} \ , \tag{4.14}$$

where Φ_i represents the i-th massless field of the theory and the $\sigma^{(1),(2)}$ are the VEVs of the scalar component of the vector supermultiplets associated with the respective abelian gauge groups. In our notation, the "undressed" $\widetilde{Y}$ direction corresponds to $\sigma^{(1)} = \sigma > 0$ while the matter fields' VEVs Φ_i and $\sigma^{(2)}$ are set to zero. This vacuum configuration is perfectly compatible with Eq. (4.13) but it is inconsistent with Eq. (4.14) due to the non-vanishing $k^{(1,2)}_{eff}$ and $\xi^{(2)}_{eff}$. This condition can now only be satisfied if some VEVs for the matter fields are turned on. For consistency with Eq. (4.13) those fields must have $n^{(1)}_i = 0$. Furthermore, since the right-hand-side of Eq. (4.14) is negative, those fields must also have $n^{(2)}_i < 0$. From Eq. (4.11), we see that there is only one possible candidate: the

$\mathbb{1}_{(0,-4)}$ field which was initially part of the field A in the antisymmetric $SU(6)$ representation. Therefore, the effects of the chiral dynamics boil down to turning the CB parameter into a dressed monopole $A\widetilde{Y}$. This is similar to the dressed monopoles that show up in [108, 109, 18, 110]. However, in all of these previous examples, the models in which the dressed monopoles appeared were chiral theories obtained from real mass deformations of parent non-chiral theories. All of these theories had tree-level CS terms. The example we present here is the first example of a dressed monopoles in a model without such a tree-level CS term and the simplest in a series of models that will be systematically explored in [116].

As an independent check, we can verify that $A\widetilde{Y}$ is in fact a gauge invariant operator. As explained above $A \to \mathbb{1}_{(0,-4)}$, thus it has charges $(0,-4)$ under the unbroken $U(1)$'s. From (4.7), computing the $U(1)_2$ electric charge generated by the mixed CS term and the $U(1)_1$ magnetic charge, $\widetilde{Y}$ has charges $(0,4)$ making the dressed operator gauge invariant. It is important to stress that gauge invariance of the dressed monopole implies the presence of the square root in the definition of the $\widetilde{Y}$.

As we will show below, this dressed monopole also possesses the correct global quantum numbers to match the field $\widetilde{M}_3$ on the magnetic side of the duality. Note that this also includes the non-abelian flavor $SU(2)$ charge which $A_{\mathbb{1}_{(0,-4)}}\widetilde{Y}$ inherits from the A field. All the one-loop non-abelian CS terms vanish:

$$\begin{aligned} k_{eff}^{SU(2)_t} &= \frac{1}{2}\left(4*(-1)+2*2*(+1)\right) = 0\,, \\ k_{eff}^{SU(2)_m} &= \frac{1}{2}\left(2*2*(+1)+2*2*(-1)\right) = 0\,, \\ k_{eff}^{SU(2)_b} &= \frac{1}{2}\left(4*(+1)+2*2*(-1)\right) = 0\,. \end{aligned} \tag{4.15}$$

The vanishing of all the non-abelian CS terms depends, once again, on a non-

trivial cancellation which is realized for this specific matter content. In a generic chiral theory, these terms could be present.

The $\hat{Y}$ Direction

Far along on the moduli space, $\hat{Y}$ describes the direction $\text{diag}(\sigma, \sigma, \sigma, -\sigma, -\sigma, -\sigma)$. This field configuration spontaneously breaks $SU(6)$ to $SU(3)_t \times SU(3)_b \times U(1)$. The subscripts "$t$" and "$b$" stand for "top" and "bottom", and refer again to the position of the embedding of $SU(3)$ in the matrix representation of $SU(6)$. Up to an irrelevant normalization, the $U(1)$ factor is associated with the generator $\text{diag}(1, 1, 1, -1, -1, -1)$. Under the unbroken gauge group the matter content of the theory decomposes as follows:

$$\begin{aligned} \overline{\square} &\to \overline{\square}^t_{(-1)} + \overline{\square}^b_{(1)}, \\ \square &\to \overline{\square}^t_{(2)} + \overline{\square}^b_{(-2)} + \left(\square^t, \square^b\right)_{(0)} . \end{aligned} \tag{4.16}$$

No abelian CS term is generated for the unbroken $U(1)$. By Eq. (4.6), no FI term is generated either. However, non-abelian terms are generated for both $SU(3)$ factors:

$$\begin{aligned} k^t_{eff} &= \frac{1}{2}\left(4 * (-1) + 2 * (+1)\right) = -1 , \\ k^b_{eff} &= \frac{1}{2}\left(4 * (+1) + 2 * (-1)\right) = 1 . \end{aligned} \tag{4.17}$$

We now argue that it is plausible that the effect of these non-abelian CS terms, combined with non-perturbative dynamics, result in the $\hat{Y}$ direction being lifted. The non-abelian CS-terms generated by the $\hat{Y}$ direction affect the equations of motions for the VEVs of the two unbroken $SU(3)$ in a manner analogous to Eqs. (4.13-4.14). Since turning on the directions Y or $\widetilde{Y}$ requires giving VEVs to some of the generators which live in these $SU(3)$ subgroups, we can see that chiral

effects forbid us from turning on the $\hat{Y}$ direction when either of the other two directions are turned on. However, if we study the different regions of the CB of this theory, we can see that in all the regions where the $\hat{Y}$ operator is defined, the $\widetilde{Y}$ operator is necessarily also defined. Ultimately it is the full dynamics that will determine whether along these regions of the CB the theory settles along the $\widetilde{Y}$ or $\hat{Y}$ directions. The effective low energy description (4.1) obtained through the compactification suggests that in all of these branches the theory settles to the $\widetilde{Y}$ direction, and so $\hat{Y}$ gets lifted.

It would be very interesting to gain a more detailed understanding of the underlying dynamics leading to the lifting of $\widetilde{Y}$. In particular one can construct a UV free completion of the IR sector, e.g. by integrating in some extra singlets, hoping to better understand the nature of the duality under consideration here. [3] A more detailed analysis of the different regions of the CB and their relationship to the properties of the unlifted directions will be provided in a future publication [116].

$U(1)$ Charges

A non-trivial check of the claimed mapping between the fields $\widetilde{M}_0$, $\widetilde{M}_3$ and Y, $A_{\mathbb{1}_{(0,-4)}}\widetilde{Y}$ is the matching of the global quantum numbers on both sides of the duality. The global quantum numbers of the fields on "the magnetic side" are listed in Tab. 4.1 and are inherited from those of the "parent" 4D theory. In the 3D theory there is an extra $U(1)$ symmetry, $U(1)_4$, which originates from the diagonal generator of the flavor $SU(5)$ in 4D. On "the electric side", the quantum numbers of the CB parameters are inherited from the Y_i's monopole operators

[3] We would like to thank Ofer Aharony for emphasizing this issue to us.

of which they are composed. These operators acquire global symmetry charges at one-loop [97] which can be computed by counting matter zero modes using the Callias index theorem [125, 98, 97, 123]. We use this fact to compute the global charges of the two relevant CB parameters Y and $\widetilde{Y}$. As explained above, the CB splits in different regions and these operators are associated to inequivalent ones. We report the detailed calculation elsewhere [116]. Carefully keeping track of the splitting and the non-perturbative contributions to the super-potential, we obtain the following charge assignments:

	$U(1)_3$	$U(1)_4$	$U(1)_{R'}$
Y_1	0	-4	10
$Y_{i\neq 1}$	0	0	-2
$Y \equiv Y_1 Y_2 Y_3 Y_4 Y_5$	0	-4	2
$\widetilde{M}_0$	0	-4	2

(4.18)

The charges of Y match those of the the operator $\widetilde{M}_0$, as claimed. For $\widetilde{Y}$:

	$U(1)_3$	$U(1)_4$	$U(1)_{R'}$
Y_2	6	-4	8
$Y_{i\neq 2}$	0	0	-2
$\widetilde{Y} \equiv \sqrt{Y_1 Y_2^2 Y_3^2 Y_4^2 Y_5}$	6	-4	2
$A\widetilde{Y}$	9	-4	2
$\widetilde{M}_3$	9	-4	2

(4.19)

We see that while $\widetilde{Y}$ by itself does not match any of the operators on "the magnetic side" of the theory, the dressed monopole, $A_{\mathbb{1}_{(0,-4)}}\widetilde{Y}$, has the same abelian global quantum numbers as $\widetilde{M}_3$. In addition, because of the $A_{\mathbb{1}_{(0,-4)}}$ field, the dressed monopole is in the $\square$ representation of the global flavor $SU(2)$, just like $\widetilde{M}_3$. Since we expect the $\hat{Y}$ operator to be lifted we do not list its quantum numbers.

4.2.2 Consistency Check from the Partition Function

Finally we discuss a further powerful check of our conjectured IR dynamics by reducing the four dimensional superconformal index[4], a topological invariant quantity counting a set of protected BPS operators in a 4D supersymmetric field theory, [126, 127] to the three dimensional partition function [128, 129] which is a measure of the 3D degrees of freedom. Because of the technical nature of this section we will not report many of the details. They will be discussed thoroughly in [116].

Starting from the result of [130, 131] of the matching between the 4D indices in the confining case, we can show the identity of the 3D partition function for the expected 3D duals through dimensional reduction. We observe in this process the appearance of the extra dressed monopole operators discussed above. This relation between the 4D index and 3D partition function has already been used to study the dimensional reduction of 4D dualities in [18, 132].

In our case, from the exact identity between the 4D index of the $SU(6)$ theory and the index of its confining phase, we obtain the relation between the partition functions for the effective duality on $R^3 \times S^1$. We can consider the compactified theories as *effective* 3D theories with the finite size effects from S^1 representing the non-perturbative dynamics. We obtain the following relation matching the

[4] The definition of the index requires only a conserved R-current; the theories do not necessarily have to be superconformal.

partition functions for the dual phases:

$$\int \frac{\prod_{i=1}^{6}(d\sigma_i \Gamma_h(\mu_1+\sigma_i)\prod_{\beta=1}^{5}\Gamma_h(\nu_\beta-\sigma_i))\delta(\sum\sigma_i)}{\prod_{i<j}\Gamma_h(\pm(\sigma_i-\sigma_j))\prod_{\gamma=1}^{2}\Gamma_h^{-1}(\sigma_i+\sigma_j+\tau_\gamma)} =$$
$$\prod_{\beta=1}^{5}(\Gamma_h(\mu_1+\nu_\beta)\prod_{\gamma=1}^{2}(\Gamma_h(\mu_1+\tau_1+\tau_2+\tau_\gamma+\nu_\beta)$$
$$\prod_{\rho=\beta+1}^{5}\Gamma_h(\tau_\gamma+\nu_\beta+\nu_\rho)\,)\prod_{\rho=\beta+1}^{5}\Gamma_h(2(\tau_1+\tau_2)+\nu_\beta+\nu_\rho))$$
$$\prod_{i_M\in\{1,2\}}\Gamma_h(\tau_{i_1}+\tau_{i_2}+\tau_{i_3}) \tag{4.20}$$

The functions Γ_h are called hyperbolic gamma functions [133] and they represent the one loop determinants of the vector and matter multiplets in the computation of the partition function from localization. The variables σ_i are the eigenvalues of the scalars in the vector multiplet as in (4.2). The parameters μ, ν and τ are holomorphic combinations of the real masses for the fields and their R-charges. They correspond to turning on a background gauge field for each global symmetry. [5] Even though in the field theory analysis we fixed the R-charges as in Table 4.1, here we consider a more general definition, consistent with the other abelian global symmetries. We observe that in this case the R-charges can be treated as unconstrained. This is consistent with the absence of superpotential in the electric theory. This procedure allows a better identification of the zero modes carried by the (dressed) monopole operators, acting as singlets in the dual theory, in terms of the elementary fields of the electric theory.

The non-perturbative effects from the finite size of the circle generate an extra superpotential in the electric theory. It breaks an abelian symmetry which is

[5] The real part of these parameters reproduce the weight of the representation for each charged matter multiplet under the (non R) global symmetries. The imaginary term is associated to the gauging of the R-symmetry and it is proportional to the squashing parameter through the formula $\omega = i(b + 1/b)$.

anomalous in the 4D electric parent. In the dual theory this symmetry is broken by the 4D superpotential (which is not modified by compactification). On the partition function this effect corresponds to a relation between the parameters μ, ν and τ. In fact the equality (4.20) is valid if the parameters satisfy the relation

$$\mu_1 + \sum_{\beta=1}^{5} \nu_\beta + 4 \sum_{\gamma=1}^{2} \tau_\gamma = 2\omega \tag{4.21}$$

The equality (4.20) can be further reduced to the $SU(6)$ theory with four antifundamentals and two antisymmetrics that we studied above by a real mass flow [133]. At the end of the mass flow we obtain the relation

$$\begin{aligned} &\int \frac{\prod_{i=1}^{6} (d\sigma_i \prod_{\beta=1}^{4} \Gamma_h(\nu_\beta - \sigma_i)) \delta(\sum_{i=1}^{4} \sigma_i)}{\prod_{i<j} \Gamma_h(\pm(\sigma_i - \sigma_j)) \prod_{\gamma=1}^{2} \Gamma_h^{-1}(\sigma_i + \sigma_j + \tau_\gamma)} = \\ &\Gamma_h(M_{\widetilde{M}_0}) \Gamma_h(M_{\widetilde{M}_3}) \prod_{i_M \in \{1,2\}} \Gamma_h(\tau_{i_1} + \tau_{i_2} + \tau_{i_3}) \\ &\prod_{\beta<\rho}^{4} (\Gamma_h(2(\tau_1 + \tau_2) + \nu_\beta + \nu_\rho) \prod_{\gamma=1}^{2} \Gamma_h(\tau_\gamma + \nu_\beta + \nu_\rho)) \end{aligned} \tag{4.22}$$

From which we can read off the quantum numbers of the operators in the spectrum. We find that the two terms parameterized by $M_{\widetilde{M}_0}$ and $M_{\widetilde{M}_3}$ have the same charges as the monopole Y and the dressed monopole $A\widetilde{Y}$ discussed above. This is an additional powerful check that the correct CB directions are Y and $A\widetilde{Y}$ as discussed previously. More precisely we have $M_{\widetilde{M}_0} = 2\omega(1 - 4\Delta_A - 2\Delta_Q) - 4m_3$ and $M_{\widetilde{M}_3} = (\omega(2 - 5\Delta_A - 4\Delta_Q) - 4m_3 + 9m_4$. The parameters m_3 and m_4 are the real masses of the abelian $U(1)_3$ and $U(1)_4$ global symmetries. The identity (4.22) holds when the condition

$$\sum_{\beta=1}^{4} \nu_\beta + \sum_{\gamma=1}^{2} \tau_\gamma = -4(m_3 - \omega(\Delta_{\widetilde{Q}} + 2\Delta_A)) \tag{4.23}$$

is imposed on the parameters.

We conclude this section with a comment on the matching of the 3D superconformal index which could be an extra check of the relations studied in this

	$SU(6)$	$SU(2)$	$SU(5)$	$U(1)_1$	$U(1)_2$	$U(1)_R$
Q	$\square$	1	1	-5	-4	0
$\bar{Q}$	$\overline{\square}$	1	$\square$	1	-4	0
A	$\begin{smallmatrix}\square\\\square\end{smallmatrix}$	$\square$	1	0	3	1/4
$M_0 \equiv Q\bar{Q}$		1	$\square$	-4	-8	0
$M_3 \equiv QA^3\bar{Q}$		$\square$	$\square$	-4	1	3/4
$B_1 \equiv A\bar{Q}^2$		$\square$	$\begin{smallmatrix}\square\\\square\end{smallmatrix}$	2	-5	1/4
$B_3 \equiv A^3$		$\square\square\square$	1	0	9	3/4
$B_4 \equiv A^4\bar{Q}^2$		1	$\begin{smallmatrix}\square\\\square\end{smallmatrix}$	2	4	1

Table 4.2: Matter content of the 4D s-confining theory along with the global symmetries and the charges of the confined mesons.

section by performing the calculation on $S^2 \times S^1$ [134]. This can be obtained from direct computation or from the matching between the partition on $T^2 \times S^2$ recently discussed in [135, 136] This check can also be performed by following a different strategy: first one can factorize the index on the S^3_b in terms of holomorphic blocks [137], and then glue the blocks together as explained in [138] to obtain the matching of the index. We leave this analysis to future investgations.

4.3 Appendix

4.3.1 Real Mass Deformation

The real mass deformation procedure is applied on a compactified $R^3 \times S^1$ theory to decouple a flavor and get rid of the KK terms, giving us with the 3D theory with the properties described above. We go through this procedure step-by-step below. The field content of the 4D electric and magnetic theories is given in Table 4.2.

The s-confining superpotential for the mesons of the 4D theory is:

$$W^{4D} = \frac{1}{\Lambda^{11}} \left(B_4^2 M_0 + B_4 M_3 B_1 + B_3 M_3 B_1^2 + B_3^2 M_0 B_1^2 \right) . \tag{4.24}$$

We now add a vector-like real mass deformation to the unique Q field and the fifth flavor of $\overline{Q}$. This can be done by "fictitiously" gauging a linear combination of the diagonal generators of the flavor groups and of $U(1)_1$ such that only these flavors are charged under this combination; we can then imagine turning on a background scalar field for this gauge group, providing us with the desired real mass deformation. The mesonic fields which are left massless (and thus remain in the spectrum) under this procedure are:

- B_1^{ab} with $a, b < 5$, which we rename b_1.
- B_3, which we rename b_3.
- B_4^{ab} with $a, b < 5$ which we rename b_4.
- $M_0^5 \equiv \widetilde{M}_0$.
- $M_3^5 \equiv \widetilde{M}_3$.

These are the fields which will be part of the s-confined description of the 3D theory.

The 3D duality can now be written by applying the real mass deformation on both sides of the 4D duality. For the electric side, this consists simply of removing one flavor. For the magnetic side, the field content is reduced to those massless mesonic fields listed above and the superpotential is obtained by setting all other fields to zero in Eq. (4.24). Doing so, we obtain the matter content displayed in Table 4.1 and the superpotential of Eq. (4.1).

CHAPTER 5

ELASTICALLY DECOUPLING DARK MATTER

We present a novel dark matter candidate, an Elastically Decoupling Relic (ELDER), which is a cold thermal relic whose present abundance is determined by the cross-section of its elastic scattering on Standard Model particles. The dark matter candidate is predicted to have a mass ranging from a few to a few hundred MeV, and an elastic scattering cross-section with electrons, photons and/or neutrinos in the $10^{-3} - 1$ fb range. [1]

5.1 Introduction

It has now been firmly established that the Standard Model (SM) of particle physics must be extended to include new particle(s) to account for the observed dark matter (DM). Many of the proposed dark matter candidates fall into a broad category of *thermal relics*, particles which were in thermal equilibrium with the hot SM particle plasma at some point in the early universe, and subsequently "froze out" as the universe expanded and cooled [140]. An attractive feature of this framework is its predictive power: the current abundance of the DM χ can be related to its microscopic properties, such as its mass and interaction cross sections.

The type of interactions which determine the χ relic abundance can vary.

[1] This paper was co-authored with Eric Kuflik, Maxim Perelstain and Yu-Dai Tsai; at the time of this writing, it was being prepared for publication by Physical Review Letters. [139]

The following three reactions will play a major role in the analysis of this paper:

- Elastic Scattering: χ+SM $\leftrightarrow$ χ+SM, where "SM" stands for any of the known Standard Model particles.
- Annihilation: $\chi + \chi \leftrightarrow$ SM+SM.
- Self-Annihilation: $\chi\chi \leftrightarrow \overbrace{\chi \ldots \chi}^{n}$, with $n \geq 3$. (Specifically, we will focus on the case $n = 3$.)

In the popular weakly-coupled massive particle (WIMP) paradigm, the relic abundance is entirely determined by the annihilation process. An alternative paradigm of self-interacting dark matter relies instead on self-annihilation [27]. Unfortunately, the dark matter predicted by this scheme is too light ($\lesssim$ 100 eV) to be consistent with the observed large-scale structure [27, 141]. Recently, an interesting variation has been proposed, dubbed the strongly interacting massive particle or SIMP [25, 26] (for extensions and variations, see [142, 143, 144, 145, 146]). In this model, the relic abundance is still set by self-annihilation, but the elastic scattering process is strong enough to sustain the thermal equilibrium between the SM and DM sectors until freeze-out occurs. In this case, the dark matter mass consistent with cosmological data is between an MeV and a GeV.

In these and all other known examples, the DM relic abundance is set by processes that change the χ particle number. In this Letter, we present a novel scenario in which the dark matter relic density is determined almost exclusively by the decoupling of the *elastic scattering*. We will refer to the dark matter candidate in this scenario as "ELastically DEcoupling Relic", or ELDER. In a nutshell, the scenario works as follows. At high temperatures, when χ is relativistic, it

is in thermal and chemical equilibrium with the SM plasma. As the universe cools to temperatures below the χ mass, the χ equilibrium density drops exponentially, and the annihilation process quickly decouples. (This feature is the same as in the SIMP scenario.) The self-annihilation and elastic scattering processes are still active, and maintain thermal and chemical equilibrium (with zero chemical potential) between the two sectors. In the ELDER scenario, the elastic scattering decouples *first*, while the self-annihilation process is still active. (This is in contrast to the SIMP case [25], where the self-annihilation process is the first one to decouple.) After the decoupling of elastic scattering, the dark matter sector enters the so-called "cannibalization" epoch [27], in which the energy released by self-annihilation keeps it at an approximately constant temperature, even as the universe continues to expand. Eventually, the self-annihilation process also decouples, at which point the comoving number density of χ is frozen. The near-constant temperature (and therefore density) of the DM in the cannibalization epoch means that the relic abundance of dark matter observed today is almost entirely fixed by the density of χ's at the beginning of this epoch, which in turn is fixed by the size of the elastic scattering cross section.

We study the scenario outlined above using both simple estimates and detailed numerical solutions of the Boltzmann equations. We find that the observed dark matter abundance can be reproduced, and all theoretical and observational constraints can be satisfied, for χ masses between a few and a few hundred MeV, while the cross-section of elastic scattering between DM and SM particles (electrons, photons, and/or neutrinos) is of the order of $10^{-3}-1$ fb in the non-relativistic limit. DM candidates with such properties arise in simple and attractive theoretical extensions of the SM: for example, a hidden-sector DM can interact with the SM sector via a TeV-scale Z' with order-one gauge couplings to

both sectors, or via a relatively light (0.01 – 1 GeV) dark photon with a kinetic mixing parameter $\epsilon \sim 10^{-8}$ [147]. We note that the model presented in [148] can realize the ELDER scenario for a range of parameters in which the theory is perturbative and all constraints are satisfied.

5.2 The elastically decoupling thermal relic

The thermal history of the ELDER is summarized in Fig. 5.1. At high temperatures, when χ is relativistic, it maintains thermal and chemical equilibrium with the SM plasma. As the universe cools, the temperature drops below the χ mass, and the subsequent thermal history is marked by two important events. First is "decoupling", when the rate of elastic scattering becomes insufficient to maintain the DM and SM sectors in thermal contact. Second is "freeze-out", at which point the rate of self-annihilation becomes insufficient to maintain chemical equilibrium in the DM sector, and the comoving dark matter density is frozen. Between these two events, chemical equilibrium within the DM sector are still maintained by self-annihilations, but the DM temperature T' is no longer equal to the SM temperature T. In this regime, the DM gas undergoes "cannibalization": $3 \to 2$ self-annihilations decrease the number density, but at the same time inject kinetic energy into the remaining gas. As the DM gas cannot exchange entropy with the SM sector at this time, its comoving entropy density is constant as the universe expands:

$$\begin{aligned} a^3 s'_\chi = a^3 \frac{m_\chi n_\chi}{T'} &= \text{constant} \\ \implies (T')^{1/2} e^{-m_\chi/T'} &\propto T^3 \end{aligned} \tag{5.1}$$

where $a \propto T^{-1}$ is the FRW scale-factor. As a result, T' decreases much slower than T as the universe expands:

$$T' \approx \frac{T_d}{1 + 3x_d^{-1} \log T_d/T}\,, \tag{5.2}$$

where $x_d \equiv m_\chi/T_d$ and T_d is temperature at which (elastic) decoupling occurs. As the DM density evolves through cannibalization stage, the comoving DM number density will reach a phase where is it changing very slowly with the expansion of the universe (see Fig. 5.1), reaching an (almost) constant value before freezeout occurs.

Let T'_f denote the DM temperature at freeze-out. Since the comoving entropies of the DM and SM sectors are separately conserved in the cannibalization epoch, the DM number density at freeze-out is given by

$$n'_f = \frac{\rho'_f}{m_\chi} = \frac{s'_f T'_f}{m_\chi} = \frac{s'_d}{x'_f}\frac{s_f}{s_d}, \tag{5.3}$$

where $x'_f = m_\chi/T'_f$, s_d and s'_d are the entropy densities of the SM and DM sectors at decoupling, and s_f and s'_f are the same quantities at freeze-out. The DM number density today is

$$n_0 = \frac{s_0}{s_f} n'_f = \frac{s'_d}{s_d}\frac{s_0}{x'_f}, \tag{5.4}$$

where s_0 is the current entropy density. Since the dark matter is non-relativistic at T_d,

$$\Omega_\chi = \frac{45}{2^{5/2}\pi^{3/2}} \left(\frac{m_\chi s_0}{\rho_c}\right)\left(\frac{g_\chi}{g_{*d}}\right)\frac{x_d^{5/2} e^{-x_d}}{x'_f}, \tag{5.5}$$

where ρ_c is the critical density ($s_0/\rho_c \approx 0.60$ eV^{-1}), g_χ is the number of degrees of freedom in the χ field (*e.g.* 2 for complex scalar and 4 for Dirac fermion), and g_{*d} is the effective number of relativistic SM degrees of freedom at decoupling. Hence, the relic abundance is exponentially sensitive to the temperature at which the elastic scattering processes decouple.

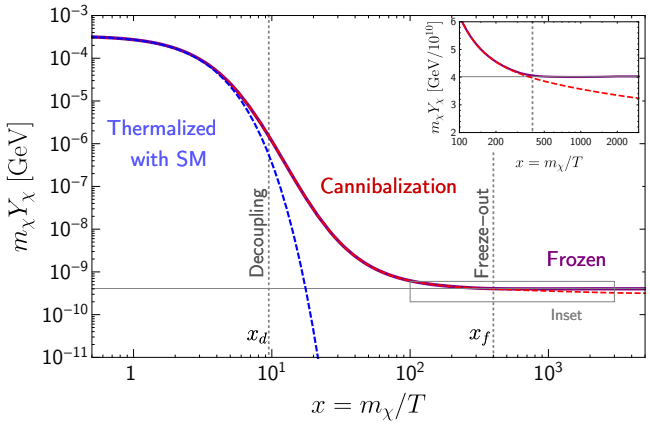

Figure 5.1: Dark matter yield, as a function of the SM plasma temperature T, for elastically decoupling dark matter with $m_\chi = 10$ MeV, $\epsilon = 8.5 \times 10^{-9}$, and $\alpha = 1$ (**purple**/solid line). For comparison, the dashed curves show the equilibrium yield assuming the DM and SM plasmas are in equilibrium (**blue**/dashed), and assuming the DM plasma is in chemical equilibrium with itself after decoupling (**red**/dashed). Decoupling of the $\chi\chi \to \gamma\gamma$ annihilations occurs roughly at $x \sim 3$.

In order to determine the temperatures at decoupling, x_d, and at freeze-out, x'_f, we parametrize the elastic scattering and self-annihilation cross-sections in the non-relativistic limit as

$$\lim_{T\to 0}\langle\sigma_{\rm el} v\rangle \equiv \frac{\epsilon^2}{m_\chi^2}, \quad \lim_{T\to 0}\langle\sigma_{3\to 2} v^2\rangle \equiv \frac{\alpha^3}{m_\chi^5}, \tag{5.6}$$

where $\sigma_{\rm el}$ is the cross-section of elastic scattering, averaged over SM species that are relativistic at $T \sim m_\chi$. At $T < m_\chi$, the equilibrium density of DM particles drops exponentially as $n_\chi^{\rm eq} \sim (m_\chi T)^{3/2} e^{-m_\chi/T}$. The self-annihilation process which maintains chemical equilibrium in the DM gas releases kinetic energy, at a per-particle rate of

$$\dot{K}_\chi = m \left.\frac{\dot{n}}{n}\right|_{\mu_\chi = 0} \simeq -m_\chi^2 H T^{-1}. \tag{5.7}$$

Elastic scattering processes transfer this excess kinetic energy to the SM gas at a

rate

$$\dot{K}_\chi \sim \Gamma_{\rm el} v_\chi^2 T \sim T^5 \epsilon^2 / m_\chi^3, \tag{5.8}$$

where $\Gamma_{\rm el} = n_{\rm SM} \langle \sigma_{\rm el} v \rangle$ is the rate at which each χ scatters elastically off the SM gas. The decoupling occurs when the DM-to-SM energy transfer can no longer keep up with the kinetic energy production; equating Eq. (5.7) with Eq. (5.8),

$$x_d \sim \epsilon^{1/2} m_\chi^{-1/4} M_{\rm Pl}^{1/4}. \tag{5.9}$$

Freeze-out occurs when the rate of self-annihilations is no longer sufficient to maintain chemical equilibrium, $(n_\chi^{\rm eq})^2 \langle \sigma_{3\to 2} v_\chi \rangle \sim \dot{n}_\chi^{\rm eq} / n_\chi^{\rm eq}$, which yields

$$x_f' \sim \frac{3}{4} \log\left(\frac{M_{\rm Pl}}{m_\chi}\right) - \frac{x_d}{2} + \frac{9}{4} \log \alpha. \tag{5.10}$$

For DM mass in the MeV–GeV range, the relic density can be conveniently approximated as

$$\Omega_\chi \sim \frac{10^6 m_{\rm MeV} \exp(-10 \epsilon_{-9}^{1/2} m_{\rm MeV}^{-1/4})}{1 + 0.07 \log \alpha}, \tag{5.11}$$

where $\epsilon_{-9} \equiv \epsilon / 10^{-9}$ and $m_{\rm MeV} \equiv m_\chi / (1\ {\rm MeV})$. As emphasized in the Introduction, the relic density is controlled by the strength of the elastic scattering, ϵ, with only weak, logarithmic, dependence on the strength of the number-changing self-annihilation process α. This is the unique feature of the ELDER scenario.

The ELDER mechanism is only possible if the self-annihilation process maintains the DM gas in chemical equilibrium until *at least* the temperature T_d, requiring

$$\begin{aligned} \alpha \gtrsim \alpha_{\rm min} &\simeq \frac{10^{-5} x_d^{7/3} m_{\rm MeV}}{\Omega_\chi^{2/3}} \\ &\approx 0.015 m_{\rm MeV} \left(1 + 0.16 \log m_{\rm MeV}\right). \end{aligned} \tag{5.12}$$

Numerical solutions to the Boltzmann equations (see below) indicate that Eq. (5.12) somewhat underestimates the lower bound of the "pure ELDER" re-

gion: for $\alpha \lesssim$ a few $\times \alpha_{\rm min}$, both self-annihilation and elastic scattering are important. For even lower α, freeze-out occurs before the elastic scattering decouples; this is precisely the SIMP scenario of [25, 26]. Together with perturbativity and unitarity constraints on the self-annihilation cross section, which can be estimated as $\alpha \lesssim 4\pi$, this bound imposes an upper bound on the DM mass. For a "pure ELDER," this implies $m_\chi \lesssim 100$ MeV. A lower bound of $m_\chi \gtrsim$ a few MeV is imposed by observational constraints, see below. In the allowed mass range, the correct relic density is obtained for ϵ ranging between 10^{-9} and 10^{-7}, while $\alpha \sim 10^{-2} - 10$.

A potential concern in the elastic decoupling scenario is its naturalness: if small changes in ϵ lead to huge changes in the relic density, it would be difficult to conceive of a reason why $\Omega_\chi \sim 1$ in the observed universe. To quantify this issue, we estimate

$$\frac{\partial \log \Omega_\chi}{\partial \log \epsilon} \approx 7 + \frac{1}{2} \log m_{\rm MeV}. \tag{5.13}$$

An order-of-magnitude change in the relic density requires a $20-30\%$ change in ϵ. We conclude that only a mild amount of tuning is required to obtain $\Omega_\chi \sim 1$.

5.3 The Boltzmann Equations

The starting point of the analysis is the microscopic Boltzmann equation for the phase-space density of the DM particle χ, with collision terms describing elastic scattering, $\chi\gamma \to \chi\gamma$; annihilation $\chi\chi \leftrightarrow \gamma\gamma$; and self-annihilation $\chi\chi \leftrightarrow \chi\chi\chi$. (For concreteness, we assume that the dominant DM coupling to the SM is via photons; couplings to $e^\pm$ or ν would produce similar results.) Since the χ velocities follow thermal distribution at all times, the microscopic Boltzmann equation

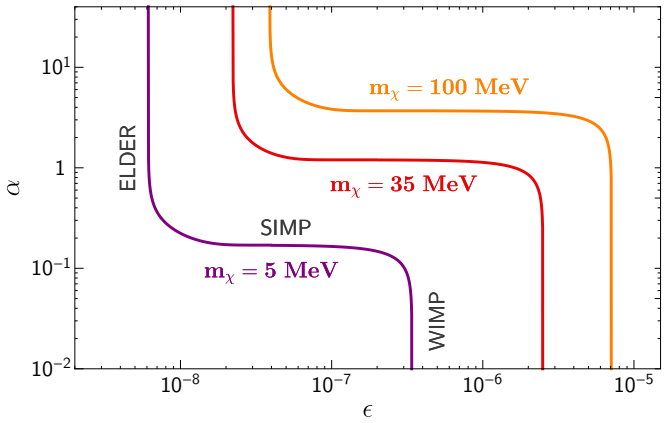

Figure 5.2: Regions of parameters corresponding to the observed relic density. For each mass, the vertical section of the line of the left/top corresponds to the elastically decoupling relic (ELDER) scenario proposed in this paper; the horizontal line to the SIMP scenario; and the vertical section on the right/bottom to the WIMP scenario.

reduces to two integro-differential equations for the DM number density $n_\chi(t)$,

$$\frac{dn_\chi}{dt} + 3Hn_\chi = -\langle\sigma_{3\to2}v^2\rangle(n_\chi^3 - n_\chi^2 n_\chi^{\rm eq}) + \ldots, \tag{5.14}$$

and energy density $\rho_\chi(t)$,

$$\frac{d\rho_\chi}{dt} + 3H(\rho_\chi + P_\chi) = \langle\sigma_{\rm el}v\cdot\delta E\rangle n_\chi n_\gamma^{\rm eq} + \ldots, \tag{5.15}$$

where

$$\begin{aligned}\langle\sigma_{\rm el}v\cdot\delta E\rangle \;=\; & \frac{1}{n_\chi^{\rm eq}n_\gamma^{\rm eq}}\int d\Pi_{\chi_1}d\Pi_{\gamma_1}d\Pi_{\chi_2}d\Pi_{\gamma_2}(2\pi)^4\delta^4(p) \\ & \times(E_{\chi_2}-E_{\chi_1})f_{\chi_1}(E_{\chi_1})f_{\gamma_1}(E_{\gamma_1})\,|\mathcal{M}|^2\,,\end{aligned} \tag{5.16}$$

and $d\Pi_i = g_i d^3p_1/(2\pi)^3$. Here, the dots denote the annihilation terms; these are unimportant in the ELDER regime, but are nevertheless fully included in the numerical analysis, as will be described in detail in Ref. [147].

The numerical solution for the evolution of the DM yield, $Y_\chi \equiv n_\chi/s$, in the ELDER scenario is shown in Fig. 5.1. The three stages of the DM evolution

(thermal equilibrium with the SM, cannibalization, and freeze-out) are clearly visible. The yield evolves very slowly in the cannibalization stage, due to slow evolution of the DM temperature (for the parameters in Fig. 5.1, $T'_f \approx 0.3T_d$, while $T_f \approx 0.025T_d$). As a result, the final DM abundance is approximately independent of when freeze-out occurs, and hence of the self-annihilation cross-section.

This feature is further illustrated in Fig. 5.2, which shows the regions of parameter space where the observed DM density is reproduced. For fixed m_χ, the ELDER scenario corresponds to the narrow vertical region of approximately constant ϵ, while α can take any value above a certain lower cutoff; these features are consistent with the estimates in Eqs. (5.11) and (5.12). For smaller values of α, self-annihilations freeze out before elastic scattering decouples, and the relic density is fixed by the strength of the self-annihilation process, α, and is independent of ϵ as long as it is large enough. The resulting horizontal region corresponds precisely to the SIMP scenario proposed in [25]. Finally, if ϵ becomes too large, annihilations become important, and since ϵ controls the annihilation cross-section, another vertical region occurs. This corresponds to the canonical WIMP scenario (or the "WIMPless" regime [149]). The numerical study clearly establishes the presence of the novel elastic decoupling scenario. In addition, it establishes precise boundaries of the different regimes, and traces out in detail the transition regions where two types of interactions play an equally important role in setting the relic density.

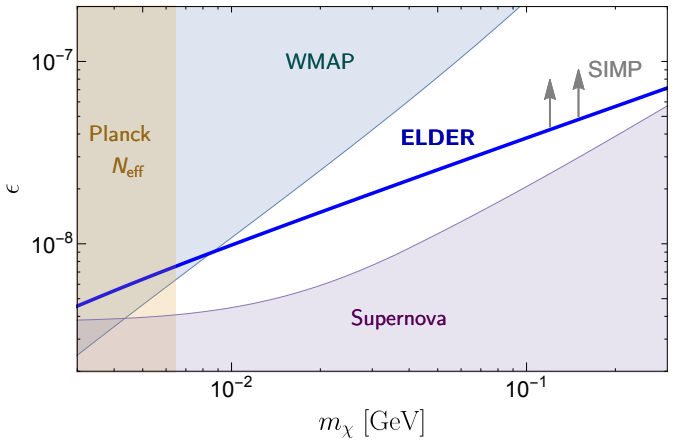

Figure 5.3: Constraints on ϵ vs. m_χ, from dark matter couplings to photons. The blue line corresponds to the ELDER scenario while the region above it corresponds to the SIMP scenario. Also shown are the exclusion limits from: supernova cooling (purple region); CMB constraints on DM annihilations into photons before recombination (blue region); and modification to $N_{\rm eff}^{\nu}$ from DM decoupling (red region).

5.4 Constraints

Since ELDER dark matter has mass and coupling strengths similar to the case of SIMPs, the same set of observational constraints is relevant for both scenarios. The strongest constraints on the strength of the χ interactions with the SM are summarized in Fig. 5.3.

In the relevant range of ϵ, the reaction $\gamma\gamma \to \chi\chi$ in the core of the supernova SN1987A would lead to energy loss rate inconsistent with observations, unless the produced χ particles become trapped in the core [150, 151, 152, 153]. Since trapping is due to elastic scattering of χ on photons in the supernova core, this constraint places a *lower* bound on ϵ. The value predicted by the ELDER scenario satisfies this bound throughout the relevant mass range. The bound can be further weakened if χ couples to e^- or ν instead of γ, as their higher density

in the supernova core implies a smaller mean free path for the same value of ϵ.

Cosmic Microwave Background (CMB) measurements limit the rate of DM annihilation into SM particles before recombination, which can modify the anisotropies of the CMB [154, 155, 156]. In our case, the relevant process is $\chi\chi \to \gamma\gamma$. The cross-section of this process in the non-relativistic regime is obtained from Eq. (5.6), which implies that annihilation occurs in s-wave. The WMAP results [157] place an upper bound on ϵ shown in Fig. 5.3. Again, the coupling predicted by the ELDER scenario is consistent with this bound. Null results of searches for anomalous high-energy photons from dark matter annihilation in the Milky Way or its dwarf satellites can also be used to place an upper bound on ϵ [158]. The bound is similar to the one implied by the WMAP data, and we do not show it in Fig. 5.3. Note that if $\chi\chi \to \gamma\gamma$ annihilation occurred in p-wave instead, the cross-sections relevant for both CMB and indirect searches would be severely suppressed relative to that at the time of dark matter decoupling, due to lower χ velocities, and the bounds would be even weaker. These bounds would also be completely eliminated if χ couples only to neutrinos.

If the ELDER decoupling occurs after the neutrinos are decoupled from the SM plasma, it can affect the temperature ratio T_ν/T_γ, resulting in a non-standard value of $N_{\rm eff}^\nu$ measured in CMB observations. This places a lower bound on the DM mass of a few MeV, with the exact number depending on g_χ: for example, $m_\chi \gtrsim 6.5$ MeV for a complex scalar χ coupled only to γ [159]. This bound can be avoided if χ is coupled to both ν and e/γ, since in this case reheating due to ELDER decoupling does not change the ratio T_ν/T_γ. (The region $m_\chi \lesssim 1$ MeV is also constrained by the Big Bang Nucleosynthesis bound on the number of relativistic degrees of freedom.) In summary, the ELDER scenario is consistent

with all constraints provided that $m_\chi \gtrsim$ a few MeV, even with the most stringent interpretation of the observational bounds.

If the DM couples to electrons, additional signatures arise in direct detection experiments searching for electron recoils [160], as well as collider searches for $e^+e^- \to \chi\chi\gamma$ [161, 162, 163]. Current direct-detection bounds from XENON10 [164] are not yet sensitive to ϵ in the range predicted by the ELDER scenario, while the collider bounds from LEP-2 depend strongly on the mass of the particle mediating the DM-SM scattering, and cannot be used to put robust constrains on ϵ. Interestingly, proposed dedicated germanium or silicon-based electron-recoil direct detection experiments [165, 166] and superconducting detectors [167] are expected to directly probe the ELDER scenario, which gives a scattering cross-section with electrons, $\sigma_{\rm scat} \sim 10^{-40} - 10^{-41}$ cm^2.

Finally, the strong $3 \to 2$ self-annihilations required in the ELDER scenario generically imply a large contribution to $\chi\chi \to \chi\chi$ elastic self-scattering. The elastic self-scattering cross-section at low velocities, $v_\chi \sim 10^{-3}$, is constrained by observations of the Bullet Cluster [21, 22, 23] and halo shapes [168, 169, 170]:

$$\frac{\sigma_{\chi\chi\to\chi\chi}}{m_\chi} \lesssim 1 \text{ cm}^2/\text{g}. \tag{5.17}$$

Note that a self-scattering cross section in the $0.1 - 1$ cm^2/g range [169, 171, 168, 170], consistent with this bound, could reconcile the N-body simulation results with the observed small-scale structure, providing an additional motivation for self-interacting DM candidates (see for instance, [172, 173, 174, 175]). The precise relation between the elastic self-scattering and self-annihilation cross-sections is model-dependent. Generically, one might expect that

$$\sigma_{\chi\chi\to\chi\chi} = a^2 \frac{\alpha^2}{m_\chi^2}, \tag{5.18}$$

where a is an order-one constant. Consistency of the ELDER scenario with the bound of Eq. (5.17) requires $a \lesssim 0.01 - 0.1$ (depending on m_χ). However, if the self-annihilation and self-scattering cross-sections both vanish at threshold, and are therefore velocity suppressed, these bounds may be alleviated [147].

Acknowledgments — We are grateful to Yonit Hochberg, Hitoshi Murayama, Aaron Pierce, Josh Ruderman, and Yue Zhao for useful discussions. This work is supported by the U.S. National Science Foundation through grant PHY-1316222. EK is supported by a Hans Bethe Postdoctoral Fellowship at Cornell. YT is also supported by Taiwan Study Abroad Scholarship.

BIBLIOGRAPHY

[1] Michael E. Peskin. Comparison of LHC and ILC Capabilities for Higgs Boson Coupling Measurements. 2012.

[2] Witold Skiba. Effective Field Theory and Precision Electroweak Measurements. In *Physics of the large and the small, TASI 09, proceedings of the Theoretical Advanced Study Institute in Elementary Particle Physics, Boulder, Colorado, USA, 1-26 June 2009*, pages 5–70, 2011.

[3] V. Agrawal, Stephen M. Barr, John F. Donoghue, and D. Seckel. The Anthropic principle and the mass scale of the standard model. *Phys. Rev.*, D57:5480–5492, 1998.

[4] Stephen P. Martin. A Supersymmetry primer. 1997. [Adv. Ser. Direct. High Energy Phys.18,1(1998)].

[5] M. Shifman. *Advanced topics in quantum field theory.* Cambridge Univ. Press, Cambridge, UK, 2012.

[6] Haiying Cai, Hsin-Chia Cheng, and John Terning. A Spin-1 Top Quark Superpartner. *Phys.Rev.Lett.*, 101:171805, 2008.

[7] G. P. Lepage. Lattice QCD for novices. In *Strong interactions at low and intermediate energies. Proceedings, 13th Annual Hampton University Graduate Studies, HUGS'98, Newport News, USA, May 26-June 12, 1998*, pages 49–90, 1998.

[8] Gavin P. Salam. Elements of QCD for hadron colliders. In *High-energy physics. Proceedings, 17th European School, ESHEP 2009, Bautzen, Germany, June 14-27, 2009*, 2010.

[9] Paul Hoyer. Lectures on Bound states. 2016.

[10] J. Terning. *Modern supersymmetry: Dynamics and duality*. 2006.

[11] Nathan Seiberg. Exact results on the space of vacua of four-dimensional SUSY gauge theories. *Phys. Rev.*, D49:6857–6863, 1994.

[12] N. Seiberg. Electric - magnetic duality in supersymmetric nonAbelian gauge theories. *Nucl. Phys.*, B435:129–146, 1995.

[13] Csaba Csaki. The Confining N=1 supersymmetric gauge theories: A Review. In *Continuous advances in QCD. Proceedings, 3rd Workshop, QCD'98, Minneapolis, USA, April 16-19, 1998*, pages 489–499, 1998.

[14] M. Srednicki. *Quantum field theory*. Cambridge University Press, 2007.

[15] Alexander M. Polyakov. Quark Confinement and Topology of Gauge Groups. *Nucl.Phys.*, B120:429–458, 1977.

[16] N. Michael Davies, Timothy J. Hollowood, and Valentin V. Khoze. Monopoles, affine algebras and the gluino condensate. *J. Math Phys.*, 44:3640, 2003.

[17] Matthew J. Strassler. An Unorthodox introduction to supersymmetric gauge theory. In *Strings, Branes and Extra Dimensions: TASI 2001: Proceedings*, pages 561–638, 2003.

[18] Ofer Aharony, Shlomo S. Razamat, Nathan Seiberg, and Brian Willett. 3d dualities from 4d dualities. 2013.

[19] K. A. Olive et al. Review of Particle Physics. *Chin. Phys.*, C38:090001, 2014.

[20] Scott Dodelson. *Modern Cosmology*. Academic Press, Amsterdam, 2003.

[21] Douglas Clowe, Anthony Gonzalez, and Maxim Markevitch. Weak lensing mass reconstruction of the interacting cluster 1E0657-558: Direct evidence for the existence of dark matter. *Astrophys. J.*, 604:596–603, 2004.

[22] Maxim Markevitch, A. H. Gonzalez, D. Clowe, A. Vikhlinin, L. David, W. Forman, C. Jones, S. Murray, and W. Tucker. Direct constraints on the dark matter self-interaction cross-section from the merging galaxy cluster 1E0657-56. *Astrophys. J.*, 606:819–824, 2004.

[23] Scott W. Randall, Maxim Markevitch, Douglas Clowe, Anthony H. Gonzalez, and Marusa Bradac. Constraints on the Self-Interaction Cross-Section of Dark Matter from Numerical Simulations of the Merging Galaxy Cluster 1E 0657-56. *Astrophys. J.*, 679:1173–1180, 2008.

[24] Manuel Drees and Gilles Gerbier. Mini-Review of Dark Matter: 2012. 2012.

[25] Yonit Hochberg, Eric Kuflik, Tomer Volansky, and Jay G. Wacker. Mechanism for Thermal Relic Dark Matter of Strongly Interacting Massive Particles. *Phys. Rev. Lett.*, 113:171301, 2014.

[26] Yonit Hochberg, Eric Kuflik, Hitoshi Murayama, Tomer Volansky, and Jay G. Wacker. Model for Thermal Relic Dark Matter of Strongly Interacting Massive Particles. *Phys. Rev. Lett.*, 115(2):021301, 2015.

[27] Eric D. Carlson, Marie E. Machacek, and Lawrence J. Hall. Self-interacting dark matter. *Astrophys. J.*, 398:43–52, 1992.

[28] Marco Farina, Maxim Perelstein, and Nicolas Rey-Le Lorier. Higgs Couplings and Naturalness. *Phys. Rev.*, D90(1):015014, 2014.

[29] Ian Low, Riccardo Rattazzi, and Alessandro Vichi. Theoretical Constraints on the Higgs Effective Couplings. *JHEP*, 04:126, 2010.

[30] Dean Carmi, Adam Falkowski, Eric Kuflik, Tomer Volansky, and Jure Zupan. Higgs After the Discovery: A Status Report. *JHEP*, 10:196, 2012.

[31] Svjetlana Fajfer, Admir Greljo, Jernej F. Kamenik, and Ivana Mustac. Light Higgs and Vector-like Quarks without Prejudice. *JHEP*, 07:155, 2013.

[32] Mikhail A. Shifman, A. I. Vainshtein, M. B. Voloshin, and Valentin I. Zakharov. Low-Energy Theorems for Higgs Boson Couplings to Photons. *Sov. J. Nucl. Phys.*, 30:711–716, 1979. [Yad. Fiz.30,1368(1979)].

[33] Andrew G. Cohen, D. B. Kaplan, and A. E. Nelson. The More minimal supersymmetric standard model. *Phys. Lett.*, B388:588–598, 1996.

[34] Maxim Perelstein and Christian Spethmann. A Collider signature of the supersymmetric golden region. *JHEP*, 04:070, 2007.

[35] Yevgeny Kats, Patrick Meade, Matthew Reece, and David Shih. The Status of GMSB After 1/fb at the LHC. *JHEP*, 02:115, 2012.

[36] Christopher Brust, Andrey Katz, Scott Lawrence, and Raman Sundrum. SUSY, the Third Generation and the LHC. *JHEP*, 03:103, 2012.

[37] Michele Papucci, Joshua T. Ruderman, and Andreas Weiler. Natural SUSY Endures. *JHEP*, 09:035, 2012.

[38] Nishita Desai and Biswarup Mukhopadhyaya. Constraints on supersymmetry with light third family from LHC data. *JHEP*, 05:057, 2012.

[39] Maxim Perelstein. Little Higgs models and their phenomenology. *Prog. Part. Nucl. Phys.*, 58:247–291, 2007.

[40] Martin Schmaltz and David Tucker-Smith. Little Higgs review. *Ann. Rev. Nucl. Part. Sci.*, 55:229–270, 2005.

[41] Kaustubh Agashe, Roberto Contino, and Alex Pomarol. The Minimal composite Higgs model. *Nucl. Phys.*, B719:165–187, 2005.

[42] Roberto Contino, Yasunori Nomura, and Alex Pomarol. Higgs as a holographic pseudoGoldstone boson. *Nucl. Phys.*, B671:148–174, 2003.

[43] Roberto Contino, Leandro Da Rold, and Alex Pomarol. Light custodians in natural composite Higgs models. *Phys. Rev.*, D75:055014, 2007.

[44] Haiying Cai, Hsin-Chia Cheng, and John Terning. A Spin-1 Top Quark Superpartner. *Phys. Rev. Lett.*, 101:171805, 2008.

[45] Maxim Perelstein, Michael E. Peskin, and Aaron Pierce. Top quarks and electroweak symmetry breaking in little Higgs models. *Phys. Rev.*, D69:075002, 2004.

[46] Tao Han, Heather E. Logan, Bob McElrath, and Lian-Tao Wang. Phenomenology of the little Higgs model. *Phys. Rev.*, D67:095004, 2003.

[47] Joshua Berger, Jay Hubisz, and Maxim Perelstein. A Fermionic Top Partner: Naturalness and the LHC. *JHEP*, 07:016, 2012.

[48] Cdric Delaunay, Christophe Grojean, and Gilad Perez. Modified Higgs Physics from Composite Light Flavors. *JHEP*, 09:090, 2013.

[49] Georges Aad et al. Search for the Standard Model Higgs boson in the diphoton decay channel with 4.9 fb^{-1} of pp collisions at $\sqrt{s}$ = 7 TeV with ATLAS. *Phys. Rev. Lett.*, 108:111803, 2012.

[50] Georges Aad et al. Search for the Standard Model Higgs boson in the decay channel $H \to ZZ^{(*)} \to 4\ell$ with 4.8 fb^{-1} of pp collision data at $\sqrt{s}$ = 7 TeV with ATLAS. *Phys. Lett.*, B710:383–402, 2012.

[51] Georges Aad et al. Search for the Standard Model Higgs boson in the $H \to \mathrm{WW}(*) \to \ell\nu\ell\nu$ decay mode with 4.7 /fb of ATLAS data at $\sqrt{s} = 7$ TeV. *Phys. Lett.*, B716:62–81, 2012.

[52] Georges Aad et al. Search for the Standard Model Higgs boson in the H to $\tau^+\tau^-$ decay mode in $\sqrt{s} = 7$ TeV pp collisions with ATLAS. *JHEP*, 09:070, 2012.

[53] Serguei Chatrchyan et al. Search for the standard model Higgs boson decaying to bottom quarks in pp collisions at $\sqrt{s} = 7$ TeV. *Phys. Lett.*, B710:284–306, 2012.

[54] T. Aaltonen et al. Higgs Boson Studies at the Tevatron. *Phys. Rev.*, D88(5):052014, 2013.

[55] S. Dittmaier et al. Handbook of LHC Higgs Cross Sections: 1. Inclusive Observables. 2011.

[56] J R Andersen et al. Handbook of LHC Higgs Cross Sections: 3. Higgs Properties. 2013.

[57] Combined coupling measurements of the Higgs-like boson with the ATLAS detector using up to 25 fb^{-1} of proton-proton collision data. 2013.

[58] Serguei Chatrchyan et al. Observation of a new boson with mass near 125 GeV in pp collisions at $\sqrt{s} = 7$ and 8 TeV. *JHEP*, 06:081, 2013.

[59] JiJi Fan, Matthew Reece, and Joshua T. Ruderman. Stealth Supersymmetry. *JHEP*, 11:012, 2011.

[60] Radovan Dermisek and Ian Low. Probing the Stop Sector and the Sanity of the MSSM with the Higgs Boson at the LHC. *Phys. Rev.*, D77:035012, 2008.

[61] Kfir Blum, Raffaele Tito D'Agnolo, and JiJi Fan. Natural SUSY Predicts: Higgs Couplings. *JHEP*, 01:057, 2013.

[62] Raffaele Tito D'Agnolo, Eric Kuflik, and Marco Zanetti. Fitting the Higgs to Natural SUSY. *JHEP*, 03:043, 2013.

[63] Graham D. Kribs, Adam Martin, and Arjun Menon. Natural Supersymmetry and Implications for Higgs physics. *Phys. Rev.*, D88:035025, 2013.

[64] Adam Falkowski. Pseudo-goldstone Higgs production via gluon fusion. *Phys. Rev.*, D77:055018, 2008.

[65] Aleksandr Azatov and Jamison Galloway. Light Custodians and Higgs Physics in Composite Models. *Phys. Rev.*, D85:055013, 2012.

[66] Nathaniel Craig, Christoph Englert, and Matthew McCullough. New Probe of Naturalness. *Phys. Rev. Lett.*, 111(12):121803, 2013.

[67] Jack H. Collins, Bithika Jain, Maxim Perelstein, and Nicolas Rey-Le Lorier. Spin-One Top Partner: Phenomenology. *JHEP*, 08:022, 2014.

[68] Paul Langacker and Ming-xing Luo. Constraints on additional Z bosons. *Phys.Rev.*, D45:278–292, 1992.

[69] Bob Holdom. Oblique electroweak corrections and an extra gauge boson. *Phys.Lett.*, B259:329–334, 1991.

[70] Guido Altarelli, Riccardo Barbieri, and S. Jadach. Toward a model independent analysis of electroweak data. *Nucl.Phys.*, B369:3–32, 1992.

[71] Riccardo Barbieri, Alex Pomarol, Riccardo Rattazzi, and Alessandro Strumia. Electroweak symmetry breaking after LEP-1 and LEP-2. *Nucl.Phys.*, B703:127–146, 2004.

[72] Haiying Cai. D-term Enhancement in Spin-1 Top Partner Model. *Phys.Rev.*, D85:115020, 2012.

[73] Max Baak and Roman Kogler. The global electroweak Standard Model fit after the Higgs discovery. pages 349–358, 2013.

[74] Johan Alwall, Michel Herquet, Fabio Maltoni, Olivier Mattelaer, and Tim Stelzer. MadGraph 5 : Going Beyond. *JHEP*, 1106:128, 2011.

[75] Search for Resonances in the Dilepton Mass Distribution in pp Collisions at sqrt(s) = 8 TeV. Technical Report CMS-PAS-EXO-12-061, CERN, Geneva, 2013.

[76] Dario Buttazzo, Giuseppe Degrassi, Pier Paolo Giardino, Gian F. Giudice, Filippo Sala, et al. Investigating the near-criticality of the Higgs boson. *JHEP*, 1312:089, 2013.

[77] Puneet Batra, Antonio Delgado, David E. Kaplan, and Timothy M.P. Tait. The Higgs mass bound in gauge extensions of the minimal supersymmetric standard model. *JHEP*, 0402:043, 2004.

[78] Alexander Maloney, Aaron Pierce, and Jay G. Wacker. D-terms, unification, and the Higgs mass. *JHEP*, 0606:034, 2006.

[79] S. Dawson, A. Gritsan, H. Logan, J. Qian, C. Tully, et al. Higgs Working Group Report of the Snowmass 2013 Community Planning Study. 2013.

[80] Howard Baer, Tim Barklow, Keisuke Fujii, Yuanning Gao, Andre Hoang, et al. The International Linear Collider Technical Design Report - Volume 2: Physics. 2013.

[81] M. Bicer, H. Duran Yildiz, I. Yildiz, G. Coignet, M. Delmastro, et al. First Look at the Physics Case of TLEP. 2013.

[82] Abdelhak Djouadi. The Anatomy of electro-weak symmetry breaking. II. The Higgs bosons in the minimal supersymmetric model. *Phys.Rept.*, 459:1–241, 2008.

[83] Ian Low, Riccardo Rattazzi, and Alessandro Vichi. Theoretical Constraints on the Higgs Effective Couplings. *JHEP*, 1004:126, 2010.

[84] Dean Carmi, Adam Falkowski, Eric Kuflik, and Tomer Volansky. Interpreting LHC Higgs Results from Natural New Physics Perspective. *JHEP*, 1207:136, 2012.

[85] Dean Carmi, Adam Falkowski, Eric Kuflik, Tomer Volansky, and Jure Zupan. Higgs After the Discovery: A Status Report. *JHEP*, 1210:196, 2012.

[86] Nathaniel Craig, Christoph Englert, and Matthew McCullough. A New Probe of Naturalness. *Phys.Rev.Lett.*, 111:121803, 2013.

[87] Don Bunk, Jay Hubisz, and Bithika Jain. Higgs Decays in Gauge Extensions of the Standard Model. *Phys.Rev.*, D89:035014, 2014.

[88] John R. Ellis, Mary K. Gaillard, and Dimitri V. Nanopoulos. A Phenomenological Profile of the Higgs Boson. *Nucl.Phys.*, B106:292, 1976.

[89] Mikhail A. Shifman, A. I. Vainshtein, M. B. Voloshin, and Valentin I. Za-

kharov. Low-Energy Theorems for Higgs Boson Couplings to Photons. *Sov. J. Nucl. Phys.*, 30:711–716, 1979. [Yad. Fiz.30,1368(1979)].

[90] Richard D. Ball et al. Parton distributions with QED corrections. *Nucl.Phys.*, B877(2):290–320, 2013.

[91] Aram Avetisyan, John M. Campbell, Timothy Cohen, Nitish Dhingra, James Hirschauer, et al. Methods and Results for Standard Model Event Generation at $\sqrt{s}$ = 14 TeV, 33 TeV and 100 TeV Proton Colliders (A Snowmass Whitepaper). 2013.

[92] Chien-Yi Chen, Ayres Freitas, Tao Han, and Keith S.M. Lee. New Physics from the Top at the LHC. *JHEP*, 1211:124, 2012.

[93] Christopher Brust, Andrey Katz, Scott Lawrence, and Raman Sundrum. SUSY, the Third Generation and the LHC. *JHEP*, 1203:103, 2012.

[94] Michele Papucci, Joshua T. Ruderman, and Andreas Weiler. Natural SUSY Endures. *JHEP*, 1209:035, 2012.

[95] Joshua Berger, Jay Hubisz, and Maxim Perelstein. A Fermionic Top Partner: Naturalness and the LHC. *JHEP*, 1207:016, 2012.

[96] Antonio Amariti, Csaba Cski, Mario Martone, and Nicolas Rey-Le Lorier. From S-confinement to 3D Chiral Theories: Dressing the Monopoles. 2015.

[97] Ofer Aharony, Amihay Hanany, Kenneth A. Intriligator, N. Seiberg, and M. J. Strassler. Aspects of N = 2 supersymmetric gauge theories in three dimensions. *Nucl. Phys.*, B499:67–99, 1997.

[98] Jan de Boer, Kentaro Hori, and Yaron Oz. Dynamics of N=2 supersymmetric gauge theories in three-dimensions. *Nucl.Phys.*, B500:163–191, 1997.

[99] Ofer Aharony. IR duality in d = 3 N=2 supersymmetric USp(2N(c)) and U(N(c)) gauge theories. *Phys.Lett.*, B404:71–76, 1997.

[100] Andreas Karch. Seiberg duality in three-dimensions. *Phys.Lett.*, B405:79–84, 1997.

[101] Kenneth A. Intriligator and N. Seiberg. Mirror symmetry in three-dimensional gauge theories. *Phys. Lett. B*, 387:513, 1996.

[102] Jan de Boer, Kentaro Hori, Hirosi Ooguri, and Yaron Oz. Mirror symmetry in three-dimensional gauge theories, quivers and D-branes. *Nucl.Phys.*, B493:101–147, 1997.

[103] Amihay Hanany and Edward Witten. Type IIB superstrings, BPS monopoles, and three-dimensional gauge dynamics. *Nucl.Phys.*, B492:152–190, 1997.

[104] Anton Kapustin and Matthew J. Strassler. On mirror symmetry in three-dimensional Abelian gauge theories. *JHEP*, 9904:021, 1999.

[105] N. Dorey and D. Tong. Mirror symmetry and toric geometry in three-dimensional gauge theories. *JHEP*, 0005:018, 2000.

[106] Vadim Borokhov, Anton Kapustin, and Xin-kai Wu. Monopole operators and mirror symmetry in three-dimensions. *JHEP*, 0212:044, 2002.

[107] Vadim Borokhov, Anton Kapustin, and Xin-kai Wu. Topological disorder operators in three-dimensional conformal field theory. *JHEP*, 0211:049, 2002.

[108] Kenneth Intriligator and Nathan Seiberg. Aspects of 3d N=2 Chern-Simons-Matter Theories. 2013.

[109] Kenneth Intriligator. Matching 3d N =2 vortices and monopole operators. *JHEP*, 1410:52, 2014.

[110] Ofer Aharony, Prithvi Narayan, and Tarun Sharma. On monopole operators in supersymmetric Chern-Simons-matter theories. 2015.

[111] Silviu S. Pufu and Subir Sachdev. Monopoles in 2 + 1-dimensional conformal field theories with global U(1) symmetry. *JHEP*, 1309:127, 2013.

[112] Ethan Dyer, Mrk Mezei, and Silviu S. Pufu. Monopole Taxonomy in Three-Dimensional Conformal Field Theories. 2013.

[113] Ethan Dyer, Mrk Mezei, Silviu S. Pufu, and Subir Sachdev. Scaling dimensions of monopole operators in the $\mathbb{CP}^{N_b-1}$ theory in $2+1$ dimensions. 2015.

[114] Csaba Csaki, Martin Schmaltz, and Witold Skiba. A Systematic approach

to confinement in N=1 supersymmetric gauge theories. *Phys.Rev.Lett.*, 78:799–802, 1997.

[115] Csaba Csaki, Martin Schmaltz, and Witold Skiba. Confinement in N = 1 SUSY gauge theories and model building tools. *Phys. Rev.*, D55:7840–7858, 1997.

[116] Antonio Amariti, Csaba Csaki, Mario Martone, and Nicolas Rey-Le Lorier. *In preparation*, 2016.

[117] K. Lee and P. Yi. Monopoles and Instantons on Partially Compactified D-Branes. *Phys. Rev.*, D56:3711, 1997.

[118] K. Lee. Instantons and Magnetic Monopoles on $\mathbb{R}^3 \times \mathcal{S}^1$ with Arbitrary Simple Gauge Groups. *Phys. Lett.*, B426:323, 1998.

[119] K. Lee and C. Lu. $SU(2)$ Calorons and Magnetic Monopoles. *Phys. Rev.*, D58:025011, 1998.

[120] T. C. Kraan and P. van Baal. Periodic instantons with nontrivial holonomy. *Nucl. Phys.*, B533:627–659, 1998.

[121] T. C. Kraan and P. van Baal. Monopole constituents inside SU(N) caldrons. *Phys. Lett. B*, 435:389–395, 1998.

[122] T. C. Kraan and P. van Baal. Constituent monopoles without gauge fixing. *Nucl. Phys. Proc. Suppl.*, 73:554–556, 1999.

[123] Csaba Csaki, Mario Martone, Yuri Shirman, Philip Tanedo, and John Terning. Dynamics of 3D SUSY Gauge Theories with Antisymmetric Matter. *JHEP*, 1408:141, 2014.

[124] Ian Affleck, Jeffrey A. Harvey, and Edward Witten. Instantons and (Super)Symmetry Breaking in (2+1)-Dimensions. *Nucl.Phys.*, B206:413, 1982.

[125] C. J. Callias. Index theorems on open spaces. *Comm. Math. Phys.*, 63:213, 1978.

[126] Christian Romelsberger. Counting chiral primaries in N = 1, d=4 superconformal field theories. *Nucl.Phys.*, B747:329–353, 2006.

[127] Justin Kinney, Juan Martin Maldacena, Shiraz Minwalla, and Suvrat Raju. An Index for 4 dimensional super conformal theories. *Commun.Math.Phys.*, 275:209–254, 2007.

[128] Daniel L. Jafferis. The Exact Superconformal R-Symmetry Extremizes Z. *JHEP*, 1205:159, 2012.

[129] Naofumi Hama, Kazuo Hosomichi, and Sungjay Lee. Notes on SUSY Gauge Theories on Three-Sphere. *JHEP*, 1103:127, 2011.

[130] V.P. Spiridonov and G.S. Vartanov. Elliptic Hypergeometry of Supersymmetric Dualities. *Commun.Math.Phys.*, 304:797–874, 2011.

[131] V.P. Spiridonov and G.S. Vartanov. Vanishing superconformal indices and the chiral symmetry breaking. *JHEP*, 1406:062, 2014.

[132] Antonio Amariti and Claudius Klare. A journey to 3d: exact relations for adjoint SQCD from dimensional reduction. 2014.

[133] Fokko van de Bult. Hyperbolic Hypergeometric Functions, http://www.its.caltech.edu/ vdbult/Thesis.pdf. *Thesis*, 2008.

[134] Seok Kim. The Complete superconformal index for N=6 Chern-Simons theory. *Nucl.Phys.*, B821:241–284, 2009.

[135] Francesco Benini and Alberto Zaffaroni. A topologically twisted index for three-dimensional supersymmetric theories. 2015.

[136] Cyril Closset, Stefano Cremonesi, and Daniel S. Park. The equivariant A-twist and gauged linear sigma models on the two-sphere. 2015.

[137] Sara Pasquetti. Factorisation of N = 2 Theories on the Squashed 3-Sphere. *JHEP*, 1204:120, 2012.

[138] Christopher Beem, Tudor Dimofte, and Sara Pasquetti. Holomorphic Blocks in Three Dimensions. *JHEP*, 1412:177, 2014.

[139] Eric Kuflik, Maxim Perelstein, Nicolas Rey-Le Lorier, and Yu-Dai Tsai. Elastically Decoupling Dark Matter. 2015.

[140] Benjamin W. Lee and Steven Weinberg. Cosmological Lower Bound on Heavy Neutrino Masses. *Phys. Rev. Lett.*, 39:165–168, 1977.

[141] Andrew A. de Laix, Robert J. Scherrer, and Robert K. Schaefer. Constraints of selfinteracting dark matter. *Astrophys. J.*, 452:495, 1995.

[142] Nicolas Bernal, Camilo Garcia-Cely, and Rogerio Rosenfeld. WIMP and SIMP Dark Matter from the Spontaneous Breaking of a Global Group. *JCAP*, 1504(04):012, 2015.

[143] Hyun Min Lee and Min-Seok Seo. Communication with SIMP dark mesons via Z? -portal. *Phys. Lett.*, B748:316–322, 2015.

[144] Soo-Min Choi and Hyun Min Lee. SIMP dark matter with gauged Z_3 symmetry. *JHEP*, 09:063, 2015.

[145] Nicolas Bernal, Xiaoyong Chu, Camilo Garcia-Cely, Thomas Hambye, and Bryan Zaldivar. Production Regimes for Self-Interacting Dark Matter. *JCAP*, 1603(03):018, 2016.

[146] Nicolas Bernal and Xiaoyong Chu. Z_2 SIMP Dark Matter. *JCAP*, 1601:006, 2016.

[147] Eric Kuflik, Maxim Perelstein, Nicolas Rey-LeLorier, and Tsai Yu-Dai. WIMPs, SIMPs and ELDERs: The Phase Diagram of Cold Thermal Relic Dark Matter. *In preparation*, 2016.

[148] Soo-Min Choi and Hyun Min Lee. Resonant SIMP dark matter. 2016.

[149] Jonathan L. Feng and Jason Kumar. The WIMPless Miracle: Dark-Matter Particles without Weak-Scale Masses or Weak Interactions. *Phys. Rev. Lett.*, 101:231301, 2008.

[150] John R. Ellis, Keith A. Olive, Subir Sarkar, and D. W. Sciama. Low Mass Photinos and Supernova SN1987A. *Phys. Lett.*, B215:404, 1988.

[151] J. A. Grifols, E. Masso, and S. Peris. Photinos From Gravitational Collapse. *Phys. Lett.*, B220:591, 1989.

[152] G. G. Raffelt. *Stars as laboratories for fundamental physics*. 1996.

[153] H. K. Dreiner, C. Hanhart, U. Langenfeld, and Daniel R. Phillips. Supernovae and light neutralinos: SN1987A bounds on supersymmetry revisited. *Phys. Rev.*, D68:055004, 2003.

[154] Douglas P. Finkbeiner, Silvia Galli, Tongyan Lin, and Tracy R. Slatyer. Searching for dark matter in the cmb: A compact parametrization of energy injection from new physics. *Phys. Rev. D*, 85:043522, Feb 2012.

[155] Mathew S. Madhavacheril, Neelima Sehgal, and Tracy R. Slatyer. Current Dark Matter Annihilation Constraints from CMB and Low-Redshift Data. *Phys. Rev.*, D89:103508, 2014.

[156] Tracy R. Slatyer. Indirect dark matter signatures in the cosmic dark ages. I. Generalizing the bound on s-wave dark matter annihilation from Planck results. *Phys. Rev.*, D93(2):023527, 2016.

[157] G. Hinshaw, D. Larson, E. Komatsu, D. N. Spergel, C. L. Bennett, J. Dunkley, M. R. Nolta, M. Halpern, R. S. Hill, N. Odegard, L. Page, K. M. Smith, J. L. Weiland, B. Gold, N. Jarosik, A. Kogut, M. Limon, S. S. Meyer, G. S. Tucker, E. Wollack, and E. L. Wright. Nine-year wilkinson microwave anisotropy probe (wmap) observations: Cosmological parameter results. *The Astrophysical Journal Supplement Series*, 208(2):19, 2013.

[158] Rouven Essig, Eric Kuflik, Samuel D. McDermott, Tomer Volansky, and Kathryn M. Zurek. Constraining Light Dark Matter with Diffuse X-Ray and Gamma-Ray Observations. *JHEP*, 11:193, 2013.

[159] Cline Boehm, Matthew J. Dolan, and Christopher McCabe. A Lower Bound on the Mass of Cold Thermal Dark Matter from Planck. *JCAP*, 1308:041, 2013.

[160] Rouven Essig, Jeremy Mardon, and Tomer Volansky. Direct Detection of Sub-GeV Dark Matter. *Phys. Rev.*, D85:076007, 2012.

[161] Andreas Birkedal, Konstantin Matchev, and Maxim Perelstein. Dark matter at colliders: A Model independent approach. *Phys. Rev.*, D70:077701, 2004.

[162] Patrick J. Fox, Roni Harnik, Joachim Kopp, and Yuhsin Tsai. LEP Shines Light on Dark Matter. *Phys. Rev.*, D84:014028, 2011.

[163] Yoonseok John Chae and Maxim Perelstein. Dark Matter Search at a Linear Collider: Effective Operator Approach. *JHEP*, 05:138, 2013.

[164] Rouven Essig, Aaron Manalaysay, Jeremy Mardon, Peter Sorensen, and

Tomer Volansky. First Direct Detection Limits on sub-GeV Dark Matter from XENON10. *Phys. Rev. Lett.*, 109:021301, 2012.

[165] Rouven Essig, Marivi Fernandez-Serra, Jeremy Mardon, Adrian Soto, Tomer Volansky, and Tien-Tien Yu. Direct Detection of sub-GeV Dark Matter with Semiconductor Targets. 2015.

[166] Samuel K. Lee, Mariangela Lisanti, Siddharth Mishra-Sharma, and Benjamin R. Safdi. Modulation Effects in Dark Matter-Electron Scattering Experiments. *Phys. Rev.*, D92(8):083517, 2015.

[167] Yonit Hochberg, Yue Zhao, and Kathryn M. Zurek. Superconducting Detectors for Superlight Dark Matter. *Phys. Rev. Lett.*, 116(1):011301, 2016.

[168] Miguel Rocha, Annika H. G. Peter, James S. Bullock, Manoj Kaplinghat, Shea Garrison-Kimmel, Jose Onorbe, and Leonidas A. Moustakas. Cosmological Simulations with Self-Interacting Dark Matter I: Constant Density Cores and Substructure. *Mon. Not. Roy. Astron. Soc.*, 430:81–104, 2013.

[169] Jesus Zavala, Mark Vogelsberger, and Matthew Walker.

[170] Annika H. G. Peter, Miguel Rocha, James S. Bullock, and Manoj Kaplinghat. Cosmological Simulations with Self-Interacting Dark Matter II: Halo Shapes vs. Observations. *Mon. Not. Roy. Astron. Soc.*, 430:105, 2013.

[171] Jesus Zavala, Mark Vogelsberger, and Abraham Loeb.

[172] David N. Spergel and Paul J. Steinhardt. Observational evidence for self-interacting cold dark matter. *Phys. Rev. Lett.*, 84:3760–3763, 2000.

[173] W. J. G. de Blok. The Core-Cusp Problem. *Adv. Astron.*, 2010:789293, 2010.

[174] Michael Boylan-Kolchin, James S. Bullock, and Manoj Kaplinghat. Too big to fail? The puzzling darkness of massive Milky Way subhaloes. *Mon. Not. Roy. Astron. Soc.*, 415:L40, 2011.

[175] Manoj Kaplinghat, Sean Tulin, and Hai-Bo Yu. Dark Matter Halos as Particle Colliders: Unified Solution to Small-Scale Structure Puzzles from Dwarfs to Clusters. *Phys. Rev. Lett.*, 116(4):041302, 2016.